Preparation, Properties, and Applications of Thin Ferromagnetic Films

Proceedings of a Workshop at the
Vienna University of Technology
June 15th and 16th, 2000

organised by the
Institute of Industrial Electronics and Material Science

Vienna, June 2000

Preparation, Properties, and Applications of Thin Ferromagnetic Films

Proceedings of a Workshop at the
Vienna University of Technology
June 15th and 16th, 2000

Institute of Industrial Electronics and Material Science
Technische Universität Wien
Gusshausstrasse 27-29/366, A-1040 Wien

Vienna, June 2000

Editor & Layout: Karl Riedling

ISBN: 3-85465-007-8

Preface

K. Riedling, H. Hauser

Institute of Industrial Electronics and Material Science, TU Vienna
Gusshausstrasse 27–29/366, A-1040 Vienna

In Spring1999, the Faculty of Electrical Engineering and Information Technology of the Vienna University of Technology has put a thematic main focus on "Sensorics and Packaging". One of the subjects of distinct interest are magnetic sensors and the related technology for microelectronic components.

The workshop "Preparation, Properties, and Applications of Thin Ferromagnetic Films" originated from a partner search call on the IDEAL-IST server of the European Commission in the course of the preparation of a European project on the application of thin ferromagnetic films. The number of responses to this partner search call, and the quality of the responding groups, was so overwhelmingly positive that we decided to invite the greater part of the interested groups to a workshop at the Vienna University of Technology. Most of our contact persons not only agreed to presenting their relevant work but also to preparing a manuscript for these proceedings. With eight presentations from the groups that had responded to the partner search, five presentations by the "core groups" of the planned project, and, last but not least, two presentations by visiting professors, the workshop turned out to provide a comprehensive overview of the state of the art of international research on thin ferromagnetic films. It need not be mentioned that various bilateral and multilateral co-operations have been initiated at this workshop, and common projects are currently being planned.

We hope that this compilation can promote and support our future work.

Vienna, June 2000

Karl Riedling

Workshop Organiser and
Editor of the Proceedings

Hans Hauser

Head of the Institute of Industrial
Electronics and Material Science

Workshop Programme

Thursday, June 15th, 2000:

10:00 – 10:30	Registration, Welcome, Introduction
10:30 – 11:30	**D. Jiles**, Ames Laboratory, Iowa State University: *The Future of Magnetoelectronic Devices*
11:30 – 12:00	**H. Hauser**, TU Wien *Magnetoresistive Sensors*
12:00 – 12:30	**G. Vértesy**, Hungarian Academy of Sciences, Budapest *High Sensitivity Magnetic Field Sensor*
12:30 – 14:00	Lunch
14:00 – 14:30	**H. Grüger**, Fraunhofer Institute for Microelectronic Circuits and Systems IMS, Dresden *CMOS Integrated Two Axes Magnetic Field Sensors – Miniaturized Low Cost Systems With Large Temperature Range*
14:30 – 15:00	**J. Hochreiter, D. Schrottmayer**, Schiebel Ges.m.b.H, Wien *DIMADS ™ — Digital Magnetic Anomaly Detection System*
15:00 – 15:30	**T. O'Donnell**, PEI Technologies, Cork *Microtransformers and Inductors using Permalloy Thin Films*
15:30 – 16:00	**J. Cabestany**, Technical University of Catalonia (UPC), Barcelona *Electronics and Methods for Sensors Based on Ferromagnetic Devices*
16:00 – 18:30	Open discussions
18:30 – ???	Transfer to a "Heurigen", Dinner

Friday, June 16th, 2000:

10:00 – 10:30	**G. Stangl**, TU Wien *Cathode Sputtered Permalloy Films of High Anisotropic Magnetoresistive Effect*
10:30 – 11:00	**U. Hilleringmann**, University of Paderborn *Deposition and Etching of Permalloy*
11:00 – 11:30	**G. A. Battiston, P. Zanella**, Istituto di Chimica e Tecnologie Inorganiche e dei Materiali Avanzati, Padua *Metal Organic Chemical Vapour Deposition at CNR – ICTIMA in Padua*
11:30 – 12:00	**P. Hudek**, Slovak Academy of Sciences, Bratislava *Submicrometer Lithography & Pattern Transfer for Magnetic Devices Fabrication*
12:00 – 12:30	**F. Schmidl**, Friedrich-Schiller-Universität Jena *Magnetic Thin Film Sensors for Non-Destructive Evaluation*
12:30 – 14:00	Lunch
14:00 – 14:30	**E. Martincic, A. Bosseboeuf**, Université Paris Sud *Activities of the PFM (Pôle Francilien Microsystèmes) on permalloy thin film deposition and magnetic devices*
14:30 – 15:00	**J. Esteve**, National Centre of Microelectronics, Barcelona *Activities at Biosensores S.L. and CNM on biosensors based on magnetic particles* [1]
15:00 – 15:30	**E. Hristoforou**, National Technical University of Athens *Miniaturised Thin Film Magnetostrictive Delay Lines for Sensor Applications*
15:30 – 18:00	Open discussions

[1] The contents of this presentation have not been published yet. The author therefore requested not to have to contribute a manuscript to these proceedings.

Contents

Preface 3

Workshop Programme 5

Preparation and Properties of Magnetic Films with Enhanced Properties for Thin Shield Layers 9

Magnetoresistive Sensors 15

High Sensitivity Magnetic Field Sensor 29

CMOS Integrated Two Axes Magnetic Field Sensors – Miniaturized Low Cost Systems With Large Temperature Range 35

DIMADS™ — Digital Magnetic Anomaly Detection System 39

Microtransformers and Inductors using Permalloy Thin Films 45

Electronics and Methods for Sensors Based on Ferromagnetic Devices 53

Cathode Sputtered Permalloy Films of High AMR Effect and Low Coercivity 57

Deposition and Etching of Permalloy 63

Metal Organic Chemical Vapour Deposition at CNR – ICTIMA in Padua 69

Submicrometer Lithography and Pattern Transfer for Magnetic Devices Fabrication 75

Magnetic Thin Film Sensors for Non-Destructive Evaluation 85

Activities of the PFM (Pôle Francilien Microsystèmes) on Permalloy Thin Films Deposition and Magnetic Devices 93

Miniaturised Thin Film Magnetostrictive Delay Lines for Sensor Applications 101

Addresses of Workshop Participants 107

Preparation and Properties of Magnetic Films with Enhanced Properties for Thin Shield Layers

J. E. Snyder[a,b], C. C. H. Lo[a], R. Chen[a,c], B. Kriegermeier[a,b], J. Leib[a,b], S. J. Lee[a], M. J. Kramer[a,b], D. C. Jiles[a,b,c], and M. T. Kief[d]

[a]Ames Laboratory,
[b] Department of Materials Science and Engineering,
[c]Department of Electrical and Computer Engineering,
Iowa State University, Ames, Iowa 50011

[d]Seagate Technology, Minneapolis, Minnesota 55435

This investigation was aimed at identifying means for improving the permeability and coercivity of Fe-S-Al thin films for use as shield layers in disk drive read heads. As a result of the need for increased data storage densities there has been a continual reduction in dimensions of these read heads. This has necessitated a decrease in thickness of the shield layers around the magnetoresistive head with an associated reduction in shielding factor. In order to counteract this we have studied means to improve the shielding characteristics of the Fe-Si-Al material through the use of alloying additions. One addition that holds promise in this respect is nitrogen. In a series of rf-sputtered soft FeSiAl(N) films, the partial pressure of nitrogen in the plasma was observed to have a profound effect on the magnetic properties, stress, and microstructure. Inclusion of 1% partial pressure (1% pp) of nitrogen caused the coercivity (H_c) to almost triple. H_c peaked for 3% pp N, then decreased steeply for N > 4% pp. Stress appears to have a major influence on the magnetic properties. Film stress correlated quite closely with H_c. The hysteresis loops suggest a stripe domain structure in which the magnetization has in-plane components which are aligned parallel, but perpendicular components which alternate up and down. Stripe domains were observed directly by magnetic force microscopy (MFM). The microstructure also changed significantly with nitrogen additions. A 1% pp N caused the originally strong (110) texture to weaken. For > 4% pp N, there was a transition from textured columnar 100 nm diameter bcc grains to a mixture of randomly-oriented, equiaxed bcc nanograins (10 nm or less) in an amorphous matrix. Transmission electron microscopy (TEM) observations appear to indicate that the grain refinement and phase separation take place by a decomposition process. Saturation magnetization also decreased with added N for > 4% pp N, indicating that one of the two phases has a lower M_s value.

Introduction

There has been considerable interest in sputtered FeSiAl(N) films as soft magnetic shield layers for disk drive read heads. Nitrogen can have a strong effect on the microstructure and magnetic properties [1], [2], yet these effects are still not well understood. In order to investigate the effect of N, a series of films was rf diode sputtered from an alloy target (85Fe-10Si-5Al wt.%) onto SiO_2/Si substrates using an Ar/N gas mixture, varying N partial pressures, and keeping total gas pressure (9.6 mTorr), forward power (1.43 W/cm^2), and film thickness (1.7 μm) constant. Magnetic properties were charac-

terized by vibrating sample magnetometry (VSM) and magnetic force microscopy (MFM). Film stress was determined from atomic force microscopy (AFM) measurements of the curvature of the film-substrate combination, and least-squares fitting to the equation of Eckertova [3]. Film structure and microstructure were determined from x-ray diffraction (XRD), transmission electron microscopy (TEM), and SEM fracture cross-sections. Film compositions were characterized by energy dispersive x-ray (EDX) analysis and parallel electron energy loss spectroscopy (PEELS).

Results

Nitrogen has a strong effect on the magnetic properties of the films (Fig. 1). 1% partial pressure (pp) N caused the coercivity (H_c) to almost triple. H_c peaked at 3% pp N, then decreased steeply for N > 4% pp. Stress appears to have a major influence on the magnetic properties. All the films showed compressive stress, the magnitude correlating closely with H_c (Fig. 1). The in-plane hysteresis loops, while very steep near the origin, all showed curved high-field portions that suggested the presence of a stripe domain structure of the type first described by Fugiwara [4], in which neighboring stripes have aligned in-plane magnetization components but their perpendicular components alternate up and down. MFM observations of the films at remanence showed stripe domains in all samples (Fig. 2), with alternating light and dark contrast showing the presence of alternating perpendicular magnetization components. Stripe width (determined from Fourier analysis) decreased with increasing N content, varying from 0.51 µm for 0% pp N to 0.25 µm for 10% pp N.

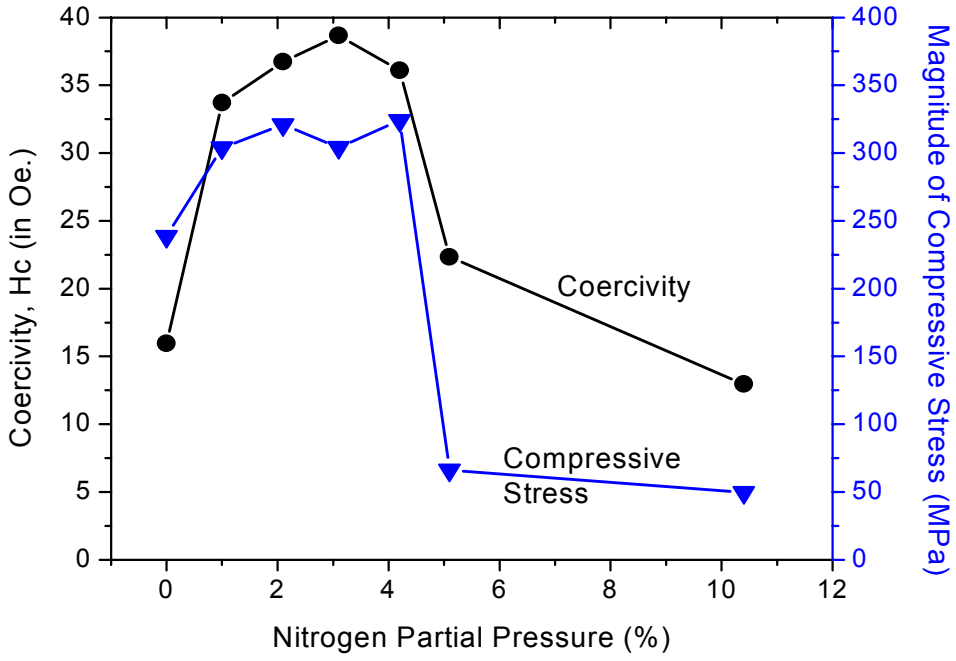

Fig. 1. In-plane coercivity (H_c) and magnitude of compressive stress as functions of N partial pressure.

The structure and microstructure also changed significantly with added N (Fig. 2). Films sputtered with 0% N showed a columnar microstructure (observed by SEM fracture cross-section), bcc crystal structure with a strong (110) texture perpendicular to the plane (from XRD and TEM), and grains approx. 100 nm in diameter (from TEM). No evidence of ordering was observed. 1% pp N caused the strong (110) texture to become very weak. The microstructure consisted of large columnar bcc grains out to 4% pp N. Between 4 and 5% pp N, there was a transition: films for 5 and 10% pp N consist of a mixture of randomly-oriented equiaxed bcc nanograins (10 nm or less diameter) in an amorphous matrix (Fig. 2). TEM observations appear to indicate that the grain refinement and phase separation take place by a decomposition process. This transition also marked a steep increase in actual N content of the films (N:Fe atomic ratio as determined by PEELS was 0.2 for 3% pp N, rising to 0.9 for 5% pp N).

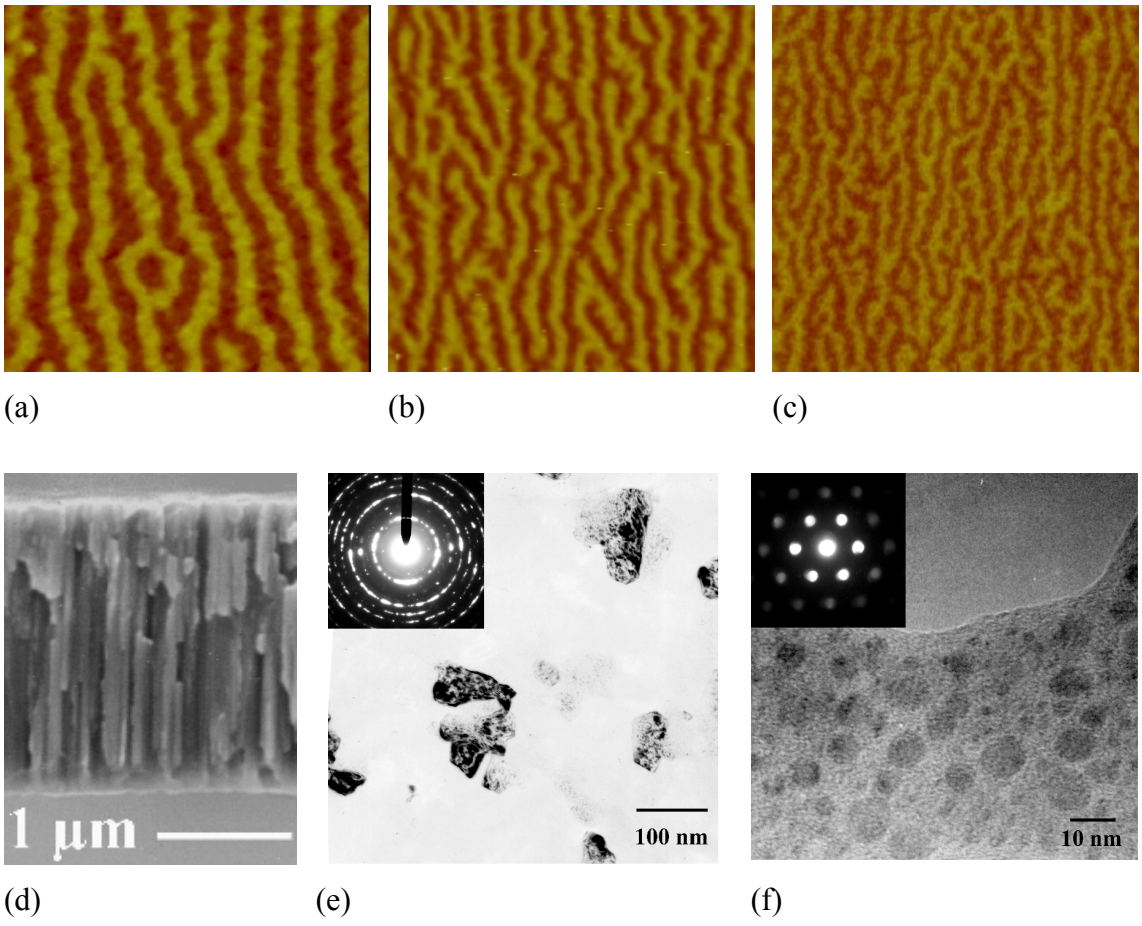

Fig. 2. Micrographs: MFM images (10 x 10 µm) of films (a) 0% pp N, (b) 3% pp N, (c) 5% pp N; (d) SEM fracture cross section of 0% pp N film, (e) Dark field TEM of 0% pp N film, (f) high resolution TEM of 5% pp N film.

Saturation magnetization (M_s) was constant from 0 out to 4% pp N, then decreased with added N (Fig. 3). By 10% pp N, it has dropped by almost 50%. This indicates that one of the two phases (bcc nanograins or amorphous phase) has a lower M_s. It contradicts the hypothesis that N first reacts with Al until it is all reacted, then reacts with Si, then goes into the Fe lattice [1]. Were this the case, one would expect M_s to first increase

with added N, as the Si and Al are “withdrawn” from the FeSiAl film, driving it towards pure Fe composition (see data in [5]).

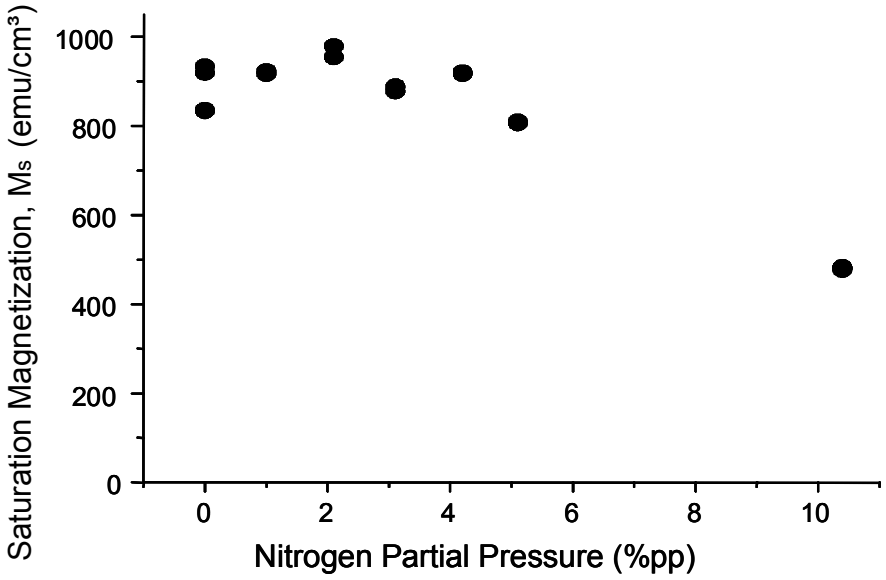

Fig. 3. Saturation magnetization (M_s) as a function of N partial pressure.

Conclusions

Nitrogen greatly affects the stress, microstructure, and magnetic properties of FeSiAl(N) sputtered films. The stress and the perpendicular texture appear to set-up perpendicular anisotropy that causes stripe domains. All the films showed isotropic in-plane compressive stress, which through the magnetomechanical effect, can cause a perpendicular magnetic anisotropy component for materials with positive magnetostriction. Compressive stress appears to adversely affect H_c. Stress magnitude and H_c variations correlate quite closely. For > 4% pp N, there was a microstructural transition to a 2-phase mixture of bcc nanograins in an amorphous matrix. Contrary to what was found in another study [2], nanograined films as thick as 1.7 μm could be produced by this r.f. diode sputtering process.

In order to optimize FeSiAl(N) films for soft magnetic shield layer applications, perpendicular anisotropy should be minimized, or films should have in-plane magnetic anisotropy, and the stripe domain structure avoided. Perpendicular anisotropy will itself adversely affect in-plane magnetic properties, and the stripe domains it causes can make reversal more difficult. Nanograined films (such as those produced near 5% pp N) should offer several significant advantages. Since the grains are much smaller than the domain sizes, there will be less pinning. There should also be much less effect of ripple (which is related to the variations in local anisotropy directions and varies with the relative sizes of grain size and spin coupling length (see e.g. [6]). Such films have a random texture and therefore no magnetocrystalline contribution to perpendicular anisotropy. However they still show enough stress-induced anisotropy to produce stripe domains, so the process would have to be optimized to decrease compressive stress or even make a small tensile stress.

Acknowledgements

This research supported by Seagate Technology, Minneapolis MN and the US Department of Energy, Office of Basic Energy Sciences. The Ames Laboratory is operated by the U.S. Department of Energy by Iowa State University under contract W-7405-ENG-82.

References

[1] Y. Chen, P. J. Ryan, J. F. Dolejsi, M. Rao, D. E. Laughlin, M. H. Kryder, F. Al-Jumaily, Z. Yang, J. Appl. Phys 84 (1998) 945.

[2] P. M. Dodd, R. Atkinson, I. W. Salter, M. S. Araghi, H. S. Gamble, J. Appl. Phys 81 (1999) 4559.

[3] L. Eckertova, Physics of Thin Films, Plenum Press, New York, 1986. p.203.

[4] N. Saito, H. Fujiwara, and Y. Sugita, J. Phys. Soc. Japan 19 (1964) 1116.

[5] R. M. Bozorth, Ferromagnetism, D. Van Nostrand Company, Inc., Princeton NJ, 1978 p. 96.

[6] H. Hoffmann, IEEE Trans. Magn. MAG-9 (1973) 17.

Magnetoresistive Sensors

H. Hauser, G. Stangl, W. Fallmann, R. Chabicovsky, K. Riedling

Institut für Industrielle Elektronik und Materialwissenschaften
TU Wien, Gusshausstrasse 27/366, A-1040 Vienna, Austria

Depending on the angle between magnetisation and current density in a thin permalloy film, the anisotropic magnetoresistive effect is utilised for high performance sensors. Both the parameters of the sputtering process and the sensor layout have to be optimised. Aiming a magnetic field resolution of some nT in a frequency range from 0 – 1 kHz, the results of Wheatstone bridge circuits are discussed.

Introduction

The magnetoresistive effect is the change of the resistivity of a material due to a magnetic field; it has been discovered by Thomson in 1856 [1]. The improvement of the technology of thin ferromagnetic films (with a thickness of 10 – 50 nm) and the utilisation of the Anisotropic Magnetoresistive (AMR) effect led to an increasing technical interest in this effect. Furthermore, a Giant Magnetoresistive (GMR) effect [2] has been discovered, which is based on the weak coupling between separate thin ferromagnetic films. The maximum resistivity change is up to 80% with the GMR effect, albeit at very high magnetic fields only.

AMR sensors feature a high sensitivity at weak magnetic fields and a small consumption of energy. Their maximum change of resistance is of the order of 3 – 4 %. These sensors can be produced in large quantities and very cost-efficiently if the processes required for their production can be handled reproducibly. Magnetoresistive sensors are used today, for example, in reading heads of magnetic data storage systems such as hard disks. They could find much wider spread applications, though, e.g., for measurements of the Earth's magnetic field, as a gradiometre, a compass, a position sensor, or for measurements of biomagnetic fields.

The sensors require thin ferromagnetic films (e.g., permalloy) with a magnetic anisotropy. There is a *hard axis* with a high requirement of magnetisation energy in one direction in the plane of the film, and, orthogonal to the hard axis in the plane of the film, an *easy axis* which indicates the magnetic preference direction. The sensitivity of the sensor depends on the width of the magnetic hysteresis, as indicated by the coercivity H_c. A second key parameter for AMR films is the relative change of the resistivity, $\Delta\rho/\rho$. This is the change of resistivity if the magnetisation vector is rotated by 90 degrees from the direction of the easy axis due to an external magnetic field.

Today, the technically most important sensors for magnetic fields are induction coils, Hall sensors, magnetoresistive and AMR sensors, fluxgates, and Superconducting Quantum Interference Devices (SQUIDs). The following Table 1 compares typical parameters of these sensors. Table 1 gives approximate values only; the maximum flux resolution depends, in general, also on the frequency. It decreases for all sensors, except

for AMR sensors, with decreasing frequency. This effect is most pronounced for the induction coils.

Sensor type:	min. B	max. B	Frequency range
Induction coils	100 fT	unlimited	0.1 mHz – 1 MHz
Hall sensors	10 nT	20 T	0 – 100 MHz
Magnetoresistive Sensors	100 pT	100 mT	0 – 100 MHz
Fluxgates	10 pT	1 mT	0 – 100 MHz
SQUIDs	5 fT	1000 nT	0 – 100 kHz

Table 1: A comparison of various magnetic sensors.

There are primary and secondary parameters of sensors: The *primary parameters* (e.g., range, band width, accuracy, resolution, linearity, hysteresis of the output signal) refer directly to the measured parameter. The *secondary parameters* (e.g., geometry, spatial resolution, working and storage temperature, chemical sensitivity, impedance, reliability, power consumption, and price) include the environment of the application and economic aspects.

Theory of the AMR sensor

The theory of the AMR sensor is based on the complex ferromagnetic processes in a very thin film. Some of the effects involved may be simplified for an easier mathematical treatment. First, the assumption is justified that the magnetisation M in a ferromagnetic material always has the magnitude of the saturation magnetisation M_S but only changes its direction. Second, the complex theory of the AMR effect (there is also an isotropic MR effect which is utilised in semiconducting layers) can be split into two simpler parts, namely, the relation between the electric resistivity and the direction of the magnetisation, and the relation between the direction of the magnetisation and an externally applied magnetic field.

Anisotropic magnetoresistive effect

The physical origin for the anisotropic magnetoresistive effect is the different shift of the energy levels of electrons with a positive and negative spin, respectively, under the influence of a magnetic field. This leads to a shift in the Fermi levels. It has not been possible yet to calculate these effects satisfactorily; the difference to experimental data is still about one order of magnitude [3]. Therefore, the most important parameters are determined experimentally.

It has been shown that the electric resistance R can be derived with a simple theory from the angle Θ between the electric current density and the magnetisation (see Fig. 1 (a)):

$$R(\Theta) = \rho_{0,n} \frac{l}{bd} + \Delta\rho \frac{l}{bd} \cos^2 \Theta = R_{0,n} + \Delta R \cos^2 \Theta \qquad (1)$$

In equation 1, $\rho_{0,n}$ and $\Delta\rho$ are material constants, l is the length of the resistive strip, b, its width, and d, its thickness. In general, l > b >> d. $R_{0,n}$ is the resistance perpendicular

to the magnetisation, and ΔR is the maximum change of resistance due to the magnetic field. For a current I in x direction, a voltage U_x results:

$$U_x = \rho_{0,n} I \frac{l}{bd} + \Delta\rho I \frac{l}{bd} \cos^2 \Theta \tag{2}$$

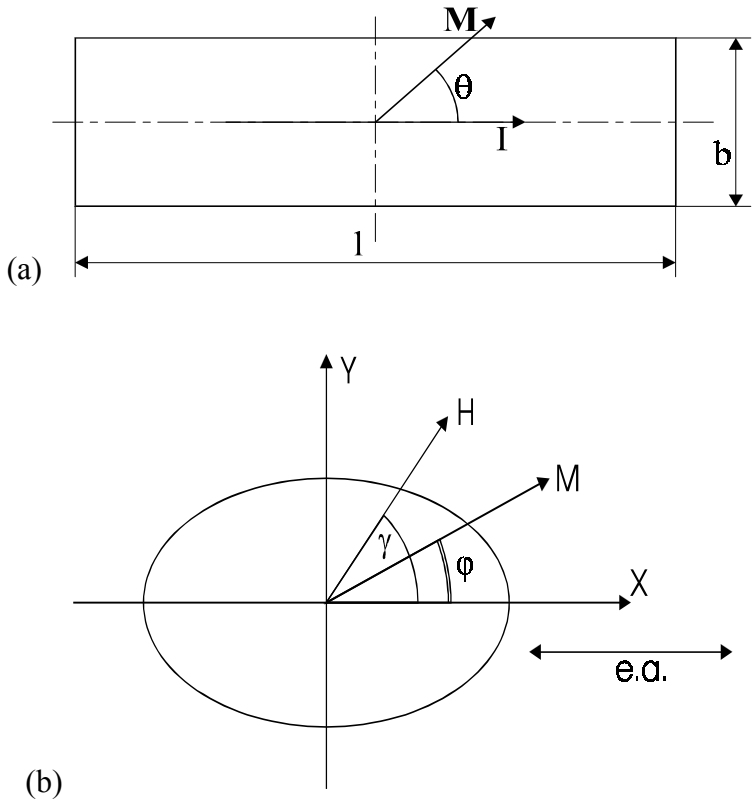

Fig. 1: (a) Geometry of a strip with magnetisation M and current direction I. (b) Geometry of an elliptically shaped thin film; the *easy axis* was assumed to be in parallel to the x axis.

It should be noted that there is also a voltage U_y perpendicular to the direction of current flow. Due to its similarity to the Hall effect, this effect is called *planar Hall effect*. It should not be mistaken for the common Hall effect, though, because its origin is totally different: In the common Hall effect, a voltage change is effected due to a magnetic field perpendicular to the film; for the planar Hall effect, the magnetic field is in the same plane as the current flow. The planar Hall effect is rarely used for practical purposes because the voltages involved are very small.

Magnetisation by an external field

The magnetisation M in the film is in a direction of minimum total energy. The most important energies involved are the energy of the external field, the anisotropy energy of the material (magnetocrystalline anisotropy energy), and the demagnetising energy (shape anisotropy energy). Most energy contributions depend on the direction. This implies that the energy required for rotating M into a given direction can be visualised by a three-dimensional energy area [4].

The spontaneous magnetisation M_S will lie in a direction with a minimum energy. The magnetocrystalline anisotropy energy area of iron has six easy axes (i.e., energy minima) in the direction of the edges of the crystal cube. Nickel has eight easy axes in the volume diagonals of the unit cell. In addition, the total energy depends on mechanical stress [5] and on the geometry. The energy planes of permalloy (Ni:Fe 81:19) are more complicated. There are 16 easy axes. However, the magnetostriction constant is close to zero in permalloy, i.e., the magnetisation has no effect on the crystal lattice dimensions.

With the total anisotropy field $H_0 = 2K/\mu_0 M_S$ (with the anisotropy constant K), the angle φ between M and the easy axis (x direction) results for $H_x = 0$ as:

$$\sin\varphi = \frac{H_y}{H_0} \tag{3}$$

for $-1 < H_y/H_0 < 1$. Outside of this range, $\sin\varphi = \mathrm{sign}\left(H_y / H_0\right)$.

Magnetoresistive sensors

The calculation of the angle Θ between M and the easy axis and the dependence of the electric resistance on the direction of M will be combined now to evaluate the sensor. We introduce the new resistances $R_{0,p}$ and R_0:

$$R_{0,p} = R_{0,n} - \Delta R \tag{4}$$

$$R_0 = R_{0,n} + \frac{\Delta R}{2} = \frac{R_{0,p} + R_{0,n}}{2} \tag{5}$$

R_0 is therefore the average resistance. We can calculate the characteristics of a simple AMR sensor using these new parameters. Figure 2 (a) depicts the dependence of the resistance on the angle between current flow and magnetisation. Equations (2) and (4) result in the resistance $R(\Theta)$:

$$R(\Theta) = R_{0,p} - \Delta R \sin^2\Theta \tag{6}$$

Equation (3) permits to calculate the resistance in dependence of the field H_y which is to be measured. Figure 2 (b) illustrates this dependence. For real measurements, the magnetisation M turns completely into the hard axis for very strong fields only. Therefore, there is a smooth transition into the saturation resistance:

$$R\left(H_y\right) = R_{0,p} - \Delta R\left(\frac{H_y}{H_0}\right)^2 \tag{7}$$

for $|H_y| \le H_0$ and

$$R\left(H_y\right) = R_{0,n} \tag{8}$$

for $|H_y| > H_0$. The resistance exhibits a strongly non-linear dependence on the external field. Furthermore, the sensitivity $\mathrm{d}R/\mathrm{d}H_y$ is very small in the proximity of the origin (and disappears entirely for $H_y = 0$). A further disadvantage of this setup is that the sign of H_y can not be determined since R is a function of H_y^2.

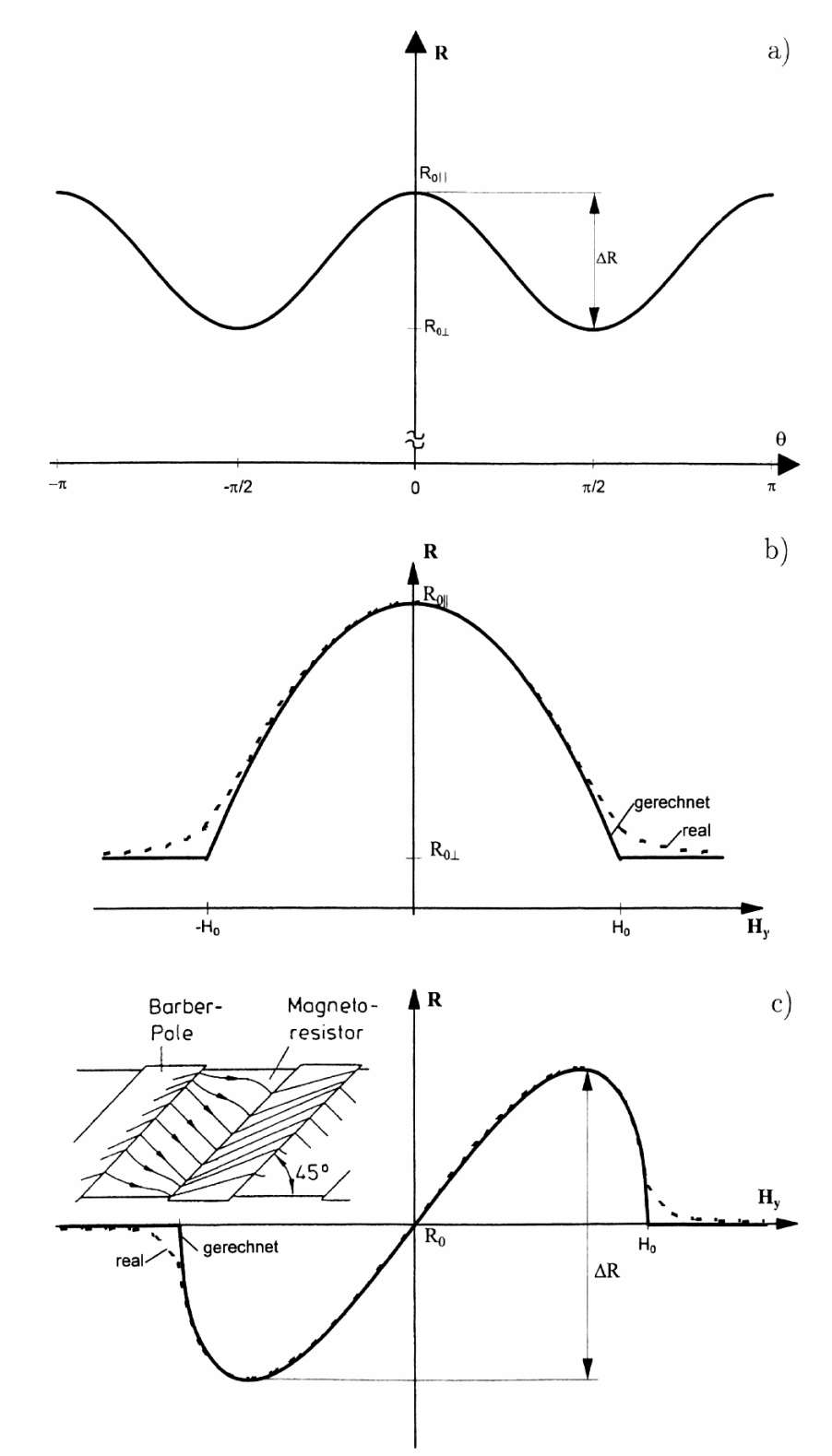

Fig. 2: (a) Resistance in x direction as a function of the angle Θ between the current I and the magnetisation M. (b) Resistance of a thin ferromagnetic film as a function of the transversal field H_y. (c) Current flow in a barber pole structure, and resistance R of a thin ferromagnetic film with a barber pole structure as a function of the transversal field H_y.

Barber pole

In order to alleviate these disadvantages, barber pole structures[1] have been introduced. Barber pole structures consist of a series of strips of high electrical conductivity that force the current flow into an angle of 45° with respect to the *x* axis, and therefore to the easy axis. Figure 2 (c) shows that the current paths are distorted at the edges of the barber poles. An optimum layout of width and distance of the barber poles is therefore crucial [7]. The well-conducting strips reduce the total resistance; they also reduce the active part of the surface where resistance changes contribute to the sensor signal.

Mathematically, barber poles are represented by introducing an additional angle ψ = 45°, which represents the angle between the easy axis and the current. The angle Θ is in this case:

$$\Theta = \varphi - \psi \tag{9}$$

The characteristics of a barber-pole AMR sensor result therefore as:

$$R(H_y) = R_0 + \Delta R \frac{H_y}{H_0} \sqrt{1 - \left(\frac{H_y}{H_0}\right)^2} \tag{10}$$

A graphic representation of the characteristics of an AMR sensor with barber poles is shown in Fig. 2 (c). For $H_y < H_0/2$, it is fairly linear with a non-linearity of less than 5%. This behaviour is only valid if the spontaneous magnetisation without an external field is in the positive *x* direction. The change of resistance changes its sign if the spontaneous magnetisation is flipped to the negative *x* direction. Flipping the spontaneous magnetisation can be utilised for determining the value of R_0 accurately as the arithmetic mean value of the two resistance values before and after flipping.

In order to convert the resistance changes into a voltage without a dc component, the sensor is realised as a Wheatstone bridge with four individual resistors. This approach demonstrates one more advantage of barber pole structures: By using barber poles under 45° and 135°, respectively, resistors with a positive and a negative ΔR in the linear range can be realised. In order to obtain a maximum output voltage, two diagonally opposite resistors have barber poles under 45°, and the other two, under 135° (see Fig. 3). This setup also compensates for a temperature dependence of the resistors.

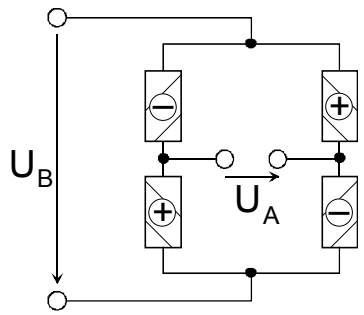

Fig. 3: Wheatstone bridge with four magnetoresistive devices. "+" indicates barber poles under 45°, and "–", under 135°.

[1] Named after the sign of a barber shop which looks very similar.

Sensitivity and measurement range

The output voltage of a Wheatstone bridge can be described by:

$$U_A = U_B \frac{\Delta R}{R_0} \frac{H_y}{H_0} \sqrt{1 - \left(\frac{H_y}{H_0}\right)^2} \tag{11}$$

The sensitivity[2] of the entire sensor results in:

$$S_0 = \frac{\Delta R}{R_0} \frac{1}{H_0} \tag{12}$$

The sensitivity can thus be increased by using materials with a high AMR effect and with a low characteristic field H_0. The sensors exhibit linear behaviour with an error of less than 5% within a range of $-H_0/2$ to $H_0/2$.

It is possible, though, to increase the measurement range arbitrarily by applying a compensating magnetic field (i.e., by a null-compensation of the bridge). Since the sensor always operates at zero field, its non-linearity has no effect. The maximum resolution depends in this case on the stability of the magnetic film.

Furthermore, the layout of the magnetoresistive elements forming a Wheatstone bridge has to be optimised. Achieving a homogeneous and small demagnetising field, an elliptical shape of the AMR array is proposed [8]. By applying a flipping field H_F , the direction of M_s in the AMR element can be inverted — this is very useful to overcome offset problems. The schematic evaluation arrangement is shown in Fig. 4. Using a compensation coil at the output of the integrator, the sensor can be operated in zero magnetic field. The linear output response (voltage V_0 versus applied field H_a) is proportional (resistor R) to the compensation coil current. Both flipping and compensation coils are thin film conductors in a meanderic form; they are also shown schematically in Fig. 4.

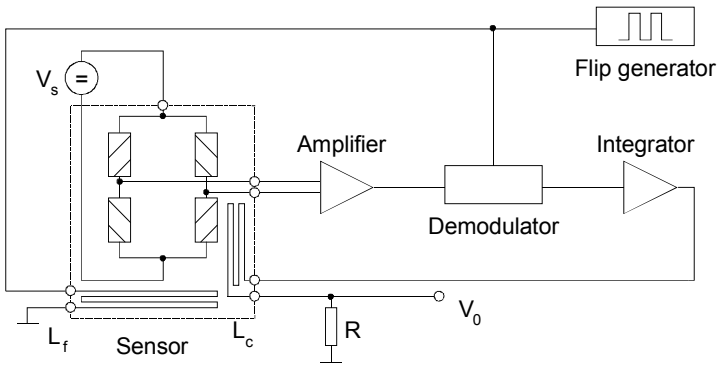

Fig. 4: Electronic evaluation circuit with flip- (L_f) and compensation (L_c) coils

[2] According to [3] there are two definitions of the sensitivity of an AMR sensor in a bridge arrangement: 1. $S_0 = \mathrm{d}U_A/\mathrm{d}H_y/U_B$, and 2. $S_U = U_{max} \times \mathrm{d}U_A/\mathrm{d}H_y/U_B$. The advantage of the second definition is that it also takes into account the maximum energy dissipation ($P_{max} = U_{B,max}^2/R$) in the sensor. The supply voltage can not be made arbitrarily high. For comparison of the sensitivities of various sensors, we use the first definition in this paper, as is done through most of the literature.

Sensor layout and film technology

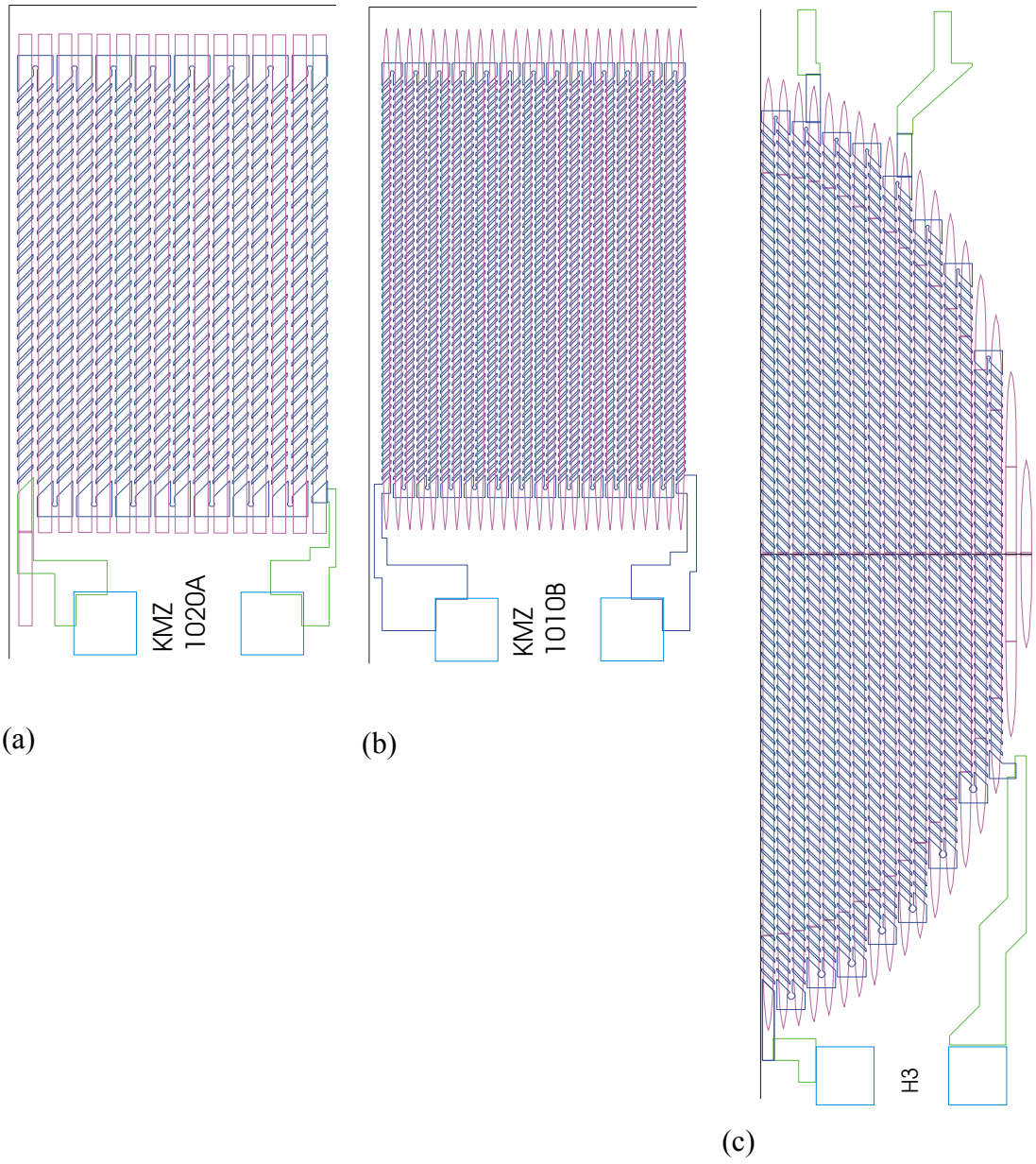

Fig. 5: Layout of KMZ 1020A (a) one of four bridge resistors, active area of the permalloy strips: 470 × 770 µm^2, KMZ 1010B (b), and H3 (c) half bridge; long axis length: 1760 µm; the AMR films are covered with barber poles (/); two bonding pads (□) belong to one resistor.

Three layouts with rectangular permalloy strips of different width and separation distance have been investigated (see Fig. 5):

a) KMZ1020A: Width 20 µm (tapering off at both ends), distance 10 µm, R_0 = 1.70 kΩ, S_0 = 3.31 (mV/V)/(kA/m), H_F = 400 A/m.

b) KMZ1010B: Width 10 µm, distance 10 µm, R_0 = 5.63 kΩ, S_0 = 1.36 (mV/V)/(kA/m), H_F = 2000 A/m.

c) H3: Width 10 µm (tapering off at the ends), distance 10 µm, R_0 = 5.63 kΩ, S_0 = 1.36 (mV/V)/(kA/m), H_F = 2000 A/m, overall elliptical shape. Ellipse axes are a = 1760 µm and b = 1000 µm.

The total sensor area was 1 × 2 mm^2 for each layout. The AMR film was characterised by $\Delta\rho/\rho$ = 1.52% and H_0 = 600 A/m.

The magnetoresistive films have been deposited by DC cathode sputtering using a triode set-up. This triode sputtering system has some advantages compared to a simple diode set-up, because the plasma is sustained independently of the target voltage, and it can be easily concentrated in the centre of the chamber by a magnetic field generated through an external coil. The arrangement is schematically shown in Fig. 6. A target consisting of 81% Ni and 19% Fe (magnetostriction free) has been used. It is connected to a negative potential of V_T = – 800 V. A negative substrate bias voltage of V_B = – 60 V and an anode voltage of V_A = +50 V are applied. The currents indicated in Fig. 6 are I_A = 3.5 A, I_C = 45 A and I_{COIL} = 2 – 6 A. The glass chamber is evacuated by a turbomolecular pump to a residual gas pressure of about 10^{-7} mbar and the argon pressure is adjusted to 2×10^{-3} mbar. During film deposition the substrates are heated and exposed to a constant magnetic field. It is important that the direction of the magnetic field is parallel to the substrate plane. The substrates are taken out of the vacuum chamber as soon as they are completely cooled down to room temperature.

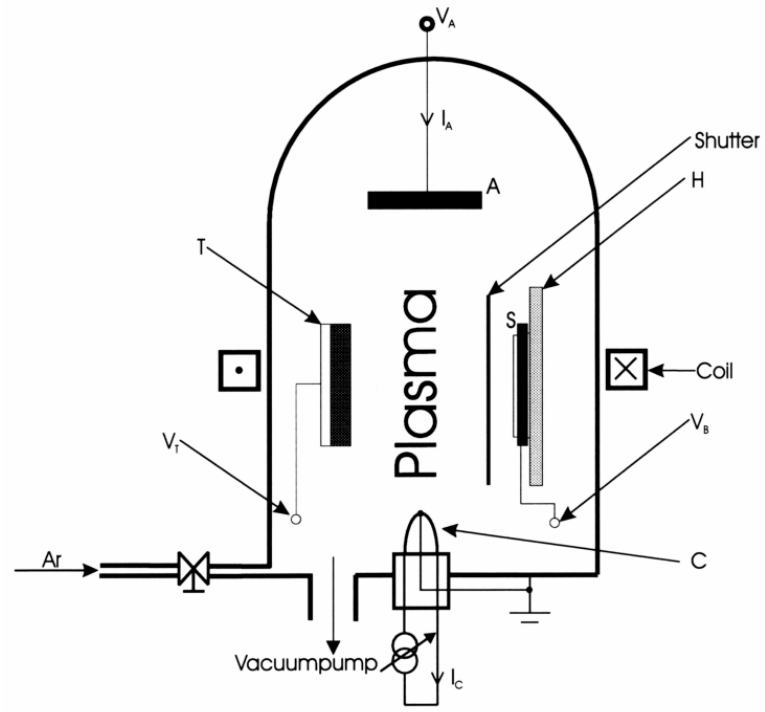

Fig. 6: DC sputtering set-up (triode system), A: anode, T: target, C: hot filament cathode, S: substrate, H: heater.

The following main parameters can influence the properties of sputtered magnetoresistive films and have therefore been varied: Method of substrate passivation, temperatures of target (T_T) and substrate (T_S), distance $a_{T–S}$ between target and substrate, and the film thickness d. Furthermore, the resistivity of the film depends also on the strength of the applied magnetic field, the direction of the field, and the film deposition rate. Film thickness measurements have been carried out with an Inficon quartz crystal film thickness monitor. The resistance has been measured by a four-wire method.

The substrate material is silicon (3" and 4" wafer with (100) orientation). The wafer surface has been passivated by a 0.5 – 0.8 µm insulation layer, consisting either of a thermal silicon dioxide or a low stress silicon nitride deposited by a PECVD process at low temperature. Sputtered silicon dioxide has also been used in some experiments.

Measurements and results

The results indicate an increasing AMR effect Δρ/ρ with decreasing ρ. Both T_S and T_T have a positive influence on the AMR effect. The target–substrate distance has been varied between 36 mm and 60 mm, yielding a change in the AMR effect by ± 0.2%. The optimum $a_{T–S}$ is in the range between 38mm and 42mm. The optimum film thickness d was about 50 nm. With these parameters we achieved an AMR effect of Δρ/ρ = 3.93% [9]. Reducing d to 20 nm, which has often been reported to be the optimum for permalloy, e.g. [10], yields a decrease of the AMR effect by 0.5%. The magnetic behaviour depends strongly on the thickness d. This is demonstrated by magnetisation curves measured by the magneto-optical Kerr effect. Reducing d from 50 nm to 20 nm, both the easy axis coercivity and the hard axis coercivity increase [6].

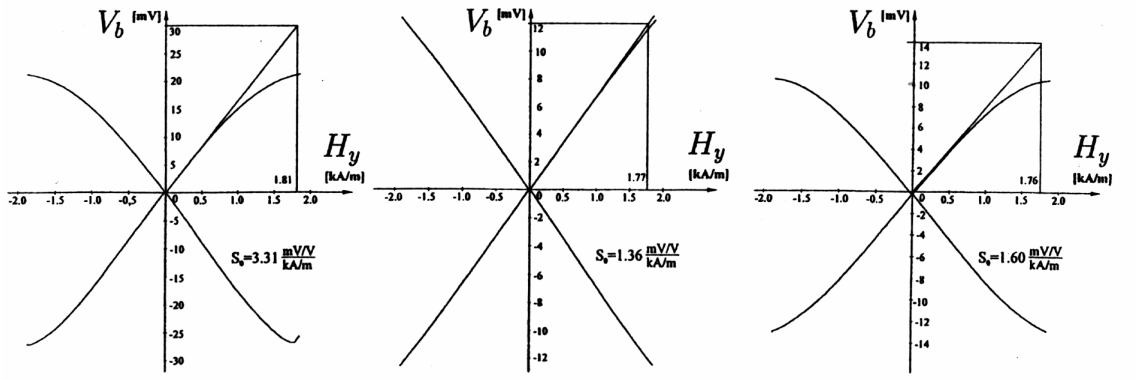

(a) (b) (c)

Fig. 7: Sensitivity of KMZ 1020A (a), KMZ 1010B (b), and H3 (c); the output voltage Vb of the half bridge versus the applied field H_y could be about 8 times greater using a full bridge with an elliptical resistor layout rotated by 90° compared to Fig. 5 (c).

Depending both on the demagnetising factor of the single strips and the total area, the sensitivity of KMZ1020A is about 2.5 times of that of the KMZ1010B. The layout H3 was designed as a half bridge and therefore its sensitivity is half of KMZ1020A. The

sensor characteristic of both magnetic states are shown in Fig. 7. Rotating the elliptical shape by 90° (in order to align the applied field perpendicular to the permalloy strips but parallel to the long axis of the ellipse) results in a sensitivity increase by $(N_b/N_a)^2$, where N_a is the demagnetising factor in the long axis direction and N_b is the demagnetising factor in the short axis direction of the ellipse. Furthermore, the signal/noise ratio is improved by achieving more homogeneous fields as compared to the KMZ layouts, which is shown in Fig. 8.

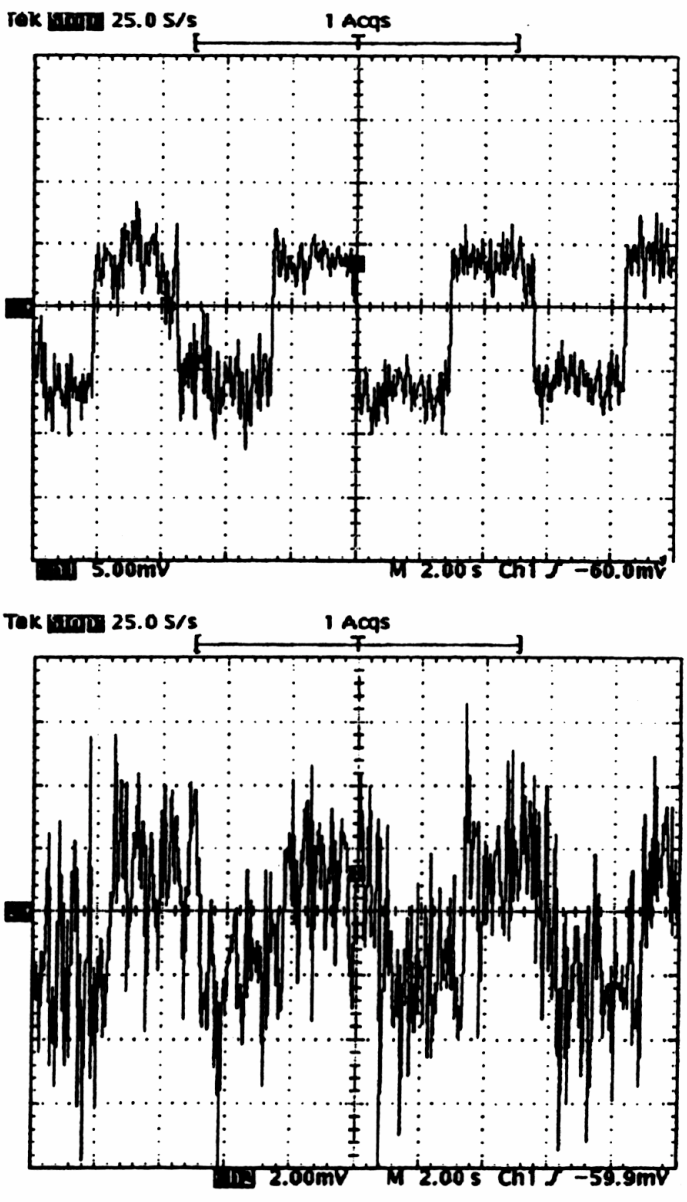

Fig. 8: Output voltage V_b versus time (2 s/div.) of the sensors H3 (5 mV/div., above) and KMZ 1010B (2 mV/div., below).

Conclusions

For a high sensitivity, the hard axis coercivity should be near zero. This is demonstrated by our recent results which show almost ideal Stoner-Wohlfahrth rotation of the spontaneous magnetisation ($H_{c;\,e:a}$ = 162 A/m, $H_{c;\,h:a} \approx 0$). Providing a high $\Delta\rho/\rho$ = 3.43%, this sample is considered to be an optimum AMR sensor material [9] (the samples of maximum $\Delta\rho/\rho$ up to 3.93% have a larger hard axis coercivity of about 20 A/m).

Using furthermore a Wheatstone bridge arrangement of elliptical shape with barber pole-structured magnetoresistors (see Fig. 5, layout H3, rotated by 90°, which means that the permalloy strips are orientated along the short axis of the ellipse) gives a sensitivity of 0.5 µV/nT at a supply voltage of 10V. The bandwidth depends on the flip frequency; in the case of a long flipping period, the bandwidth could be in the MHz range.

With these sensors it is possible to detect the distortion of the earth's magnetic field — caused by ferromagnetic objects which have to be located — with a gradiometer arrangement. Various industrial and automotive electronics applications can be considered because of the low production cost.

Acknowledgements

The authors are grateful to Prof. W. Fallmann and to Prof. G. Fasching for making these investigations possible, and to P. Aigner, R. Kloibhofer, and W. Krenn for technical assistance. Financial support was provided by the company Dipl.-Ing. Hans Schiebel Elektronische Geräte GmbH and by the Forschungsförderungsfonds für die Gewerbliche Wirtschaft (FFF) under grant no. 3/9893.

References

[1] Thomson, W.: Proc. R. Soc. London A 8 (1857), 546 – 550.

[2] Baibich, M. N. et al.: Phys. Rev. Lett. 61 (1988), 2472.

[3] Dibbern, U.: Magnetoresistive Sensors; in: G. opel, W., Hesse, J. und Zemel J. N. (ed.): Sensors, Vol. 5, Magnetic Sensors (Vol. Editors.: Boll, R. und Overshott, K. J.), 342 – 379. Weinheim: VCH 1989.

[4] Fasching, G. M.: Werkstoffe für die Elektrotechnik. 3. Auflage. Wien – New York: Springer 1994.

[5] Hauser, H. and Fulmek, P.: The Effect of Mechanical Stress on the Magnetization Curves of Ni- and FeSi-Single Crystals at Strong Fields. IEEE Trans. Magn. 28 (1992), 1815 – 1825.

[6] Fulmek, P. and Hauser, H.: Simulation of the Magnetization Process in Anisotropic Ferromagnetic Materials by Energy Areas. Elsevier Studies in Applied Electromagnetics in Materials, Vol. 5 (1993), 327 – 330.

[7] Feng, J. S. Y., Romankiw, L. T. and Thompson, D. A.: Magnetic self-bias in the barber pole MR structure. IEEE Trans. Magn. 13 (1977) S. 1466 bis 1468.

[8] Hauser, H.: Magnetfeldsensor II. Austrian Pat. Appl. No. 1928/96 (1996).

[9] Aigner, P., Stangl, G. and Hauser, H.: Cathode Sputtered Permalloy Films of High Anisotropic Magnetoresistive Effect. J. Phys. IV 8 (1998) 461 – 464.

[10] Song, Y. J. and Joo, S. K.: Magnetoresistance and magnetic anisotropy of permalloy based multilayers. IEEE Trans. Magn. 32 (1996), 5 – 8.

High Sensitivity Magnetic Field Sensor

G. Vértesy, A. Gasparics, J. Szöllösy

Hungarian Academy of Sciences, Research Institute for Technical Physics and Materials Science, H-1525 Budapest, P.O.B. 49, Hungary

A high sensitivity sensor has been developed recently, suitable for measuring DC and/or middle frequency AC magnetic field. The device has a sensitivity better than 100 pT, it operates in a wide temperature range, it is simple and cheap. Good stability and linearity, and low crossfield effect of the sensor have been measured. Due to its construction, the sensor is very suitable for miniaturisation. It may be realised using thin permalloy films, which is expected to add some more advantages, without sacrificing the good properties of the conventional setup.

Introduction

Magnetic field sensors play an important and continuously increasing role in many fields of science and of modern technique. Fluxgate type sensors are solid-state devices for measuring the absolute strength of a surrounding magnetic field or the difference in the field strength between two different points within a magnetic field. Their measuring range and their resolution are just within the gap between inexpensive sensors such as the magnetoresisitive or Hall type sensors and very expensive magnetometers based on quantum effects such as SQIUDs and others. In the present work a new type of magnetic field sensor, which belongs to the family of fluxgate sensors, is shown.

Fluxset sensor

A magnetic field sensor (Fluxset) has been developed recently [1] for measuring DC and AC (up to 200 kHz frequency) low level magnetic fields with high accuracy. Its principle of operation is close to the pulse-position type fluxgate magnetometers [2]. The particular advantage of these magnetometers is an output signal that can be simply converted into a binary signal. The measurement of a small magnetic field is reduced to a high accuracy time measurement through the displacement of the magnetization curve produced by the field. The probes are suitable for axial measurement of the magnetic field. The transverse sensitivity is negligible. The device has a small size, it is versatile, inexpensive and sufficiently robust to meet the demands of the industry.

The probe of the sensor (the measuring head itself) is made of two solenoids wound on each other. The inner and outer solenoids are called driving and pick-up solenoids, respectively. An elliptically shaped driving coil was applied in order to decrease the air gap between the core and the coil. The pick-up coil is located outside of the driving coil. The geometry of the probe is shown in Fig. 1.

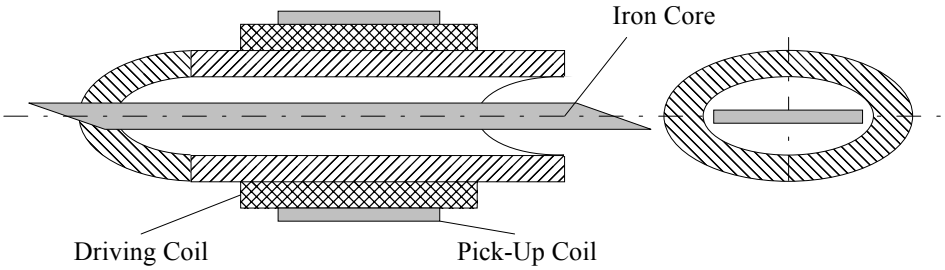

Fig. 1: The geometry of the Fluxset sensor.

The sensing element of the probe is an amorphous alloy ribbon with high initial permeability and low saturation. This core is periodically saturated by a triangle-shaped magnetic field produced by the current in the driving coil (see Fig. 2). The signal of the pick-up coil (shown also in Fig. 2) is transformed into pulses, the edges of which control the counting of a clock. Without an external field the time intervals between the pulses are equal. In an external field the magnetization cycle of the core is shifted, and the time intervals between pulses, corresponding to the parallel and anti-parallel saturation, will be no longer symmetrical. Any distortion in the local magnetic field caused by the soft magnetic core is eliminated by the symmetry of its hysteresis loop.

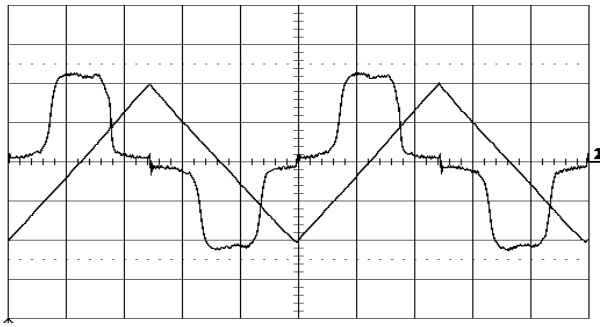

Fig. 2: Oscilloscope plot of the current of driving coil (triangle) and the voltage induced in the pick-up coil with zero external field.

For the ideal operation of the device, the material of the sensing element was optimised. A 0.6 mm wide, 20 μm thick amorphous alloy ribbon core with almost zero magnetostriction was prepared by the melt spinning method. Surface polishing and heat treatment of the ribbon were performed. This process resulted a significant improvement both in the sensitivity and in the signal/noise ratio [3].

The size of the probe core has a large effect on the sensitivity of the device. Three different numerical models based on electromagnetic field calculation (a 3D FEM model, an axisymmetric analytical model, and an integral equation model [4]) were investigated, and the results of these simulations were tested by the comparison of the calculated relative sensitivities with the measured ones [5]. The results of the calculations agreed well with the results of experiments, and a large influence of the sensor core on the sensitivity was shown. By increasing the length of the core, the sensitivity can be significantly improved. In the high sensitivity version of the sensor 40 mm long cores were applied, versus 5 mm long cores in the high frequency version of the device.

High sensitivity version

Based on the above considerations, the Fluxset sensor was developed in two different (high sensitivity and high frequency) versions. The high sensitivity version operates at DC or in low frequency range (below 100 Hz); the size of the probe is relatively large (20 – 40 mm). The linearity is better than 1%, the calibration is 0.12 mV/1 nT. The low field stability and the large sensitivity of the device were proved by observatory measurements [1].

The low frequency and high sensitivity version of the sensor were tested by the detection of the generated magnetic field in natural (unshielded) environment. Three different arrangements were investigated in order to determine the noise limited sensitivity of the sensor. The noise signal of the whole measurement system (*System noise*) was recorded when the sensor had no core material. After that, the core was inserted into the probe and the noise of the external magnetic field together with the system noise was detected (*Measured noise*). An additional magnetic field with 1 nT amplitude at 2 Hz was applied in order to calibrate the output signal of the measurement system (*Measured field*). The results of these measurements can be seen in Fig. 3. It can be well observed that the source of the noise arises mainly from the noisy magnetic environment. It means that the sensor has higher sensitivity than the geophysical applications need. The sensitivity of the sensor was determined by a spectral analysis of the detected signals. The system has approximately 20 Hz bandwidth, so this frequency range was investigated. The amplitude spectra (calculated from 500 points) can be seen in Fig. 4. The calculated average levels of the noise and its 2 Hz frequency component together with the equivalent magnetic field value are summarised in Table 1.

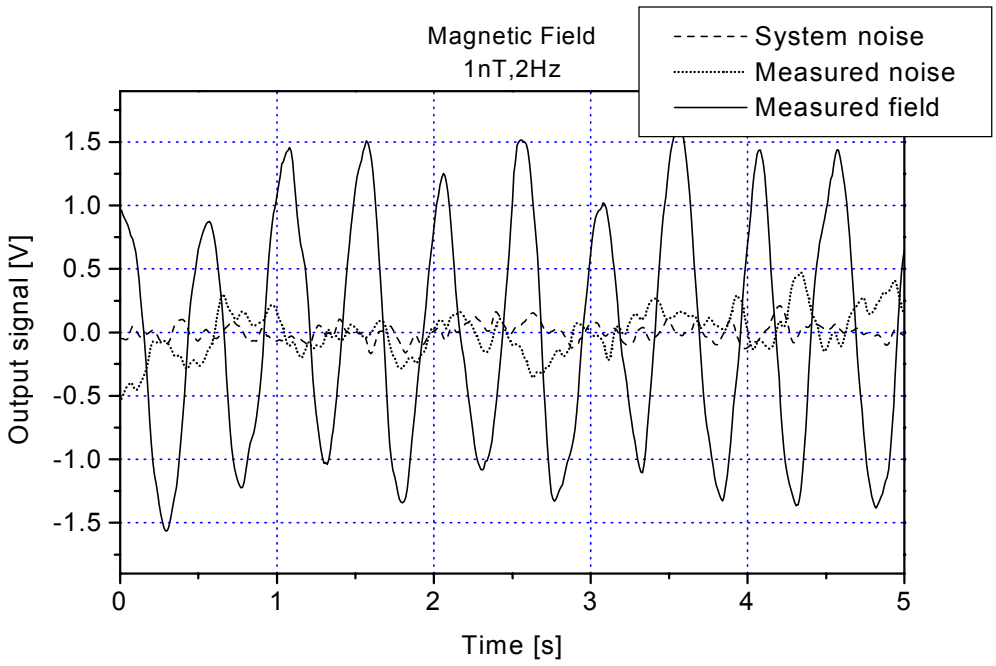

Fig. 3: The time dependent output signal of Fluxset sensor. Without core (System noise), with core (Measured noise) and in the presence of 1 nT amplitude ac magnetic field (Measured field).

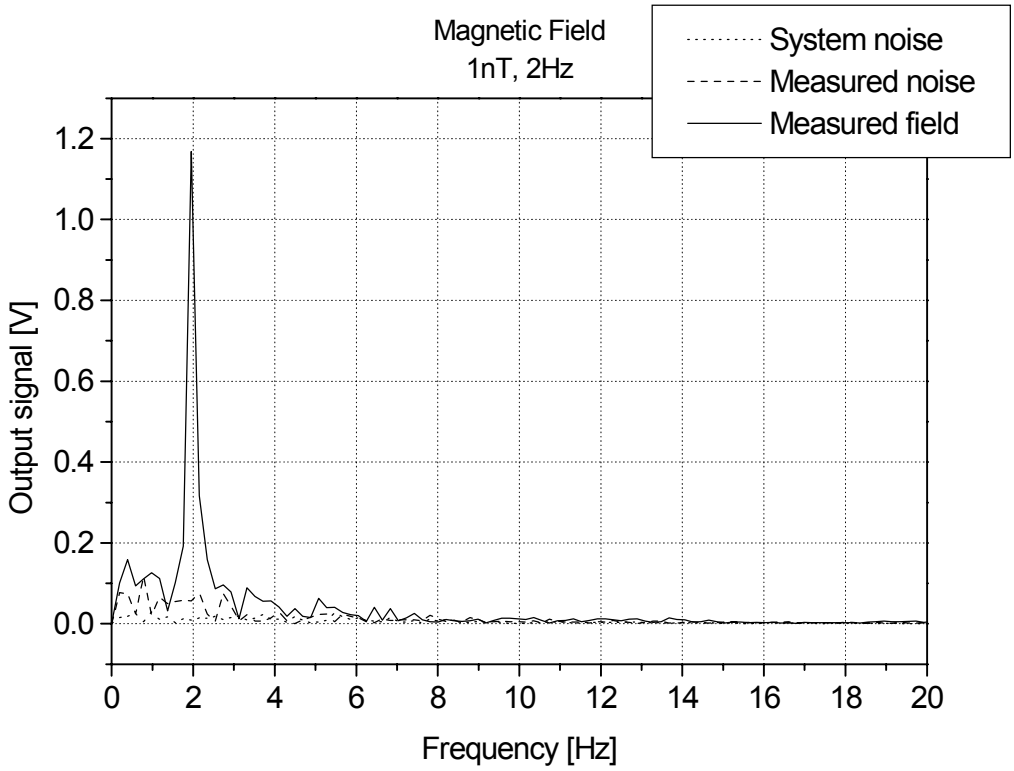

Fig. 4: The amplitude spectra of the detected signals.

The results show that the noise limited sensitivity of the measuring system, which means, how small a signal can be separated from the noise, is in the range of 10 – 50 pT. (The measured magnetic noise of the environment is two or three times higher: 50 – 150 pT.) The obtainable level of the sensitivity depends obviously on the bandwidth of the measurement system: the smaller the bandwidth is, the larger the reachable sensitivity. If the bandwidth was 20 Hz, 56 pT resolution was detected. By decreasing the bandwidth down to 1 – 2 Hz, 10 pT resolution can be achieved. (7.6 pT at 2 Hz; see Table 1.) In general, it can be concluded that Fluxset sensor has about 100 pT sensitivity, which can be higher or lower in accordance with its application.

Measured signal:	Determined [V]	Calibrated [pT]	Determined at 2Hz [V]	Calibrated at 2Hz [pT]
System Noise	0.06554	56.1	0.0089	7.592
Measured noise	0.18094	154.9	0.0564	48.300
Measured field	1.16832	1000	1.1683	1000

Table 1: The calculated average levels of the noise and its 2 Hz frequency component together with the equivalent magnetic field values.

The temperature dependence of the output signal of the probe (the measuring head only) was measured, keeping the probe in fixed position in the laboratory, without magnetic shielding. The temperature of the probe was modified from –196 °C till 200 °C, and the output signal was measured. the noise was also measured, similarly to the measurement shown in Fig. 4, as a function of the temperature, at three temperature values (-196 °C, -97 °C and +20 °C), and the amplitude spectra were calculated. No temperature dependence was found.

High frequency version

This version was developed mainly for the application in eddy current testing. The frequency range of the sensor was extended up to 200 kHz driving frequency, which makes it possible to measure ac magnetic fields of up to a frequency of 100 kHz. The size of the probe is small (5 mm). The sensitivity is not so high as in the case of the other version (10 – 50 nT). The main advantage of this version is the high spatial resolution. The behaviour of the sensor was tested in an inhomogeneous magnetic field environment, the spatial resolution of the sensor was determined by a bobbin coil arrangement at 1 and 10 kHz. The two exciting bobbin coils generate the magnetic field in opposite directions relative to each other. The results of this test and the calculated magnetic field of the exciting coils can be seen in Fig. 5. The spatial resolution of the sensor has been found to be several tenths of a millimetre (significantly less than the length of the probe).

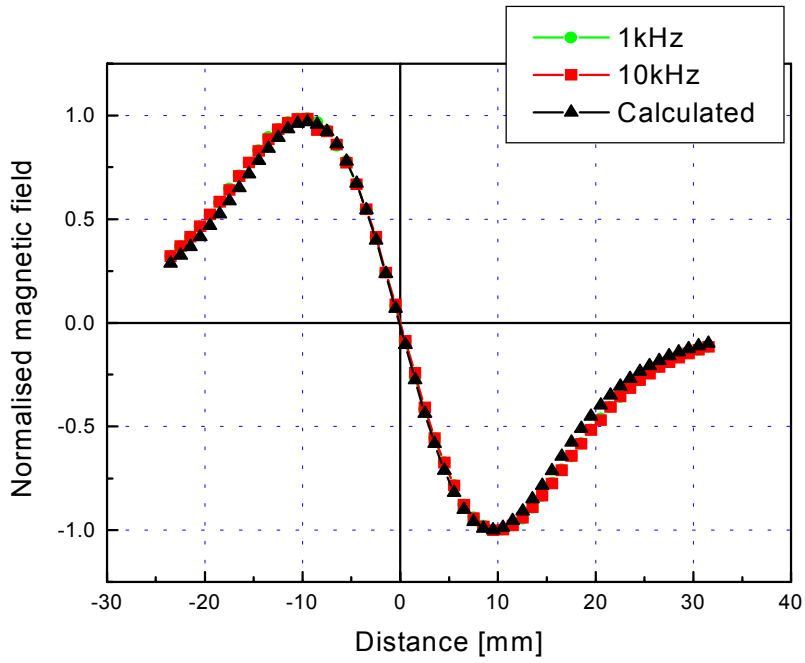

Fig. 5: Results of the spatial resolution test of the Fluxset sensor for two measuring frequencies, compared with the calculated values.

Application possibilities

This sensor is ideal for geophysical, geological applications and in detecting of electromagnetic smog. In differential mode of operation this device is suitable for the measurement of stray and residual fields, which makes it possible to detect the presence of different ferromagnetic impurities in the non-ferromagnetic materials. By the application of a sensor matrix the magnetic image of different objects can be taken. Because of the negligible transverse sensitivity, 3D magnetometers can be built using Fluxset sensors. The advantageous properties of the high frequency version of the sensor (relatively large sensitivity, relatively wide frequency range, small size, good spatial resolution, together with the simple construction) make this device ideal in non-destructive material evaluation, mainly in eddy current testing.

Conclusions

The results of measurements performed on Fluxset sensors showed that this type of sensor reaches the parameters usual for low-noise and long term stable magnetometers based on the conventional second-harmonic principle of fluxgate magnetometers. In certain fields (simple construction, wide temperature range of operation, higher frequency limit, price) it can be better than conventional fluxgates.

The simple construction of the sensor makes possible its miniaturisation, using a thin permalloy film as a core material, and integrated coils instead of windings. This development is expected to add some more advantages, without sacrificing the good properties of the conventional setup. The sensor could be mounted on a chip together with the integrated electronic circuit.

Acknowledgements

The work was supported by the Hungarian Scientific Research Fund through grants T-023559 and F-030579.

References

[1] G. Vértesy, A. Gasparics, J. Szöllösy, Sensors and Actuators A, in press

[2] P. Ripka, Review of fluxgate sensors, Sensors and Actuators A, 33 (1992) 129

[3] G. Vértesy, A. Gasparics, Z. Vértesy, J. Magn. Magn. Mater., 196-197 (1999) 333

[4] D. Ioan, M. Rebican, G. Ciuprina, P. Leonard, Studies in Applied Electromagnetics and Mechanics 14, Electromagnetic Nondestructive Evaluation (II), Eds.: R. Albanese et al, IOS Press, Amsterdam, 1998, p.152 and p. 160

[5] A. Gasparics, G. Vértesy, D. Ioan, Proc. 5th Japan-Hungary Joint Seminar on Applied Electromagnetics in Materials and Computational Technology, Budapest, Hungary, September 24-26, 1998, p. 117

CMOS Integrated Two Axes Magnetic Field Sensors – Miniaturized Low Cost Systems With Large Temperature Range

H. Grüger, R. Gottfried-Gottfried

Fraunhofer Institute for Microelectronic Circuits and Systems IMS Dresden
Grenzstrasse 28, D-01109 Dresden, Germany

Fluxgate magnetic field sensors offer a wide range of applications in the µT range and below. The thin film fabrication of the solenoids in the metallisation layers and the core in the intermetal dielectrics of a CMOS process has been successfully developed in recent years [1], [2]. These monolithic integrated fluxgate magnetic field sensors offer interesting properties in a low cost market segment.

Introduction

For applications like electronic compasses or the detection of the earth magnetic field and its variations (e.g. caused by vehicle traffic) measurements with a resolution of 0.1 to 0.01 µT are required. Fluxgate magnetic field sensors offer this resolution without use of superconductivity. The principle of the fluxgate can be described as follows (Fig. 1) [3]:

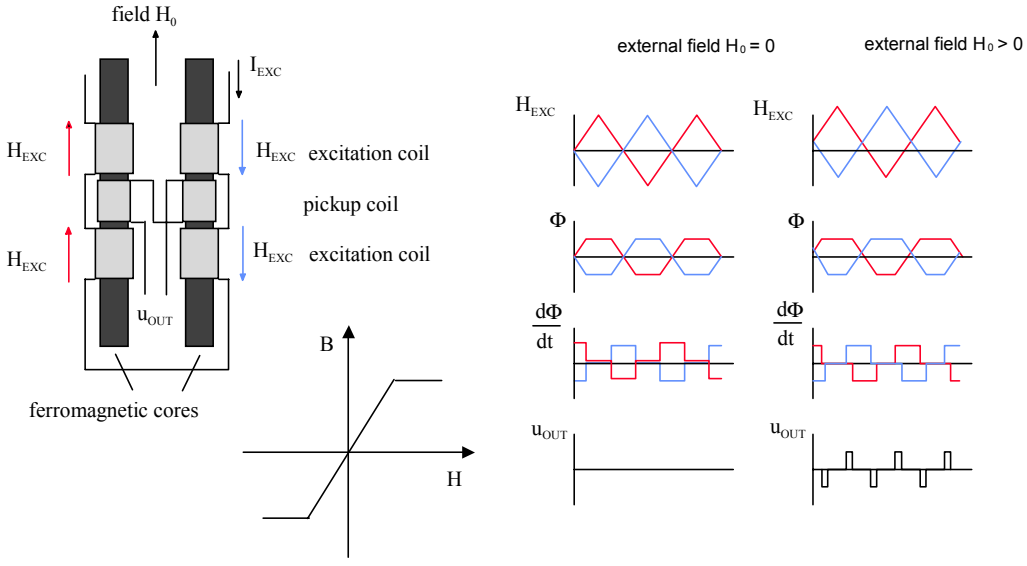

Fig. 1: Principle of fluxgate magnetic field sensors.

A ferromagnetic core is alternating driven into saturation, the magnetisation is a function of the applied field of the excitation coil. Pick-up coils measure dΦ/dt. A differential arrangement of pick-up coils leads to a symmetric dΦ/dt when no external field is applied. The integrated signal is zero. With an external field the symmetry is broken, dΦ/dt shifts and the integrated signal depends on the external magnetic field. The frequency of the signal is twice the excitation frequency; a second harmonic readout can be used.

The ranges of linear signal can be enhanced by a zero point operation mode with the use of further compensation coils.

Sensor system setup

Each fluxgate sensor consists of a three dimensional solenoid with two parallel ferromagnetic cores (Ni_{81}-Fe_{19}) which were embedded in the intermetal dielectrics of the CMOS process between the two metallisation layers (Fig. 2 (a), (b)) leading to 192 windings per millimetre.

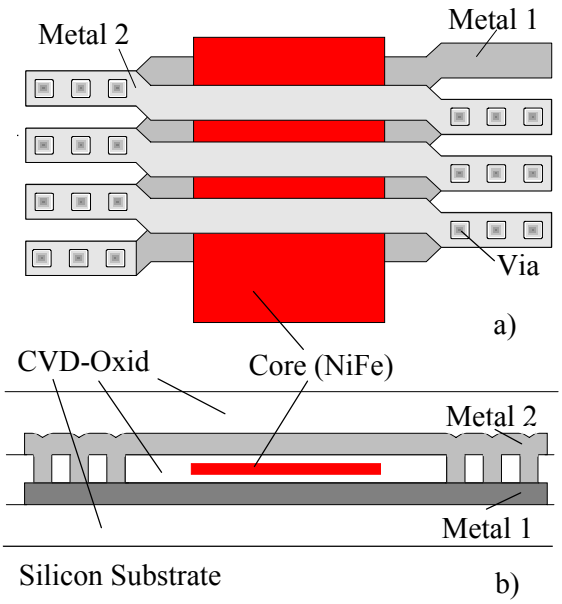

Fig. 2: CMOS-compatible, three dimensional solenoids. (a) top view, (b) cross sectional view.

The readout electronic is set up by a CMOS ASIC which uses even harmonic detection and zero field compensation for driving with internal excitation frequencies in the range of 300 kHz. The microelectronic system has the capability for monolithic integration on one chip. The chip area is approximately 4 mm x 7 mm. Sensor and ASIC are mounted on a ceramic substrate in chip on board (COB) technology. On this board (Fig. 3) additional resistors for sensitivity adjustment and driving amplitude and the capacitors for low pass filtering are placed. The two axes sensor system has a size of 15 mm x 15.24 mm x 3 mm. It can operate in the –40 °C to 125 °C temperature range. Low drifts of sensitivity and offset are achieved. The angle mismatch of the two axes is minimised

due to the nanometer accuracy of the deposition of the solenoids in the CMOS process. The setup is designed that after connection of the 5 V supply voltage analogue signals of both axes are available without further electronic components. The magnetic field values are given relative to the 2.5 V reference potential. The bandwidth can be changed by the value of two capacitors on the board.

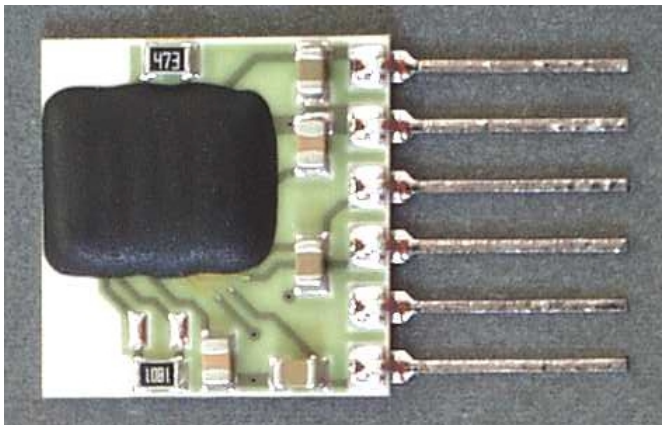

Fig. 3: Photograph of the fluxgate sensor module.

Features of FGS1/COB07

The **f**lux**g**ate **s**ensor system in **c**hip **o**n **b**oard technology was named FGS1/COB07. The sensitivity can be adjusted between 5 and 30 mV/µT by replacing one resistor. A fine adjustment of the sensitivity is possible with a second parallel resistor. Using values of a E24 resistor assortment for the parallel resistors the sensitivity is within 1% of the desired value at a fixed temperature. The sensitivity drift from –25 °C to 105 °C is typically 100 ppm. The same drift values are valid for the offset voltage. The working temperature range can be extended to –40 °C … 125 °C.

The output voltage is in the range from 0.5 to 4.5 V, the zero field value is 2.5 V. The output can be used relative to a 2.5 V reference potential (U_{AGND}) on one connection of the board.

In Fig. 4 the excellent linear behaviour and the hysteresis behaviour of one specimen of the sensor system with deviations below 20 mV for both axes are shown. Using the default 30 Hz low pass filter a noise value (rms) of 2 mV respectively 67 nT at 25 °C is measured. By changing the capacitors of the first order low pass filter, the bandwidth can be changed. The resistor of the low pass filter (34 kΩ ± 15%) is on chip integrated. Due to the internal refresh rate of the ASIC of approximately 2.5 kHz, the bandwidth is limited. The system has an operating power consumption of 165 mW (33 mA, 5 V).

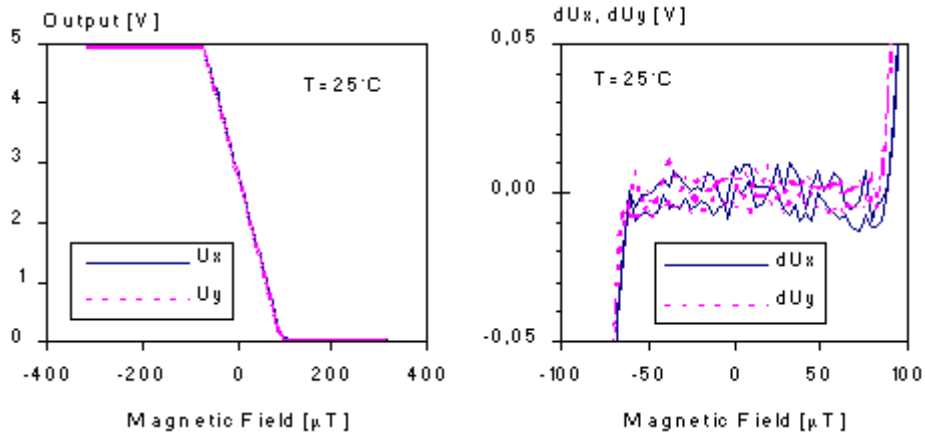

Fig. 4: Sensor output and deviation from linear regression of a sample (A0202011).

Optimisation of the shape of the cores and coils and the use of improved materials seems to be a challenge for the future which should permit a reduction of the sensor noise in the range of up to two orders of magnitude. A stable deposition process on 6 inch wafers is indispensable. An improved ASIC layout could be helpful to enlarge the bandwidth and to reduce the chip size.

Summary

A miniaturised two axes fluxgate magnetic field sensor system has been developed in a CMOS compatible process. This low cost system offers the capability of the detection of magnetic fields in the ±100 µT range, typically values of the earth magnetic field, with a sensitivity of 5 to 30 mV/µT. Temperature drifts of sensitivity and offset voltage of typically 100 ppm from –25° C to 105 °C and a working temperature range of –40 °C to 125 °C are realised. The bandwidth can be up to 400 Hz. Using the default 30 Hz low pass filter the noise (rms) is typically 2 mV corresponding to 67 nT.

References

[1] B. Sauer, R. Gottfried-Gottfried, Th. Haase, H. Kück: CMOS-compatible Integration of thin ferromagnetic Film; Sensors and Actuators A, 41-42, (1994),582-584

[2] S. Ulbricht, B. Sauer, R. Gottfried-G., R. Jähne, U. Wende, W. Budde: A Monolithically Integrated Two-Axis Magnetic Field Sensor System; Proc. of the 22nd European Solid-State Circuits Conference ESSCIRC´96, 17-19 September 1996, Neuchâtel, Switzerland, 132-135

[3] F. Primdahl: The fluxgate magnetometer; J. Phys. E: Sci. Instrum., 12, (1979), 241-253

DIMADS™ — Digital Magnetic Anomaly Detection System

J. Hochreiter, D. Schrottmayer
Schiebel Elektronische Geräte GmbH, A-1050 Wien, Austria

Introduction

An estimated 100 million unexploded land mines and a minimum of the same amount of unexploded ordnances (UXOs) left over from this century's various wars and conflicts lie scattered in 64 countries, still lethal decades after the peace treaties have been signed. Many of those are still effective, each day claiming the limbs and lives of about 70 people, mostly civilians, in places like Cambodia, Angola, Ethiopia, Afghanistan, and Bosnia. But even in the heart of Europe companies are confronted with the danger of UXOs all the time during digging work in towns like Vienna, Berlin and Dresden, where many times a year bombs and grenades from Second World War are found. Therefore it is very important to detect those threats as early as possible to save human life and health.

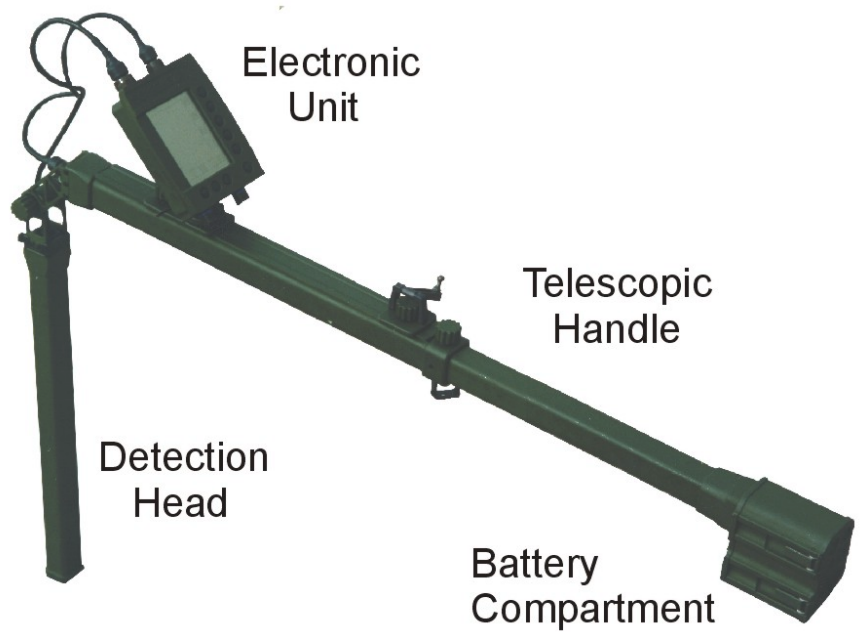

Fig. 1: Basic components of the DIMADS™.

DIMADS is a handheld device designed to locate ferromagnetic objects such as unexploded ordnance, drums or pipes under ground or under water and has been developed by Schiebel Elektronischer Geräte GmbH [1], an Austrian Company specialised in the manufacturing of mine and ordnance detection equipment. It features a unique pair of three-axis sensor arrays that provide highly accurate target information.

The DIMADS^{TM} consists mainly of the detection head, the Electronic Unit, the Telescopic Handle and the Battery Compartment (see Fig. 1). Magnetic field data from six fluxgate sensors are sampled, corrected for sensitivity and alignment of each sensor and transmitted via an RS485 link to the Electronic Unit. On the microcomputer controlled Electronic Unit data may be visualised on a number display, as moving graphs or bar graphs (see Fig. 2). Recorded data can be stored on the Electronic Unit and be later transferred to a PC for post processing of the acquired data.

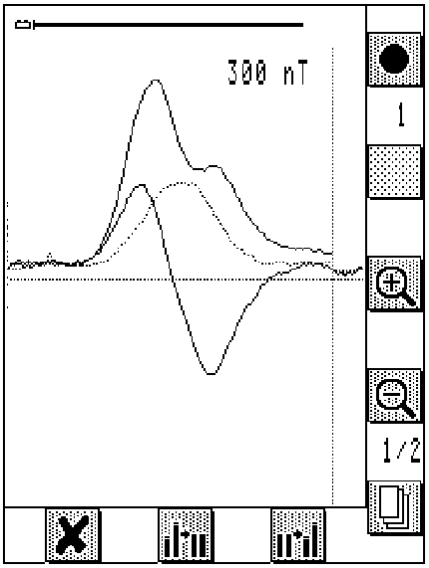

Fig. 2: Typical data displayed at the DIMADS^{TM}.

Background

The presence of ferromagnetic objects in the ground results in magnetic anomalies superimposed on the background geomagnetic field. Consequently, the use of magnetic detection techniques to locate buried Unexploded Ordnance (UXO), drums and pipes has become one of the standard methods used by the UXO community. Detection techniques include the use of total field and vector field magnetic measurements. Usually both methods are used to take magnetic field gradient measurements (gradiometer). Detection of buried objects is not a simple exercise as both man-made and naturally occurring magnetic clutter, as well as the time-varying component of the Earth's mag-

[1] Schiebel Elektronische Geraete GmbH, founded in 1951, is an Austrian, Vienna-based company working in the field of advanced electronic technology systems. For the past twelve years the focus has been on the development, testing, and manufacturing of state-of-the-art mine and ordnance detection equipment. SCHIEBEL has built an international reputation for producing quality military products.

netic field complicate detection. In order to maximise detection and assist in the identification of UXO, a real understanding of the typical magnetic signatures expected for different types of targets is important. This is not always straightforward because the magnetic signature is strongly dependent on the outer dimensions, relative permeability, history, and wall thickness of the ferrous ordnance, not only the mass. Thus, the magnetic signature should not be scaled with the ferrous mass.

The Detection Head

The detection head is the sensing element of the DIMADS™. Electronic and mechanic components of the detection head are selected to produce lowest magnetic moments in order to keep self-detection low. Two three-axis sensor arrays are located on top and on bottom of the detection heads tube-in-tube construction. The electronics for the operation of the fluxgate sensors and the micro controller is placed in between the sensor arrays.

The sensor arrays measure the components of the Earth field in three orthogonal directions, and their sensing directions are aligned about parallel to each other. The outputs of these six sensors are A/D converted and processed by a micro controller, which applies a factory generated calibration matrix for precise sensor sensitivity calibration and alignment.

From these measurements the vertical gradient (field difference at vertical distance d) of each field component as well as the vertical gradient of the total field is calculated (see Fig. 3).

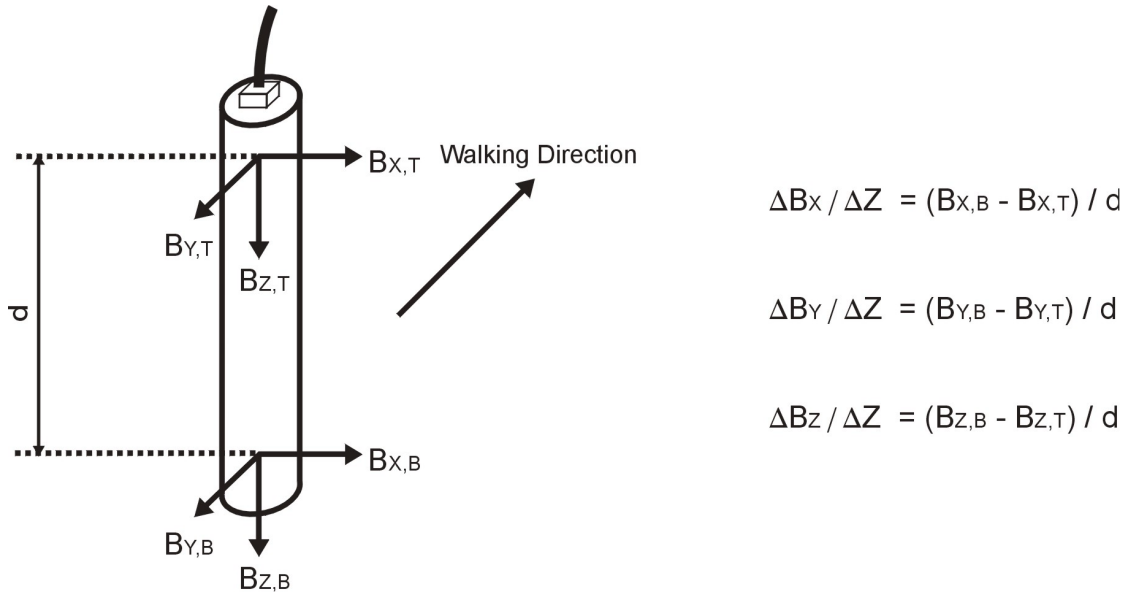

Fig. 3: Calculation of the vertical gradient of the total magnetic field.

The Electronic Unit

The Electronic Unit is the user interface to the handheld detection system. It records magnetic data from the Detection Head as well as positioning data and stores them on user request. It provides different kinds of data presentation in real time and in post processing and provides the possibility to transmit data to a PC for further processing in real time or after recording.

The Electronic Unit also features an in-field re-calibration procedure in order to reduce long time drift of sensor properties (e.g. remanent magnetisation of the Detection Head) as well as to eliminate other external field gradients. Switching of the Detection Head's sampling rate in order to eliminate the mains frequency is also initiated via selectable averaging time spans.

First data processing is accomplished in the Electronic Unit supplying the operator with corrected gradient and total field data as well as with computed properties such as object depth. Object orientation has to be investigated by scanning the magnetic signature on the ground surface accounting for the position of maximum and minimum signals as well as the shape of the signature.

Post processing

Post processing by correlation of samples in close vicinity serves many purposes. It is a possibility to

- apply spatial filters in order to handle changing (back-)ground and sensor drift,
- eliminate clutter from measured data,
- enhance object estimates by presentation of different signals,
- enhance therefore the useful resolution of the device.

Produced maps are also a means of quality ensurance documenting the non-existence of ferrous objects in the covered area up to the detection limit (see Fig. 4).

Sensor requirements

Magnetic field sensors for the localisation of buried objects have to be able to reliably detect magnetic field gradients in the order of a few nT/m on top of the Earth field background (around 48 μT in Vienna). This requirement states hard limits to alternative sensors. Most important characteristics are sensor offset and directional stability, sensitivity and temperature coefficients of those, power consumption, bandwidth, size, and the necessary electronic interface.

Using a gradiometer configuration almost any static sensor error can be squeezed into the sensor offset, because of a carefully handled, unidirectional carried detector. E.g., a misalignment of two sensors of 5 seconds of an arc produces a worst case error of ±1 nT. This is about the same number as the sensitivity change of good solid state fluxgates due to thermal expansion per degree Celsius. Usually there is also a trade off between the power consumption and the gain-bandwidth product of the sensor.

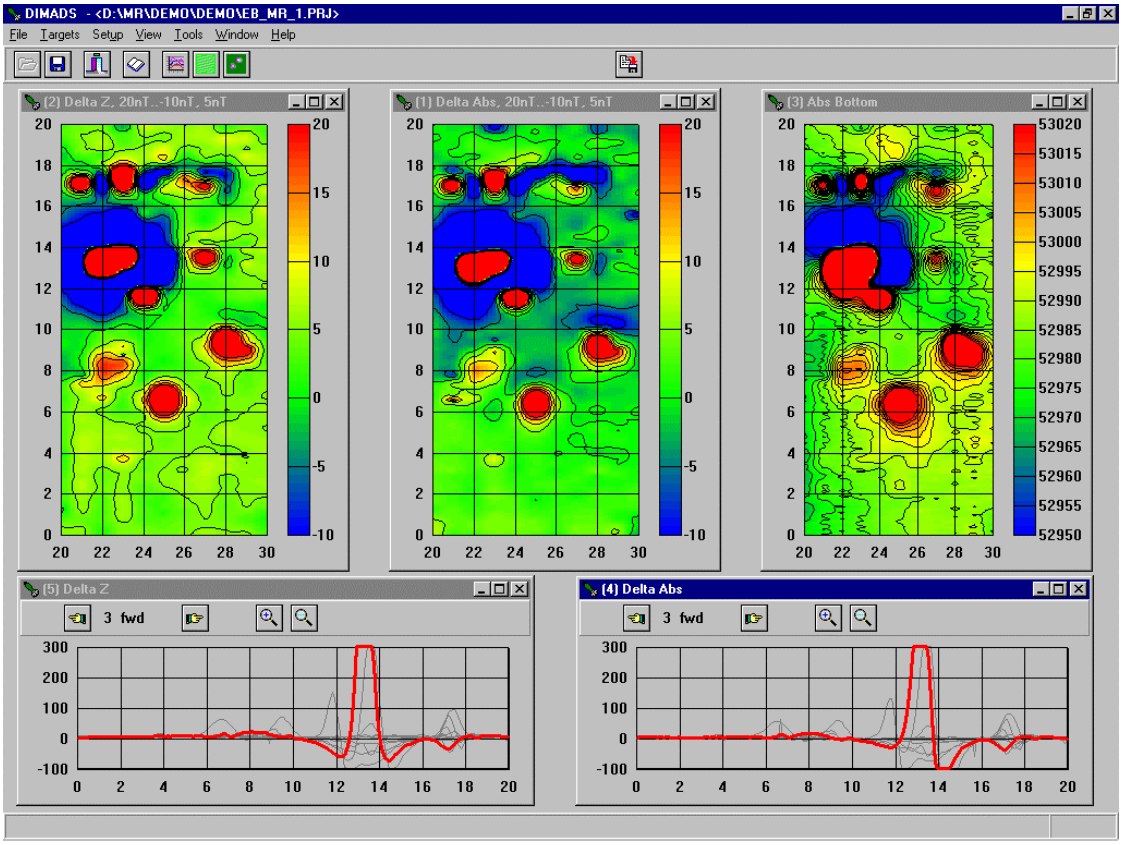

Fig. 4: Maps produced by post processing of DIMADS™ detection data.

Even if magnetoresistive sensors will not reach the performance of fluxgates for the above measurement purpose, there might arise applications for arrays of sensors which enhance their performance by a higher spatial sampling density.

Summary

Important applications of magnetic anomaly detectors are in the area of UXO clearance. Schiebel's DIMADS is a handheld device designed to locate ferromagnetic objects such as unexploded ordnances, drums or pipes under ground or under water and is based on fluxgates. A gradiometer is built by two three-axis sensor arrays that provide highly accurate target information. Magnetic field data is displayed, recorded, and post processed for later calculation of target properties.

Magnetoresistive sensors could be used instead of fluxgates. The intention would be an increase of mechanical and thermal stability and to reduce production costs. Schiebel is supporting research activities[2] in the area of thin ferromagnetic films and is interested to investigate the possibility of this technology for UXO detection.

[2] The research activities are funded by FFF Forschungsförderungsfonds für die Gewerbliche Wirtschaft, project number 802303.

Microtransformers and Inductors using Permalloy Thin Films

Terence O'Donnell[#], Magali Brunet[#], Paul McCloskey[#], Joe O'Brien[†], Seán Cian Ó Mathúna[†]

[#]PEI Technologies,
[†]National Microelectronics Research Centre,
Prospect Row, Lee Maltings, Cork, Ireland

Introduction

Most electronic products require a power supply, either to regulate battery voltages or to provide voltage step-up/down functions for different parts of the system. A vital part of most power supplies are the magnetic components, either inductors, which provide an energy storage function, or transformers which provide an isolation, and/or voltage step up/down function. To date progress in the integration of magnetic components has been slow — the vast majority of magnetic components are still fabricated using wire conductors wound on discrete cores.

However in recent years there has been growing research interest in the integration of magnetic components directly onto silicon substrates and the integration of these magnetic components with other circuitry [1], [2]. This research is mostly motivated by the aim of achieving miniature low power (typically several Watts) power supplies, suitable for use in hand held electronic equipment. Generally these supplies have high switching frequencies (several MHz and greater) to facilitate the use of low inductance ($\approx$ 1 μH) values. An example of the state of the art is the 1 W DC-DC converter recently presented by Sugahara et al. [1]. This converter included an IC which included power switches, control circuitry and inductors all integrated onto a single chip. There is, however, still considerable room for improvement in the performance of this type of magnetic component.

This paper discusses the design and fabrication of thin film magnetic components suitable for applications in low power dc-dc conversion. Section 2 reviews the structure and properties of thin film magnetics and discusses the impact of fabrication techniques on the performance of these devices. Sections 3 and 4 describe the fabrication methods used and presents test results for thin film inductors.

Design considerations

In general the fabrication of thin film magnetic components require the deposition of conductors, insulation layers, and magnetic material. Although details of the structures of components vary, in general they have either a toroidal structure, or a pot-core structure as shown in Fig. 1.

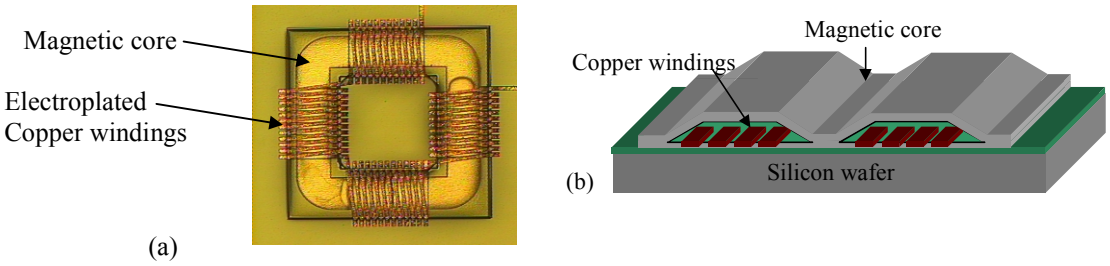

Fig. 1: Two basic structures for thin film magnetic components, (a) toroidal with conductors wound around the magnetic material, (b) pot-core with magnetic material wrapped around the conductors.

Inductors and transformers have similar structures with the difference being that an inductor consists of a single continuous winding around the magnetic core, whereas in general a transformer will have at least two electrically isolated windings. Among the more important performance criteria for theses components is the inductance achievable and the efficiency.

Inductance & efficiency

In general the footprint area available for this type of magnetic component will be limited. Maximum feasible footprint size is approximately 5 mm x 5 mm. Thin film components should achieve an adequate inductance in this limited footprint area. Current applications in low power dc-dc conversion require inductances of approximately 5 µH at frequencies of 1 – 2 MHz. However with future increases in switching frequency these requirements are likely to move towards 500 nH – 1 µH at frequencies up to 10 MHz.

Efficiency of the components must also be high, e.g. the efficiency of many conventional magnetic components is in excess of 95%. However thin film magnetic components fabricated to-date have efficiencies in the range of 70 – 80% [3]. Maintaining a high efficiency means that losses in the component must be minimised. Losses will be either I^2R losses in the windings, or losses in the magnetic core which are composed of both hysteresis and eddy current losses.

The low frequency inductance of an inductor can be approximated by the following expression;

$$L = \mu_o \mu_r N^2 \frac{A_e}{l_e} \tag{1}$$

where N is the number of turns wound around the core, μ_r is the relative permeability of the core material, A_e is the effective cross sectional area of the core and l_e is the effective magnetic path length. It is immediately obvious from this expression that the inductance can be increased by ensuring a large number of turns, a high permeability for the core material, and a thick core.

A high number of turns requires a high turns density, i.e. small track width and spacing so that many turns can be fitted in a given area. However reducing track width has the

effect of increasing the conductor resistance, which has a negative impact on device efficiency, so that there is a design trade-off between inductance and winding resistance. Conventional magnetic components generally have low winding resistance (< 1 Ω). Achieving this low resistance requires the deposition of thick conductors, at least 10's of µm thick, which suggests that the most feasible method for conductor deposition is electroplating.

One approach which ensures thick conductors, and small track widths and spaces is to use high-aspect ratio conductors, i.e. conductors which have a high thickness to width ratio. In this way footprint area is not sacrificed in achieving a large conductor cross sectional area.

High inductance can also be achieved by increasing the core cross sectional area, i.e. in a limited footprint area this means using thick magnetic cores (large A_e). However most thin film magnetic materials are metal alloys, which generally have a relatively high conductivity (when compared to ferrite materials). Thick layers of such material are very susceptible to eddy current formation. The formation of eddy currents in the core increases the core loss and also tends to decrease the inductance. However both these effects can be minimised by ensuring that core layers are thin. A Finite element simulation of the inductance and losses for the simple structure shown in Fig. 2 can be used to show the effect of core thickness on the inductance and losses.

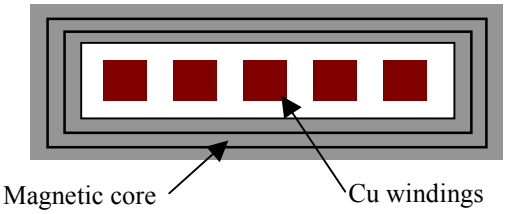

Fig. 2: Simple pot-core type magnetic component structure simulated to compare the effect of different core layer thickness on inductance and losses.

In the graph in Fig. 3 simulation results for three different magnetic core constructions are compared, (a) the core is implemented as a single 12 µm permalloy layer, (b) the core is implemented as two, 6 µm thick core layers, and (c) core is three, 4 µm thick layers.

In all three cases the inductance and losses remain constant up to a certain frequency. However above this frequency the inductance rapidly decreases and the losses increase due to the effect of eddy currents. Thus inductance decreases rapidly above 1 MHz, 4 MHz and ≈ 7 MHz for the 12 µm, 6 µm and 4 µm thick layers respectively. The graph in Fig. 4 highlights the relationship between these frequencies and the skin depth in the permalloy core, given by

$$\delta = \sqrt{\frac{1}{\mu\sigma\pi f}} \qquad (2),$$

where µ is the permeability, and σ the conductivity of the core material. In Fig. 4 the inductance is plotted against the ratio of layer thickness to skin depth for the above three core constructions.

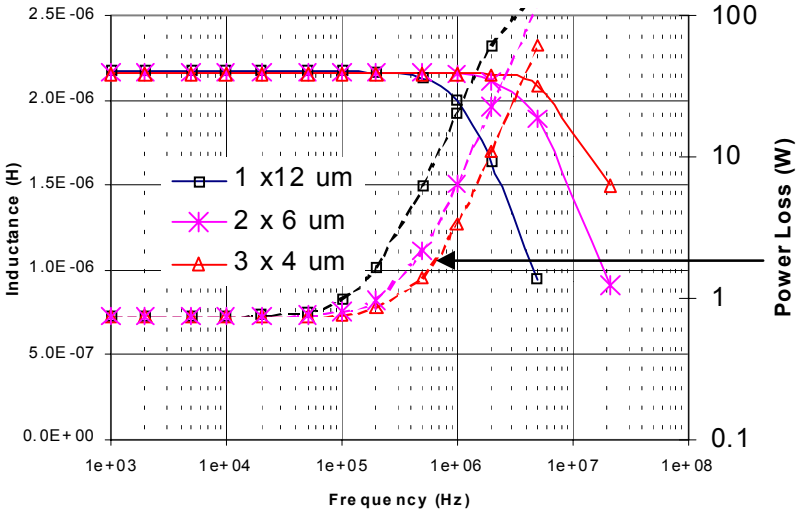

Fig. 3: Simulated results for inductance vs. frequency for three different core configurations, (a) a 1 x 12 µm thick core, (b) a 2 x 6 µm thick core, (c) a 3 x 4 µm thick core.

The graph clearly shows that the inductance begins to decrease when the ratio of lamination thickness to skin depth is greater than one. Thus lamination thickness must be less than one skin depth at the operating frequency of the component in order that inductance is maintained.

As equation (2) indicates, the skin depth in the core material depends on the permeability and the conductivity. Permalloy generally has a permeability in the range of 600 – 2000 and a resistivity of approximately 20 µΩcm. Materials with higher resistivity have the advantage of lower eddy current loss and also allow the deposition of thicker layers as the skin depth is greater.

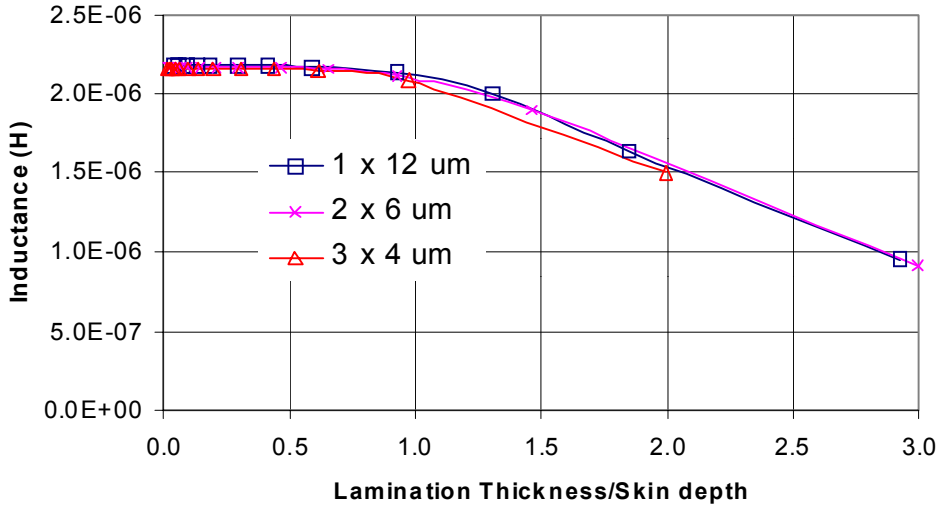

Fig. 4: Inductance plotted against the ratio of lamination thickness to skin depth.

Thus much research remains to be done in the area of higher resistivity magnetic materials. Recently an electroplated alloy of Fe and Co was reported to have a resistivity of 125 μΩcm [5]. Other high resistivity materials which have been investigated include Fe-Zr-O [4] and CoHfTaPd [1]. These latter materials have been deposited by sputtering. Sputtering has advantages for the deposition of laminated layers of magnetic and insulating materials, as both the magnetic and insulating material can be deposited in the same process step. Electroplating is not feasible as a method for the deposition of laminated multi-layers as the deposition of the magnetic and insulating materials require different processes. For higher resistivity materials, which can be deposited in thicker layers, electroplating is a more feasible core deposition method.

Fabrication

The fabrication of both toroidal and pot-core structure thin film components is currently being investigated. Both types of component use similar methods for the deposition of the conductors, core, and insulating layers, although the order of the process steps is different depending on the structure.

Conductor deposition

The conductors of the transformer were fabricated using the electrodeposition of copper. The basic process is shown in the Fig. 5.

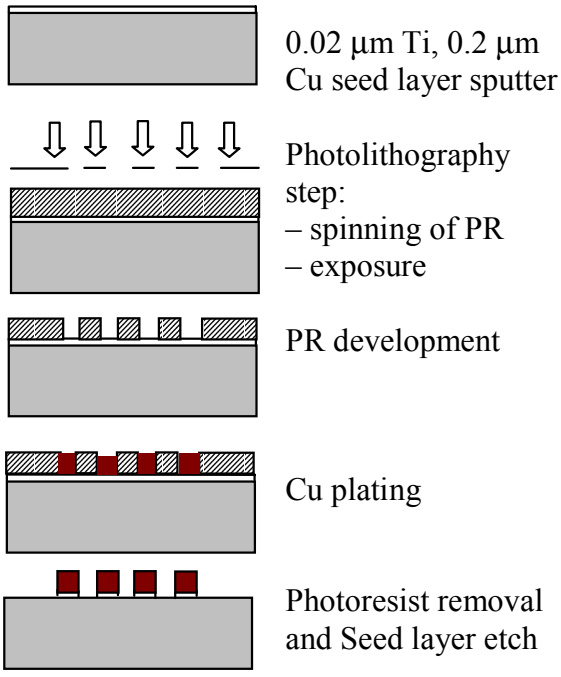

Fig. 5: Basic electroplating process for the copper conductors.

As discussed in the design considerations, the reduction of the losses in the copper tracks demands that thick conductors be deposited. In this case, the use of a thick photoresist is required (10's of μm thick) instead of the standard photoresist.

For positive photoresists like the AZ-4000 series, a standard thickness of 25 µm with good structural resolution can be obtained. When considering thicker layers, negative photoresists like EPON Resin SU8 [5] have an advantage over positive photoresists in that they can give very high aspect ratios. For example aspect ratios of 18:1 with straight side walls have been achieved in a one step process. The use of this photoresist for the formation of high aspect ratio transformer tracks is currently being investigated.

Magnetic core deposition

Electroplated permalloy ($Ni_{80}Fe_{20}$) is deposited to form the magnetic core of the inductors/transformers. The basic process used is similar to that outlined in Fig. 5 for the copper deposition. In order to reduce hysteresis loss anisotropy is induced in the magnetic core by depositing the permalloy in the presence of a magnetic field, supplied by permanent magnets placed in the appropriate position on each side of the electroplating bath.

Insulation layer deposition

The insulating material used to insulate the windings from the core is BCB or Benzocyclobutene. The Cyclotene 7200-35 series is photosensitive and can thus be patterned using a photolithography step. BCB offers a good degree of planarization, good pattern properties if used as a photoresist, less shrinkage at lower cure temperatures and no hydrophilic properties.

Results

Using the processes outlined in the previous section toroidal type thin film inductors have been fabricated. The graph in Fig. 6 shows measured results of inductance and winding resistance for an inductor fabricated in a 1.6 mm x 1.6 mm square footprint area.

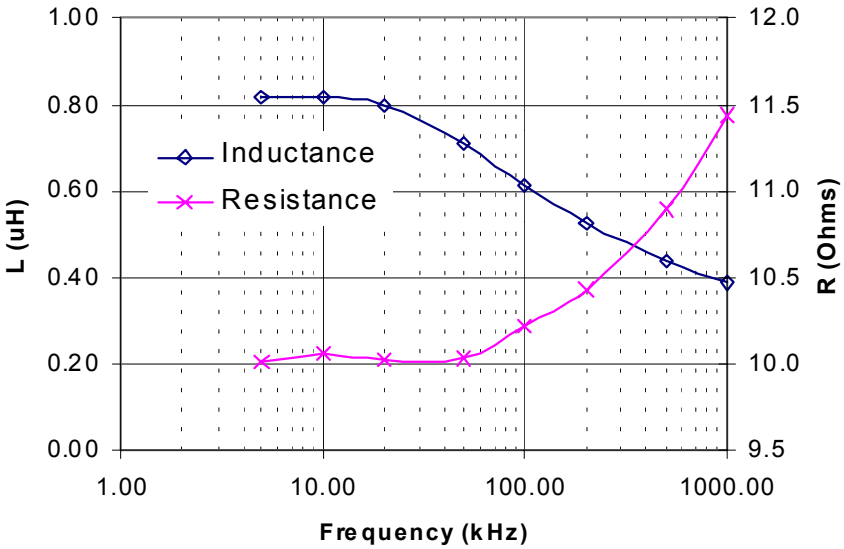

Fig. 6: Inductance and resistance measurements for the toroidal inductor shown in Fig. 1 (a).

The inductance remains constant up to a frequency of approximately 20 kHz and begins to decrease above this. Also the resistance begins to increase significantly for frequencies above 50 kHz. These effects are due to a combination of hysteresis loss and eddy currents in the magnetic core. In this particular device the permeability of the magnetic material was measured to be approximately 4000, and the core thickness approximately 4 μm, thus eddy current loss should not be significant for frequencies less than 2 MHz. However the core material was not deposited in the presence of a magnetic field so that hysteresis losses are significant, which possibly explains why the losses start to increase above 50 kHz.

Also the dc winding resistance of the components is quite high at 10 Ω. This is due to the fact that the conductor thickness is approximately 2.5 μm because a standard photoresist was used for the fabrication.

In order to improve device performance a pot-core structure device is currently being investigated. This structure has the following advantages compared to the toroidal structure:

- windings are confined to a single layer, thus fabrication is simplified and problems with contact resistance are eliminated;
- thick conductors with low resistance are easier to implement with this structure;
- the structure lends itself more readily to the deposition of an anisotropic core material and thus the reduction of hysteresis loss in the core.

The SEM image in Fig. 7 shows thick electroplated conductors which are to form the windings of the transformer. These conductors are 70 μm wide, with a 70 μm spacing and 80 μm thick.

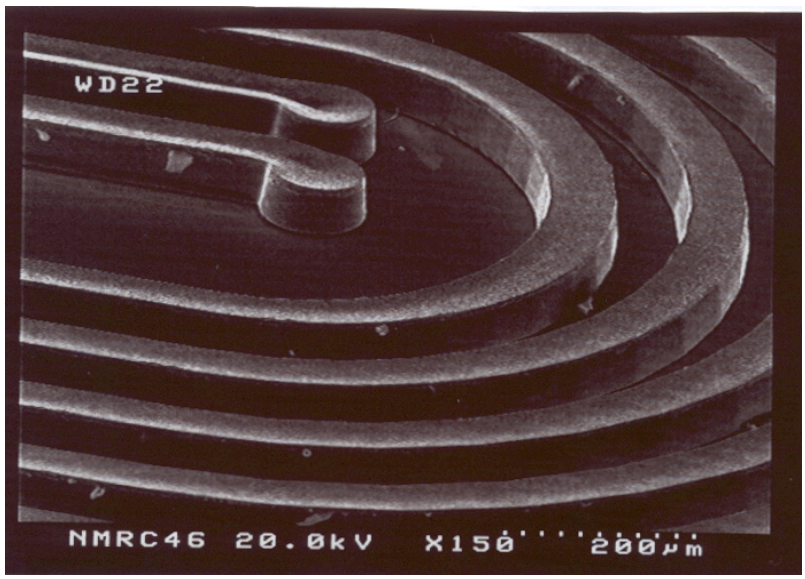

Fig. 7: SEM image of thick electroplated windings for pot-core type transformer.

Conclusions

The integration of magnetic components onto silicon substrates is likely to find increasing application in low power dc-dc converters, especially as switching frequencies increase. Thin film magnetic components with adequate performance will require the deposition of thick conductor layers and low loss magnetic cores. The use of high aspect ratio conductors is one means of achieving low resistance windings in a limited footprint area. Low loss cores demand the deposition of laminated multilayers of magnetic material, or the development of high resistivity materials suitable for deposition as single layers.

References

[1] "*Characteristics of a Monolithic DC-DC Converter utilizing a Thin Film Inductor*", S. Sugahara et al., Proceedings of the International Power Electronics Conference, IPEC-2000, Tokyo, April 3-7, 2000, pp326 - 330.

[2] "*New micromachined inductors on Silicon Substrates*", J. Park et al., IEEE Transactions on Magnetics, vol. 35, no. 5, Sep. 1999.

[3] "Measured Performance of a High-Power-Density Microfabricated Transformer in a DC-DC Converter", C. Sullivan et. al., Proceedings of the Power Electronics Specialists Conference, 1996, pp278-294.

[4] "*Thin Film Inductor for micro switching converters using a high resistive Fe-Zr-O film*", Y. Sasaki et al., Proceedings of the International Power Electronics Conference, IPEC-2000, Tokyo, April 3-7, 2000, pp315-319.

[5] "*Micromagnetic Components for Miniaturised Power Management*", R. Filas et al., Proceedings of the International Power Electronics Conference, IPEC-2000, Tokyo, April 3-7, 2000, pp320-325.

[6] "*SU-8: a low-cost negative resist for MEMS"*, J. H. Lorenz, Micromech. Microeng., 7 (1997), 121-124.

Electronics and Methods for Sensors Based on Ferromagnetic Devices

J. Cabestany, J.M. Moreno, M. Garcia

Electronic Systems and Sensors Centre
Technical University of Catalonia (UPC)
Jordi Girona, 1-3; Building C5
E-08034 Barcelona, Spain

csse@eel.upc.es
http://csse.upc.es

Introduction

Magnetic sensors are specific detectors that don't directly measure the physical characteristic of interest. They detect changes in magnetic fields that have been created or modified, and from them derive information and conclusions about properties (position, presence, electrical currents,...).

One of the main characteristics of this kind of sensors is that they need a special and adapted "signal processing" part for a proper operation and the posterior manipulation of useful information.

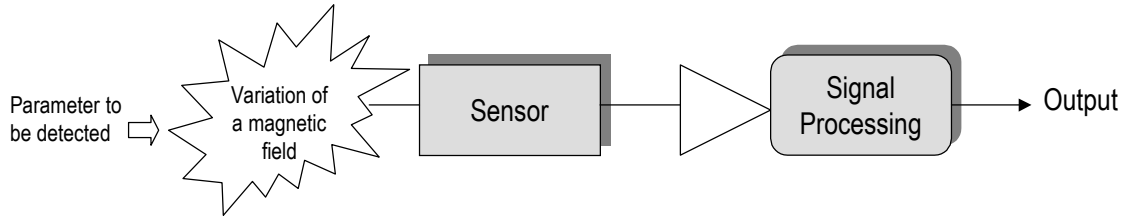

Fig. 1: Magnetic sensors detect changes in magnetic fields. Signal Processing parts are required.

There exists a wide range of available technologies for the implementation of magnetic sensors, with a detectable field range associated to each one [1]. From all of them we will focus our attention on the magnetoresistive ones with a resolution in the range of nT (10^{-9} Tesla), and more specifically, on Anisotropic Magnetoresistive (AMR) devices. AMR sensors are well suited for the measurement of both linear and angular position and displacement in the Earth's magnetic field.

These devices are usually made of a nickel–iron thin film (Permalloy) deposited on a silicon wafer, and patterned as a resistive strap. The intrinsic properties of this film cause the resistance value to change in the presence of a magnetic field. The relative change is in the range of a 2% to 3%. A very typical configuration is an arrangement of

four films connected in a Wheatstone bridge configuration in order to allow the measurement of field magnitude and direction along a single axis.

Today ferromagnetic materials for AMR sensors can be deposited as thin films and structured as small strips with the following typical dimensions: 40 nm thick, 10 μm wide, and 100 μm long. The electrical resistance of AMR material depends on the angle between the direction of the magnetisation, and the direction of the current going through it. It is possible to draw the change in resistance ΔR/R as a function of the above mentioned angle, giving us a curve with a linear portion and a non-linear section. Technological efforts have been made for obtaining a specific method for biasing just in the linear part of the characteristic.

Main advantages for these devices are the exhibition of a large bandwidth, a very fast reaction to the perturbation and their compatibility with the silicon wafer technology. This permits to include the AMR sensors in commercial IC packages, and to assemble them with other circuit and systems. Additional characteristics are a relatively high sensitivity, a small size, and good noise immunity.

Model for a sensor system.

As it was introduced before, it is almost obligatory to consider an electronic system around the Permalloy film sensor, in order to obtain the desired characteristics. The primary application in a Wheatstone bridge configuration represents the use of a simple operational amplifier with its parameter adjustment needs. When more generic models are considered, it is possible to go to sophisticated systems with many possibilities and improved characteristics.

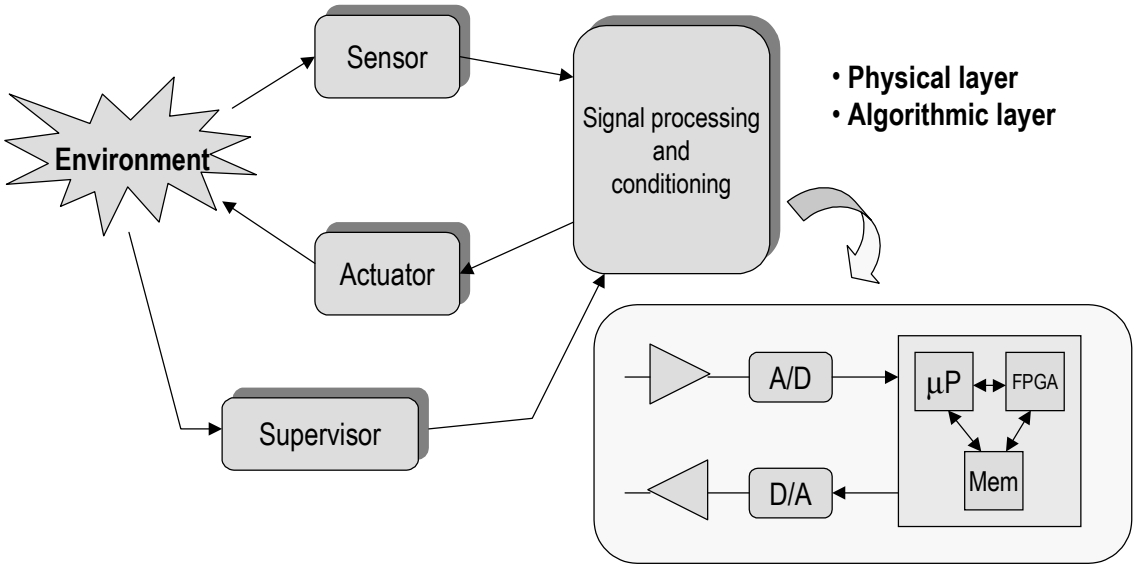

Fig 2: Sensor system with generic possibilities. A physical layer and a software part can be considered in the signal processing and conditioning subsystem.

Figure 2 represents the global organisation of an embedded system using sensors and actuators to handle a specific application. Besides the reactive part of the system (con-

stituted by the specific sensor and actuator elements), special attention must be paid to the signal processing and conditioning subsystem. Usually, it is composed of the components appearing in the block. A/D and D/A converters are used for interfacing the sensor and actuator components with the necessary electronics contained in the subsystem (depending on the specific sensor and application, resolution will be in the range of 12 to 16 bits). The actual processing part is composed of a microprocessor or microcontroller (MCU) unit, together with a digital subsystem implemented on a FPGA device, and connected with a memory system containing the code to be executed by the MCU, and (eventually) the configuration of the FPGA device.

The configuration presented in Fig. 2 permits the integration on the same system of most part of the requirements needed when considering AMR sensors. As can be seen [2], AMR sensors exhibit good characteristics, but they are less linear when compared with other magnetic sensors. They also present a dependence with temperature. All these circumstances suggest us that it is important to have compensation mechanisms and strategies. This can be done in an embedded way using the capabilities offered by the signal processing subsystem, usually with an algorithmic method programmed on it.

Other interesting advantages offered by the electronic signal processing part is the compensation possibility of some undesirable effects like automatic gain adjustment and real time offset cancellation.

Making some additional considerations it is possible to progress towards the "Smart sensor" concept [3]. Among other factors, the following main aspects must be considered:

- Real time computing characteristics. This can be reached by many of the actual MCU on the marked. The concurrency of special DSP (Digital Signal Processors) devices must be considered when needed. Actual technological approaches permit the use of synthetizable IP cores, certified by vendors, and compatible with state-of-the-art technology.
- Communication interfaces according to standard protocols. When these interfaces are integrated with the sensor or built near the system, it will be very easy to communicate with computing systems, house control engines or automotive control parts.
- Introduction of "intelligence" into the system. This is indicated in Fig. 2 by means of a supervisor block, giving the possibility to adapt some parameter values. The adaptive control can be implemented through an algorithm introducing knowledge in an algorithmic way, or alternatively, using specific techniques like artificial neural networks (ANN) or fuzzy systems.
- Auto-calibration and auto-diagnosis capabilities.

When the application target is decided for the sensor system, the electronic engineer job will begin. It is important to decide the particular technological approach to be used. This decision will be taken after particular considerations on desired functionality and characteristics of the global system. Special constraints, like power consumption or size can be very important in order to take the final decision.

Electronic Systems and Sensors Centre capabilities.

The Centre is a part of the Technical University of Catalonia (UPC) in Spain, and their staff is a part of the Department of Electronic Engineering. Among the different competencies, two main sections must be considered:

- Electronic systems team. Their main expertise is on the specification and design of electronic circuits and systems. Used technologies are, among others, ASIC devices design when it is required, FPGAs programming for digital or mixed systems implementation, and/or MCUs and DSPs for standard programmable solutions.
- Sensor systems team. They are using commercial or custom devices with special interfaces when it is required by the application constraints. Special expertise on IR and UV devices must be pointed out.

The Electronic Systems and Sensors Centre has participated in several industrial projects and contracts. Three main actions can be mentioned:

- ELENA (Esprit EU project). The complete title was "Enhanced Learning for Evolutive Neural Architectures", and the main objectives were to obtain knowledge and solutions for the emerging field of the evolving ANN solutions. A good result was to obtain a hardware solution for an electronic implementation of this kind of structures.
- FIPSOC (Esprit EU project). The result of this industrial project was the prototype of the first European mixed (analogue/digital) system on a chip, including a FPGA part and a complete microcontroller, compatible with the Intel 8051 part. This new family of devices will be commercialised along 2000 and it is specially matched to the requirements of some specific sensors systems. The FIPSOC device itself, depending on specific application constraints, can implement the main electronic part represented in Fig. 2.
- PIEZOTAG (Craft EU action). It is a project for the specification and implementation of a new low cost, piezoelectric powered pressure measurement technology.

As it can be seen, the activity and expertise of the Centre is well matched with the system and, specially, electronic requirements to be configured around Permalloy films sensors. Special interface design experience and the knowledge on ANN is enough for the participation in a smart magnetic sensor design initiative.

References

[1] Carusso M.J., Bratland T., Smith C.H., Schneider R. *"A new perspective on Magnetic Field Sensing"* Sensors December 1998

[2] Gardner J.W. *"Microsensors. Principles and Applications"* Wiley 1994

[3] Frank R. *"Understanding Smart Sensors"* 2nd edition Artech House 2000

Cathode Sputtered Permalloy Films of High AMR Effect and Low Coercivity

G. Stangl, P. Aigner, H. Hauser, J. Hochreiter, K. Riedling

Institut für Industrielle Elektronik und Materialwissenschaften
Technische Universität Wien, Gusshausstrasse 27 – 29,
A-1040 Vienna, Austria

The anisotropic magnetoresistive (AMR) effect of dc sputtered Ni 81% – Fe 19% films has been increased up to $\Delta\rho/\rho$ = 3.93% at 50 nm thickness. Investigations have been concentrated on the influence of the target current, the target-substrate distance, and of the temperature of both target and substrate material. As a function of the applied magnetic bias field, the easy axis coercivity of the permalloy film is between 100 A/m and 200 A/m due to induced anisotropy. The dc magnetisation curves represent an almost ideal Stoner–Wohlfarth behaviour with a hard axis coercivity between 0 and 20 A/m.

Introduction

The anisotropic magnetoresistive (AMR) effect is widely utilised in sensor applications, related with the detection of weak magnetic fields [1]. The resistance ρ in the plane of a thin ferromagnetic film with uniaxial anisotropy varies with the angle between the current density and the spontaneous magnetisation. To achieve a high sensitivity, the coercivity in the hard axis magnetisation direction must be very low and the specific resistance variation $\Delta\rho/\rho$ must be as high as possible. Depending on both material composition and film thickness, it is (theoretically) about 4% in a 50 nm thin Ni 81% – Fe 19 % (magnetostriction free) permalloy film.

Experimental

The magnetoresistive films have been deposited by cathode sputtering (triode process). Figure 1 shows the arrangement schematically [2]. The target is connected to a negative potential of U_T = –800 V and the substrate is biased by U_S = –60 V. The cathode current is I_C = 43 A, the anode current is I_A = 3.5 A, and the anode voltage is U_A = +50 V against ground potential. The following parameters have been varied: Both target and substrate materials, the temperatures of target (T_T) and substrate (T_S), the distance $a_{T\text{-}S}$ between target and substrate, and the film thickness d. This value has been determined by resonance frequency measurements with an accuracy of better than 1%. Depending on the applied magnetic field direction, the specific resistance variation has been measured by a four-wire method.

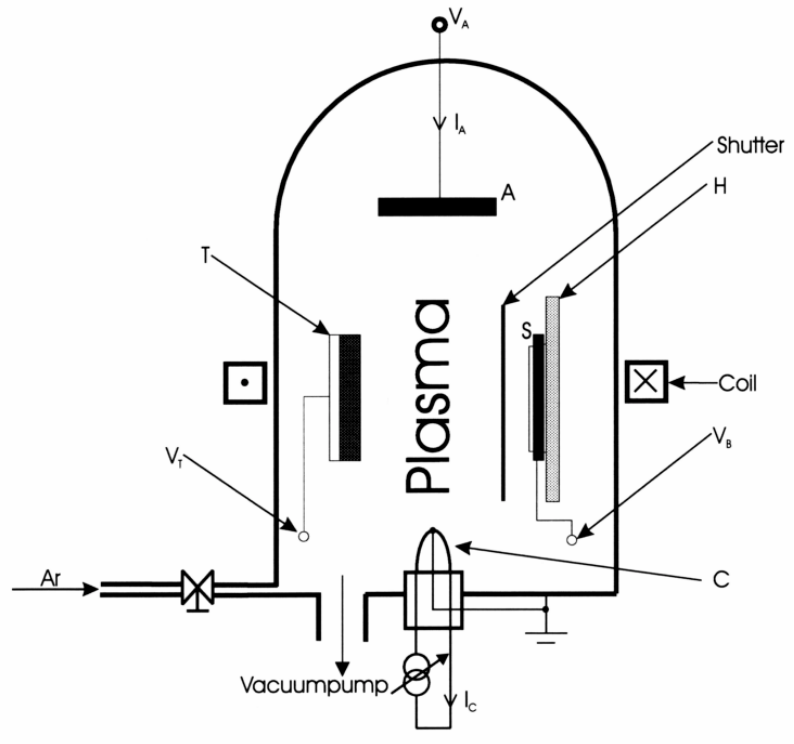

Fig. 1: Cathode sputtering set-up.

Figure 2 shows the experimental arrangement for measuring the dc magnetisation curves by the transversal Kerr effect [3]. Red laser light (diode D1) is focused (lens L1) onto the sample and reflected by its surface to the receiver (L2, D2). In order to reduce the signal noise, a 4% part of the light (beamsplitter BS1, L3, D3) is subtracted (–) and the resulting signal is bandpass filtered (BP). It is displayed versus the magnetising current *I* (frequency up to 200 Hz) of a ferrite C-yoke by a storage oscilloscope (X/Y). The applied field *H* is proportional to *I* and the magnetisation *M* is represented by the amplitude of the photocurrent of D2 (arbitrary units).

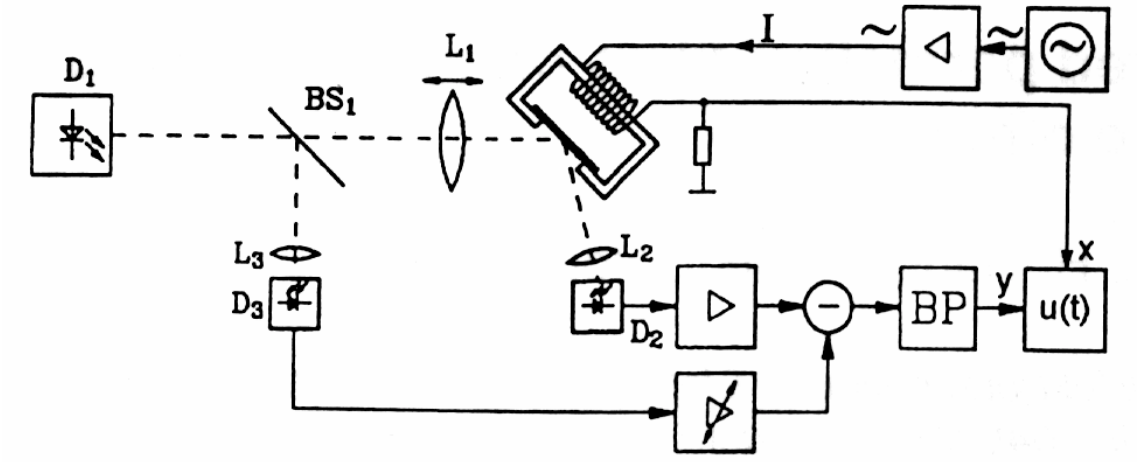

Fig. 2: Set-up for magneto-optical magnetisation curve measurements.

Results and discussion

no.	T_S [°C]	T_T [°C]	Sputter rate [Å/s]	d [nm]	$a_{T\text{-}S}$ [mm]	Δρ [μΩcm]	ρ [μΩcm]	Δρ/ρ [%]
172	41	350	5.1	50	60	0.35	17.14	2.06
173	54	454	4.5	50	60	0.39	15.97	2.47
175	250	560	4.1	50	60	0.40	11.36	3.52
176	74	560	3.8	50	40	0.25	8.02	3.08
177	255	560	3.4	50	40	0.25	6.62	3.73
186	268	560	3.0	50	36	0.23	6.76	3.43

Table 1: Parameters and results for samples sputtered from a melted and rolled NiFe target.

Table 1 shows the parameters and results for some samples, sputtered from a melted and rolled NiFe 81:19 target (purity 99.3%). A sintered target of the same alloy (purity 99.996%) was used for the samples of Tab. 2. The bias magnetic field was H_x = 260 A/m. The substrate material was Si-Si_3N_4 for samples no. 132 – 154, and Si-SiO_2 for samples no. 172 – 186, respectively.

no.	T_S [°C]	T_T [°C]	Sputter rate [Å/s]	d [nm]	$a_{T\text{-}S}$ [mm]	Δρ [μΩcm]	ρ [μΩcm]	Δρ/ρ [%]
132	38	< 44	0.8	50	45	0.14	71.34	0.20
134	150	< 44	0.7	50	45	0.25	63.32	0.26
137	41	< 44	0.7	100	45	0.25	57.88	0.43
138	51	< 44	0.7	150	45	0.31	40.79	0.76
151	100	< 100	0.8	200	45	0.35	36.58	0.96
152	100	~ 100	0.7	50	45	0.17	59.91	0.28
152*	100	~ 100	0.7	50	42	0.61	21,53	2.82
153	265	~ 100	0.7	50	42	0.30	61.46	0.49
154	100	~ 100	0.7	50	42	0.25	51.81	0.49
178	272	560	3.0	50	40	0.17	4.42	3.93
182	238	560	3.1	50	40	0.21	5.79	3.54
184	275	560	2.7	50	38	0.21	5.43	3.78
185	274	560	2.9	20	36	0.16	5.03	3.27

Table 2: Parameters and results for samples sputtered from a sintered NiFe target; the sample 152* has been annealed later at 400 °C.

The results indicate an increasing AMR effect Δρ/ρ with decreasing ρ (as a function of the grain size). A low sputtering rate (0.7 – 0.8 Å/s) yields also a low AMR effect. Both T_S and T_T have a positive influence on the AMR effect. If T_S is about 270 °C, Δρ/ρ is increased by up to 0.5%. The maximum T_T of 560 °C increases the AMR effect by 1% up to 3.93%. The target-substrate distance has been varied between 36 mm and 60 mm,

yielding a change in the AMR effect by ~0.2%. The optimum $a_{T\text{-}S}$ is in the range between 38 mm and 42 mm. The optimum thickness d was about 50 nm. Reducing d to 20 nm, which has often been reported to be the optimum for permalloy, e.g. [4], yields a decrease of the AMR effect by 0.5% (samples 184 and 185).

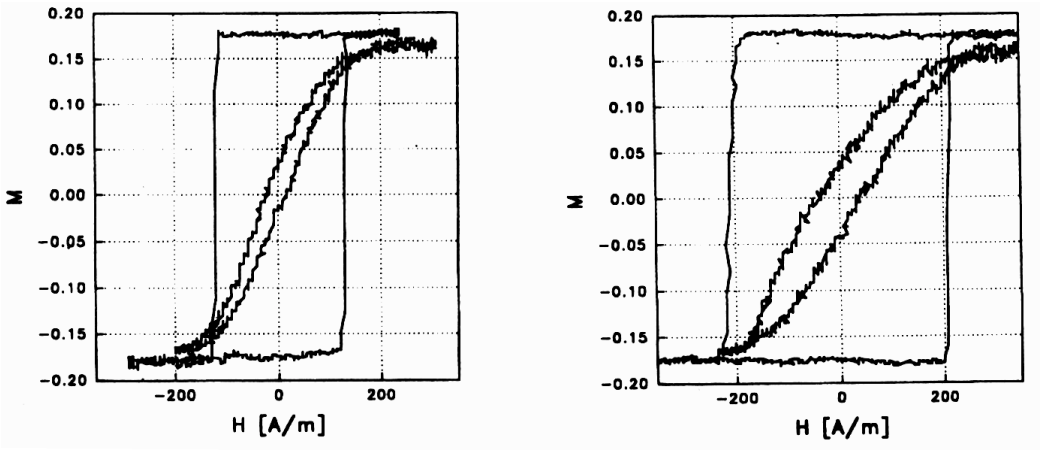

Fig. 3: Magnetisation M (photodetector current, arbitrary units) versus applied field H of sputtered permalloy films, thickness 50 nm (left: sample 184) and 20 nm (right: sample 185).

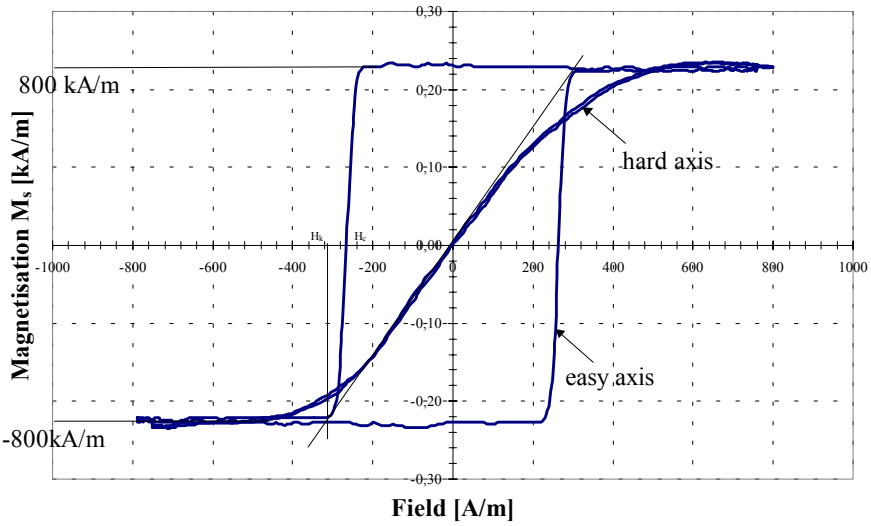

Fig. 4: Magnetisation M (photodetector current, arbitrary units) versus applied field H of sample 186.

The magnetic behaviour also depends strongly on the thickness d. This is demonstrated by the magnetisation curves of the two samples above (see Fig. 3). By reducing d from 50 nm to 20 nm, both the easy axis coercivity and the hard axis coercivity are increasing. For a high sensitivity, the latter value should be near zero. This is demonstrated by sample 186 (see Fig. 4), which shows almost ideal Stoner-Wohlfahrth rotation of the

spontaneous magnetisation. Providing a high $\Delta\rho/\rho = 3.43\%$, this sample is considered to be an optimum AMR sensor material.

Finally, both grain size and orientation have been investigated by atomic force microscopy and the compositions of the sputtered films have been determined by secondary ion mass spectroscopy [2].

Conclusion

A substantial increase of the anisotropic magnetoresistive effect was achieved by increasing both target and substrate temperatures. This is caused mainly by larger grains and a reduced specific resistance of the permalloy film. The magneto-optical characterisation of the samples indicated a good performance for sensor applications due to a low coercivity.

Acknowledgements

The authors are grateful to Prof. W. Fallmann and to Prof. G. Fasching for making these investigations possible. Financial support was provided by Dipl.-Ing. Hans Schiebel Elektronische Geräte GmbH and by the Fonds zur Förderung der Gewerblichen Wirtschaft (FFF) under Grant no. 3/9893.

References

[1] Dibbern, U., Magnetoresistive Sensors in: Göpel W., Hesse J. and Zemel J. N. (Ed.), Sensors. (Volume 5: Magnetic Sensors (vol. Ed.: Boll R. and Overshott K. J.), VCH Verlagsgesellschaft, Weinheim 1989) pp. 341 – 380.

[2] Aigner G., Herstellung dünner Permalloy-Schichten für magnetoresistive Sensoren (Diplomarbeit, Technische Universität Wien, Vienna, 1997) pp. 5 – 49.

[3] Hauser H., Haberl F., Hochreiter J., and Gaugitsch M., Appl. Phys. Lett. **64** (1994) 2448 – 2450.

[4] Song Y.J. and Joo S.K., IEEE Trans. Magn. **32** (1996) 4788 – 4790.

Deposition and Etching of Permalloy

R. Otterbach, U. Hilleringmann

University of Paderborn, FB 14/120, Warburger Straße 100,
33098 Paderborn, Germany

In this paper a technique for realisation of structures with a minimum feature size of less than 100 nm and the chance of its modification for pattern transfer in permalloy films is presented. During the process flow, necessary masking layers are formed utilising the conformity of an LPCVD-deposition. By adaptation of the process flow, this technique was successfully applied for MOS transistors with channel lengths down to 40nm. Likewise diamond paths just as aluminium paths of 100 nm width were realized. Due to the missing dry etching process with sufficient accuracy, the adaptation for pattern transfer in permalloy films is a feasible challenge.

Introduction

For various applications the ferromagnetic property of several transition metals and their alloys has already been taken into account. Especially in the data storage industry and for the fabrication of magnetic sensors and actuators permalloy (NiFe), other Fe-based materials, copper, and cobalt are well established. In consideration of the requirements of each application, exacting challenges for the applied process technology have to be overcome.

For anisotropic magnetoresistive sensors the composition of the applied films dominates the features of the arising sensors. The deposition of these homogeneous films determines several properties of the film, e.g. the specific resistance and the magnetoresistive effect. These sensors require a large magnetoresistive effect to ensure a high ratio of the signal in relation to the operation voltage. Binary or ternary alloys consisting of Ni, Fe and Co are widely used.

All the years round the data storage industry fabricates devices with either decreased geometric dimensions or a distinctly increased data capacity. On the other hand the increasing miniaturisation raises the problem of pattern transfer into the surface of the applied ferromagnetic films with the necessitated accuracy.

Therefore, novel sensor concepts could not evade the increasing miniaturisation of the sensor devices and the associated electrical system. Increasingly selective deposition and wet etching techniques of permalloy films do not provide a sufficient accuracy. Dry etching techniques are not at disposal as well. Hence, novel techniques for pattern transfer into permalloy films have to be developed.

Consequently, the deposition of permalloy films and the pattern transfer determine increasingly an impediment to the development of sensors with improved sensitivity.

Deposition

The deposition of thin films is widely used in process technology. Like several other metals magnetoresistive layers are deposited by vacuum evaporation, cathode sputtering, or electroplating. Although these techniques are widely used in process technology the deposition of magnetoresistive films requires special care. Contamination and variations of the composition have an unfavourable effect on the magnetic properties of the arising film. Especially the amount of oxygen in the atmosphere during the deposition has to be controlled very carefully.

Vacuum evaporation is always taken into account if smooth surfaces have to be covered with a metal layer. Nevertheless, for alloys the composition of the arising film could vary due to a different partial pressure of the components in the atmosphere and inhomogeneous source materials. Therefore in process technology this technique has been established mainly to deposit the metal layer onto the backside of a silicon wafer.

In process technology cathode sputtering is well established. This technique covers even rough surfaces rather conformally with a metal layer. Beside of the application in standard CMOS process, self-adjusting contacts are fabricated in a CMOS process with improved packaging. Therefore, nickel, cobalt and titanium layers were sputtered. Furthermore, barrier layers are deposited by reactive sputtering of TiN. These layers separate the Al/n-Si system of thin diffusions to prevent the effect of spiking. Finally, for special issues aluminium and titanium films are applied for masking layers, e.g. high rate etching of diamond.

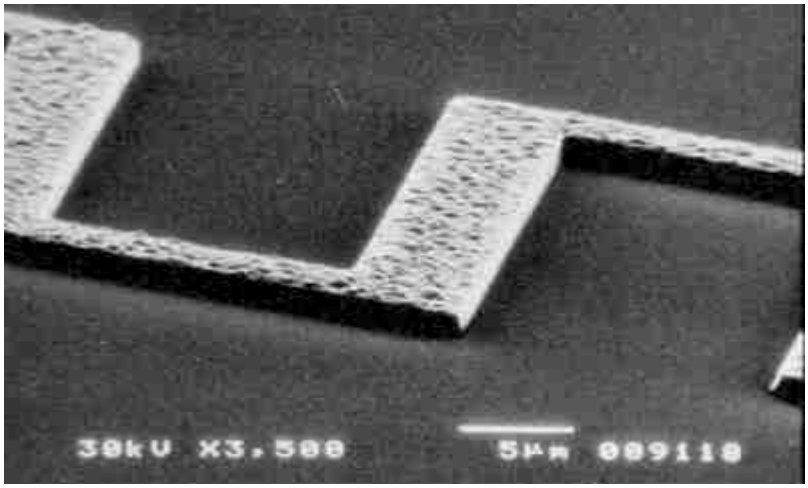

Fig. 1: Copper path fabricated by electroplating and following lift-off.

Copper paths on a silicon wafer have been formed utilising electroplating. Since the removal of copper was not accomplished by reactive ion etching a lift-off technique was applied. Figure 1 depicts a deposited copper path.

Within the scope of the suggested project the LPCVD deposition of metal films utilising metal organics should be analysed as well.

Pattern transfer

Principally two different procedures are available if single structures have to be formed utilising the planar technology. The selective deposition frequently applies structured photoresist layers during the deposition, and the following lift-off step removes the material which adheres to the photoresist. In contrast, selective removal of material is realised by a wet or dry etching utilising an inert masking layer.

Due to a lower accuracy and insufficient resolution in relation to device dimensions, the selective deposition is accomplished dominantly if the removal of material is not possible. Either the incompatibility with prior process steps, the hardness, or the chemical inertness of the applied film prevent the removal of material, e.g. membrane fabrication of diamond-based pressure sensors. For permalloy the selective deposition as well as the wet chemical etching are well established.

Several nickel containing films just as permalloy are etched by H_2SO_4/H_2O_2. During the CMOS process with improved packaging nickel is applied to fabricate self-adjusting ohmic contacts. After spacer formation and ion implantation the metal layer was sputtered. The additional high temperature treatment in a Rapid Thermal Annealing (RTA) apparatus results in a metal silicide at the transition between the doped silicon of drain and source and the nickel layer. In contrast, nickel does not react with silicon oxide. Therefore the metal silicide with distinctly increased conductivity arises only on drain and source of the transistors as well as on polysilicon gates and paths. Finally, the H_2SO_4/H_2O_2 solution removes surplus nickel selectively in relation to nickel silicide. Furthermore, this technique has also been applied utilising titanium or cobalt layers in combination with other wet solutions.

Generally, anisotropic dry etching processes provide an improved accuracy in comparison with wet etching or selective deposition. On the other hand, these processes require volatile products. Since the reaction products of commonly applied etching gases in combination with nickel layers are involatile, dry etching of these films describes a further challenge. Nevertheless silicon, silicon oxide, silicon nitride, diamond, aluminium, titanium, and tungsten have been etched successfully.

Nanometer scale structures

Utilising the conformity of an PECVD deposition, nanometer scale masking layers were formed. These structures were transferred into the layer below. In consequence, structures with minimum feature sizes of less than 100 nm were realised in several materials utilising an anisotropic dry etching process, e.g. an MOS transistor with 40 nm channel length.

Exemplary for the various applications, the process flow during fabrication of an aluminium mask with 100 nm width on CVD diamond is presented. The best conditions for the removal of CVD diamond by reactive ion etching is provided by an O_2/CHF_3 plasma. Due to a distinctly increased adhesion of an aluminium layer on CVD diamond during the final etching process in comparison to silicon oxide or nitride, the substrate was covered with a 200 nm thick aluminium layer first, as depicted in Fig. 3 (a). After pattern transfer the remaining share of the aluminium layer masks the surface of the diamond during the concluding etching step.

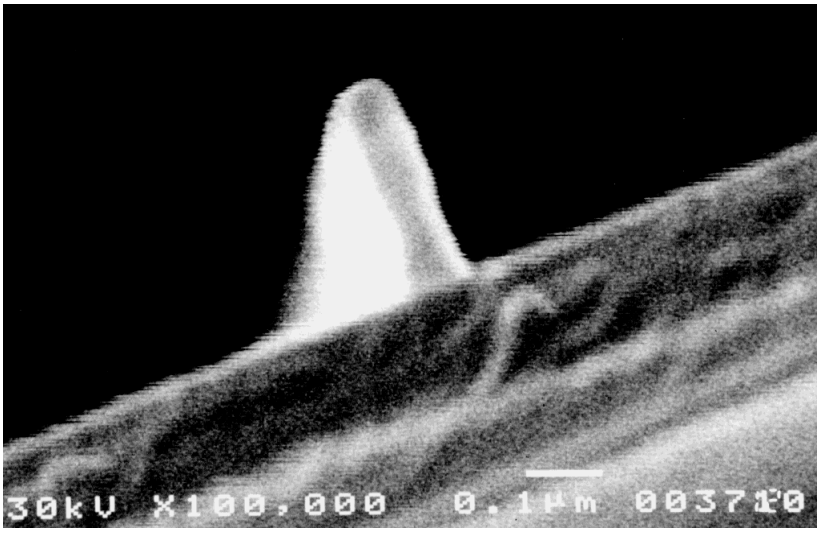

Fig. 2: MOS transistor gate with 60 nm channel length.

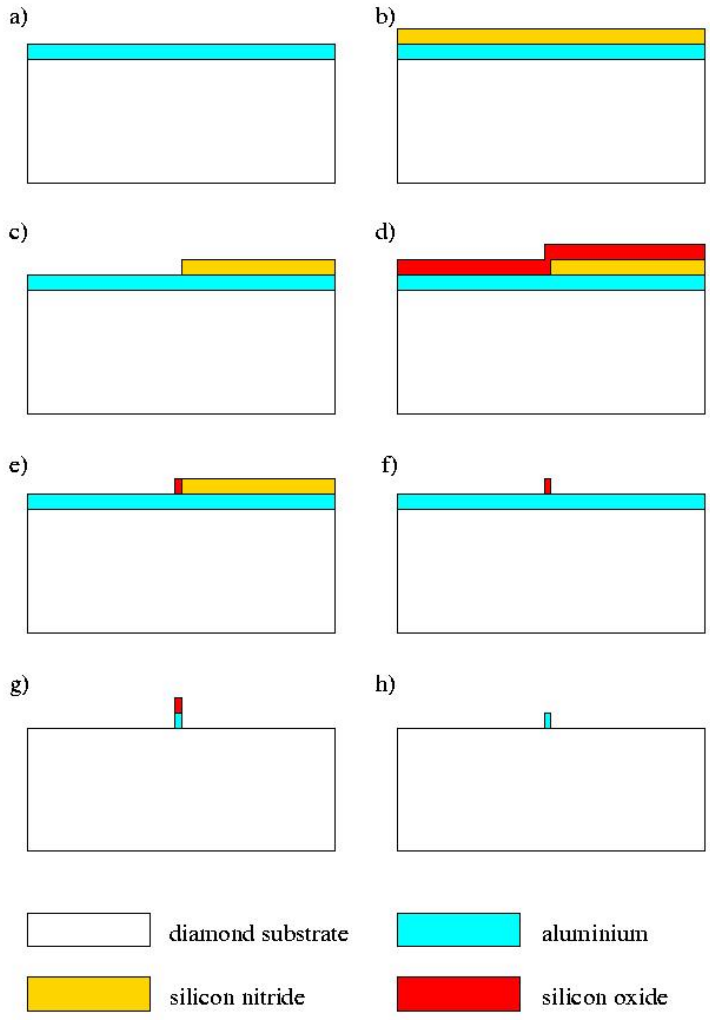

Fig. 3: Fabrication of masking layers for nanometer scale structures.

Standard photolithography provides only an insufficient resolution for the fabrication of structures with a minimum feature size less than 100 nm. To overcome this impediment, a 150 nm silicon nitride sacrificial layer was deposited on top of the aluminium film (Fig. 3 (b)). Due to the temperature limitation by the choice of aluminium this process step has been performed in an PECVD reactor.

Only the location of the arising structures is determined by the following conventional photolithography step. For that purpose the nitride layer was etched anisotropically in a reactive ion etching reactor utilising 25 sccm CHF_3, 3 sccm O_2 and a photoresist mask containing the structures which have to be transferred.

After removal of the remaining photo resist by an oxygen plasma in a barrel reactor, a 150 nm PECVD silicon oxide layer was deposited. As depicted in Fig. 3 (e), the oxide was etched without any mask exactly in the same thickness as it was deposited before, using an anisotropic reactive ion etching process. Due to the conformity of the PECVD process, a thin silicon oxide structure next to the nitride boundary was formed. Consequently, the thickness of the deposited oxide film determines the width of the arising structure.

Furthermore, in the next step the remaining silicon nitride was removed by anisotropic dry etching with a sufficient selectivity relative to the silicon oxide (Fig. 3 (f)). Thereupon the oxide paths must be transferred into the aluminium layer. Since aluminium reacts with surrounding oxygen at its surface, a combined etching process was applied. A low process pressure in the reactor during the first step results in an increased share of physical removal of material due to an increasing bias voltage. This was used to crack the Al_2O_3 surface in an $SiCl_4/Cl_2$ plasma. Since this process provides only an insufficient selectivity relative to oxide, the process parameters were changed after an etching time of 1 minute. Subsequently, the remaining aluminium layer was etched utilising a distinctly increased process pressure of 80 mTorr in comparison to 40 mTorr during the first step and an additional part of CH_4 in the reactive atmosphere. The addition of methane results in an increased anisotropy of the etching process due to an improved passivation of vertical surfaces. Finally the remaining silicon oxide can be removed.

Conclusion

The presented technique for pattern transfer of structures with a minimum feature size of less than 100 nm is already applied successfully. Nevertheless the adaptation for permalloy films raises the problem of pattern transfer. Selective deposition as well as wet etching provides only an insufficient accuracy, dry etching processes with commonly applied etching gases are hindered by involatile etching products. Therefore the development of a novel technique for pattern transfer determines a further challenge.

References

[1] Sensors Vol. 5, Edited by W. Göpel, J. Hesse, J. N. Zemel, VCH-Verlag, 1989

[2] A. Soennecken, U. Hilleringmann, K. Goser: Floating Gate Structures as Nonvolatile Analog Memory Cells in 1.0 µm-LOCOS-CMOS Technology with

PZT Dielectrica, ESSDERC'91, Montreux, Microelectronic Engineering 15, 1991, S. 633 - 636

[3] U. Hilleringmann, S. Adams, K. Goser: Micromechanic Pressure Sensors with Optical Readout and “on Chip” CMOS-Amplifiers Based on Silicon Technology, Microsystem Technologies'94, Hrsg. H. Reichl, A. Heuberger, VDE-Verlag, Berlin, 1994, S. 713 - 722

[4] U. Hilleringmann, K. Goser: Optoelectronic System Integration on Silicon: Waveguides, Photodetectors, and VLSI CMOS Circuits on One Chip, IEEE Trans. on Elec. Dev., Vol. 42, No- 5, 1995, pp. 841 - 846

[5] J. T. Horstmann, U. Hilleringmann, K. Goser: Characterization and Matching Analysis of 50 nm-NMOS-Transistors, ESSDERC'96, Hrsg. G. Baccarani, M. Rudan, Editions Frontieres, 1996, S. 253 - 256

[6] L. M. H. Heinrich, J. Müller, U. Hilleringmann, K. F. Goser, A. Holmes, D.-H. Hwang, R. Stern: CMOS-Compatible Organic Light-Emitting Diodes, IEEE Transaction on Electron Devices, Vol. 44, No. 8, 1997, S. 1249 - 1252

[7] J. T. Horstmann, U. Hilleringmann, K. F. Goser: Matching Analysis of Deposition Defined 50-nm MOSFET's, IEEE Transactions on Electron Devices, Vol. 45, 1998, S. 299 - 306

[8] U. Hilleringmann, V. Mankowski, K. Goser: Chip Size Optically Controlled 12 kV Switch on Silicon, ESSDERC'98, Hrsg. A. Touboul, Y. Danto, J.-P. Klein, H. Grünbacher, Editions Frontieres, 1998, S. 596 - 599

[9] G. Wirth, U. Hilleringmann, J. T. Horstmann, K. F. Goser: Mesoscopic Transport Phenomena in Ultrashort Channel MOSFETs, Solid-State Electronics 43, 1999, pp. 1245 - 1250

[10] R. Otterbach, U. Hilleringmann: High Rate CVD-Diamond Etching for High Temperature Pressure Sensor Applications, ESSDERC'99, Editions Frontieres, Editors: H. E. Maes, R. P. Mertens, G. Declerck, H. Grünbacher, 1999, S.320 - 323

[11] J. T. Horstmann, U. Hilleringmann, K. Goser: Matching Analysis of NMOS-Transistors with a Channel Length down to 30 nm, IECON'99 Conference Proceedings, Vol. 1, San Jose, 1999, S. 23 - 28

[12] U. Hilleringmann: Mikrosystemtechnik auf Silizium, Teubner Verlag, Stuttgart, 1995, ISBN 3-519-06158-9

[13] U. Hilleringmann: Silizium-Halbleitertechnologie, 2. Auflage, Teubner-Studienskripten, Stuttgart, 1999, ISBN 3-519-10149-1

Metal Organic Chemical Vapour Deposition at CNR – ICTIMA in Padua

G. A. Battiston, F. Benetollo, G. Carta, R. Gerbasi, G. Rossetto, G. Torzo, P. Zanella

Istituto di Chimica e Tecnologie Inorganiche e dei Materiali Avanzati (ICTIMA)
Area della Ricerca del CNR, Corso Stati Uniti 4, 35127 Padua, Italy

The ability to obtain a huge variety of thin film materials at low temperatures is the reason of the tremendous expansion of Metal Organic Chemical Vapour Deposition (MOCVD) techniques. Attention has been focused on suitably tailored metal organic precursors to synthesise specific materials. The obtained products are detailed. Oxide thin films (such as TiO_2, ZrO_2, and Al_2O_3) have been deposited either by using new or unusual oxygenated precursors or oxygen free precursors. Metallic films such as platinum, copper, and nickel have also been grown. Some examples of epitaxial semiconductor (III-V) films are reported. Finally, the possibility of achieving a Fe-Ni metal alloy is reported.

Metal Organic Chemical Vapour Deposition (MOCVD) has been shown to be a viable process for the preparation of high quality thin films. Its versatility and the low deposition temperature make the process particularly interesting for industrial applications. Since materials in form of thin films are essential for many advanced technologies, interest and research on MOCVD are continually growing and expanding [1].

The basic step of MOCVD is the decomposition of volatile precursors at a suitable temperature in contact with the substrate on which the desired thin film is deposited while gaseous side products are easily eliminated. The reaction is carried out inside special reactors (thermal, plasma, laser, or photo activated). It is evident that precursors play a crucial role with their peculiar properties:

- Volatility: The precursors must be present in appreciable concentration in gas form inside the reactor in order to assure a fair deposition rate.
- Stability and reactivity: The precursors must be stable both thermally and towards moisture and oxygen to allow easy manipulation. However, they must react under the deposition conditions. Precursors in the liquid phase are preferable (to solid phase) in that they offer more precise control of the evaporation rate than solids because the surface area of a powder cannot be controlled well.
- Purity: This is a crucial requirement especially when electronic grade materials are deposited.
- Environmental compatibility and safety: The precursors should be manipulated without risks for operator safety and environmental contamination.
- Cost: even though reported last, this is a limiting factor for industrial applications.

In recent years synthetic chemistry has been increasingly involved with the aim of producing promising new precursors with tailored properties that have been tested in preliminary research work. The full significance of these efforts cannot be appreciated without a multidisciplinary approach involving the synthesis of precursors, the growth of high quality materials on a large scale, and fundamental studies including thermodynamics, kinetics, chemical engineering, and optimisation of process conditions by using modelling. In this context we have developed our research, and here several recent results will be considered on the following specific subjects.

MOCVD of oxide thin films

Metal oxides form a class of very attractive materials due to the wide range of their technological applications. In principle, their synthesis appears easy and straightforward for the most part of metals even under the MOCVD conditions. The route to the oxides is based on the decomposition of oxygenated compounds (single-source precursors) or on the reaction of oxygen-free metal compounds with oxygenating agents (O_2, H_2O, etc.).

The significant results are summarised in Table 1.

	Precursors	Reactant gas	Source temp.	Growth Temp.	Growth rate	Crystal phase	Ref.
TiO_2	$Ti(OiPr)_4$	O_2	50°C	400°C	~2 µm/h	anatase	[2],[3]
TiO_2	$Ti(OiPr)_4$	N_2, O_2	50°C	120°C Plasma	~1 µm/h	amorphous	[4]
ZrO_2	$Zr[N(C_2H_5)_2]_4$	O_2	30- 60°C	500-580°C	~4 µm/h	monoclinic	[5]
ZrO_2	$Zr[OC(CH_3)_3]_4$	O_2	40°C	350°C	~6 µm/h	cubic	[6]
ZrO_2	$(C_5H_5)_2Zr(CH_3)_2$	O_2, H_2O	70-80°C	400-450°C	~7 µm/h	cubic monoclinic	[7]
ZrO_2-Co_2O_3	$(C_5H_5)_2Zr(CH_3)_2$ $Co(C_5H_5)_2$	O_2, H_2O	70-80°C	400-450°C	~2 µm/h		[8]
ZrO_2-MnO_x	$(C_5H_5)_2Zr(CH_3)_2$ $Mn(hfac)_2THF$	O_2, H_2O	70-80°C	400-500°C	~2 µm/h		[6]
ZrO_2-TiO_2	$Zr[OC(CH_3)_3]_4$ $Ti(O^iPr)_4$	O_2	40-50°C	400°C	1-2 µm/h	cubic	[9]
Al_2O_3	$(CH_3)_2Al(O^iPr)$	O_2	25°C	560 °C	~2 µm/h	amorphous	[10]
Al_2O_3	R_2Al acac R= Me, Et, ^{i}Bu	O_2, H_2O	20-80°C	400-520°C	2-4 µm/h	amorphous	[11]

Table 1: Deposition data of oxide thin films

MOCVD of epitaxial materials

New indium precursors as Et_2InNMe_2 [12] and Me_2InPz [13] (PzH = pyrazole) have been successfully used for MOVPE of InP homoepitaxial layers. The new sources do not present the drawbacks of the conventional $InMe_3$ precursor (high pyrophoricity and high reactivity towards nucleophilic agents), and their lower vapour pressure allows a better control of the epilayer thickness in the growth of MQW structures. Besides, the Me_2InPz has been used in the growth of nanostructures of InP on GaAs substrates obtaining islands of InP with a size distribution peak around 100 nm.

The two-dimensional – three-dimensional transition has been studied for InAs and InP layers grown on (001) GaAs substrates by MOVPE with conventional precursors [14]. The combined use of SFM and RBS allowed the determination of the surface morphology of the samples and of their equivalent layer thickness with a precision better than 0.1 monolayers. The critical thickness for the 2D–3D transition has been found to occur after a deposition of (1.2 ± 0.1) ML for InAs/GaAs, and after a deposition of (2.2 ± 0.2) ML for InP/GaAs, independently of the temperature and of the growth rate. For coverages slightly exceeding 1 ML for InAs, and 2 ML for InP, the surfaces of the samples appear partially covered by small bi-dimensional structures whose dimensions appear to be independent of the system under study and consequently of the misfit.

MOCVD of metallic thin films

Platinum films were deposited at 80 Pa varying the reactor temperature in the range 380 – 420 °C and the sublimation temperature of platinum acetylacetonate ($Pt(acac)_2$) in the range 120 – 180 °C. The molar ratio oxygen/precursor at the inlet was in the 20 – 130 range. The growth rate of 0.4 μm/h above 400 °C was independent from deposition temperatures higher than 400 °C indicating a diffusion limited process. The presence of oxygen led to good-quality metallic films of polycrystalline platinum on all the substrates. The X-ray diffraction patterns always exhibit polycrystalline cubic structure, highly textured in the (111) direction [3].

We prepared new Pt precursors $(C_5H_4CH_3)Pt(CH_2CHCH_2)$ (Methylcyclopentadienyl platinum allyl), complexes of Pt containing methylcyclopentadienyl ($C_5H_4CH_3Pt(CH_3)_3$), and allyl ligands ($C_5H_5PtCH_2CHCH_2$) [15]. Pt deposition was carried out with the first precursor under mild conditions (25 – 30 °C source temperature, N_2 carrier gas, 300 °C substrate temperature). Appreciable growth rate (1.5 – 2.0 μm/h), and a smooth and bright surface were obtained. But the most remarkable feature was the purity of the deposited platinum.

Copper films have been deposited at 100 Pa and 370 °C by using the new precursor $HB(Pz)_3Cu(PCy_3)$ where Pz is pyrazole, and PCy_3 is tricycloexphosphine in nitrogen or oxygen environment; the films resulted homogeneous, adherent to substrate, and without carbon contamination [16]. Traditional precursors as copper(II) acetylacetonate hydrate and hexafluoroacetylacetonate have also been used in oxygen environment either at low or atmospheric pressure MOCVD. The films sometimes resulted carbon contaminated, and the presence of CuO was detected.

Nickel thin films were obtained at 450 °C in N_2 or O_2 environment as polycrystalline films with preferred orientation (111) and little contamination of carbon and nickel oxide by using the new precursor nickel bismethylacetoacetatemethyl [17].

Kinetics and modelling

The control of the film quality is strongly coupled to the control of conditions in the deposition chamber as temperature, gas feed composition, chamber pressure, and gas flow rates. A theoretical study of the kinetics and transport phenomena is the basis for reproducing the desired properties in the film.

Studies of the growth rate were carried out in order to derive the various kinetic control regimes and the corresponding kinetic laws. As an example for the formation of titanium oxide films the developed model considered the occurrence of a heterogeneous reaction in the film formation and a parasitic reaction in the gas phase [18]. It was therefore possible to find the best conditions for high uniformity in the reactor and the correlation between growth parameters and surface properties (Fig. 1).

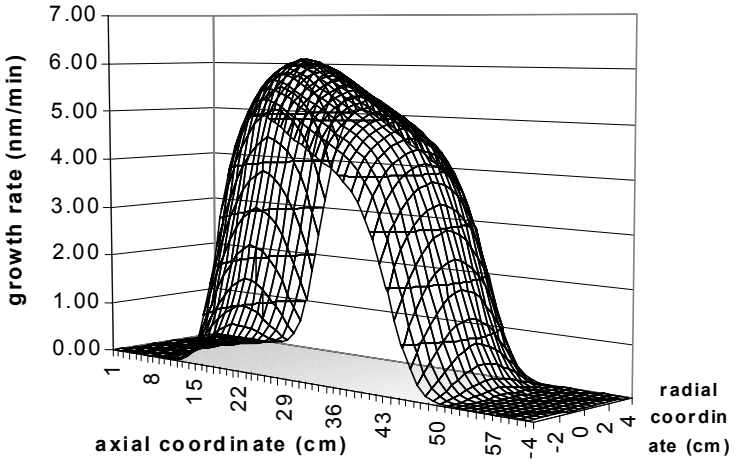

Fig. 1: Growth rate of TiO_2 as a function of position in a reactor pipe with cylindrical symmetry, at 400 °C and 70 Pa.

Optimisation is, in a first instance, a criterion of uniformity regarding some relevant film characteristics, such as thickness, crystallite orientation, adherence, or crystalline phase. Really conclusive results on the optimisation can be achieved only throughout an economic evaluation of the costs on the basis of customer specifications. This kind of evaluation depends on parameters specific of country, man power salary, local law, etc. Also the geometry of reactor plays a fundamental role according to customer requests or process specifications. Modelling is a fundamental step for any economic evaluation. In view of an industrial application, evaluation of costs and economic optimisation of the process have been accomplished [19].

Perspectives of achieving a metal alloy Fe-Ni

As reported in the literature the most promising precursors for Ni deposition are $Ni(CO)_4$, $Ni(dmg)_2$, $Ni(MeCp)_2$, and $Ni(hfa)_2$. Deposition temperature, costs, safety, easy manipulation, growth rate, and a combination of those can steer the choice of a particular precursor.

Precursors for the chemical vapour deposition of iron allow high film purity at temperatures as low as 200 °C. Iron pentacarbonyl $Fe(CO)_5$ was extensively used as precursor with growth rates up to 1 μm/h. Ferrocene $Fe(Cp)_2$ has been studied to a lesser extent because it requires higher deposition temperatures (400 – 500°C) due to its thermal stability.

Only one paper, to our knowledge, deals with co-deposition Fe-Ni via MOCVD. Lane *et. al.* [20] prepared permalloy thin films by using a carbonyl derivative of the two metals as precursors, at atmospheric pressure. The maximum values of magnetoresistance occurred at a composition of about 90% Ni, 10% Fe, and the maximum sensitivity occurred at about 80% Ni, 20% Fe.

The main drawback of Ni-Fe carbonyls is their extreme toxicity that limits their practical use. The design of new volatile precursors of both metals, with comparable chemico-physical properties will be the route to obtain environmentally friendly alloys.

References

[1] a) P. Zanella, G. Rossetto, N. Brianese, F. Ossola, M. Porchia and J.O. Williams, *Chem. Mater.* 1991, **3**, 225.
b) A.C. Jones, P.O' Brien, CVD of Semiconductors, Precursor Synthesis, Development and Applications, VCH, Weinheim, 1996.
c) T.T. Kodas, M. Hampden-Smith, The Chemistry of Metal CVD, VCH Weinheim, 1994. d) M.L. Hitchman, K.F. Jensen, Chemical Vapor Deposition, Academic Press, London 1993.

[2] G.A. Battiston, R. Gerbasi, M. Porchia, A. Marigo, *Thin Solid Films* 1994, **239**, 186.

[3] G.A. Battiston, R. Gerbasi, M. Porchia, A. Gasparotto, *Chem. Vap. Deposition* 1999, **5,** 13.

[4] G.A. Battiston, R.Gerbasi, A. Gregori, M. Porchia, S. Cattarin and G.A. Rizzi, *Thin Solid Films* 2000, in press.

[5] A. Bastianini, G.A. Battiston, R. Gerbasi, M. Porchia and S. Daolio, *Journal de Physique IV, Supplement au Journal de Physique II* 1995, **5**, 525.

[6] G.A. Battiston, R. Gerbasi, and G. Cavinato 5th Italian Meeting on Nanophase Materials, Roma 28-29 October 1999, 63.

[7] S. Codato, G. Carta, G. Rossetto, G.A. Rizzi, P. Zanella, P. Scardi and M. Leoni, *Chem.Vap. Deposition* 1999, **5**, 159.

[8] G. Rossetto et al. in press.

[9] P. Stocco Thesis, University of Padua, 1999.

[10] D. Barreca, G.A. Battiston, R. Gerbasi and E. Tondello, *Mater.Chem*. 2000, *in press*.

[11] G.A. Battiston, G. Carta, R. Gerbasi, M. Porchia, L. Rizzo and G. Rossetto, *J.Phys, IV*, 1999, **9**, 675.

[12] G. Rossetto, R. Franzheld, A. Camporese, M.L. Favero, G. Torzo, D. Ajò and P. Zanella, *J. Crystal Growth* 1995, **146**, 51.1

[13] K. Locke, J. Weidlein, F. Scholz, N. Bouanah, N. Brianese, P. Zanella and Y. Gao, *J. Organometal.Chem*. 1991, **420**, 1.

[14] M. Berti, A.V. Drigo, G. Rossetto and G. Torzo, *J. Vac. Sc. Technol. B* 1997, **15**, 1794.

[15] G. Rossetto, P. Zanella, G. Carta, R. Bertani, D. Favretto and G.M. Ingo, *Appl. Organometal. Chem.* 1993, **13**, 509.

[16] G.A. Battiston, R. Gerbasi, C. Pettinari, A. Drozdov, work in progress.

[17] E. Faggin, Thesis, University of Padua, 1999.

[18] A. Scattolin, Thesis, University of Padua, 2000.

[19] G.A. Battiston, R. Gerbasi, A. Tiziani, A. Figuears and G. Garcia, Mat. Sc. Forum, in press.

[20] P.A. Lane, P.J. Wright, P.E. Oliver, C.L. Creeves, A.A. Pitt, J.M. Keen, M.C.L. Ward, M.E.G. Tisley, N.A. Smith, B.C. Cockaine and H. Harris, *Chem. Vap. Deposition*, 1997, **3**, 97.

Submicrometer Lithography and Pattern Transfer for Magnetic Devices Fabrication

P. Hudek[1], I. Kostic

Institute of Informatics, Slovak Academy of Sciences
Dúbravská 9, SK-842 37 Bratislava, Slovakia

Miniaturisation is an ongoing trend, driven by the insatiable demand for more complex, powerful, and compact micro-devices. Advances in micro-lithography and pattern transfer are critical in supporting this trend. The continuing growth in development of new sensor systems has been the direct result of these improved methods. Lithography is a significant economic factor, currently representing over 35% of the sensor-on-chip manufacturing cost. The intention of this contribution is to inform on the current work in the micro-lithography using high-resolution direct electron-beam writing together with dry plasma pattern transfer processes with associated technologies that are in use in our research institute, including a broad supplementing special micro-processes which can enhance the resulting micro-patterning process.

Introduction

The combination of the tool, resist layer, and the associated process is referred to as "lithography", a term from the Greek, meaning "writing on stone", an ancient art used for engraving, painting, etc. Modern-day micro-lithography is a hybridisation of new and old technologies. These techniques have been perfected over the past 30 years in support of semiconductor device fabrication.

Lithography in microelectronics is a technological process step, in which the patterns are drawn into a recording medium (*resist*) into which the desired device pattern is written (*the mask*) by using photons, electrons, or ions (see Fig. 1). During the process, fine-line relief-patterns are formed into radiation-sensitive thin resist films, which selectively protect an underlying wafer substrate against chemical or physical attack. By exposing the resist-coated wafer the behaviour of the exposed and unexposed resist areas will be differentiated. This allows for easy removal of exposed (Positive-Tone) or unexposed (Negative-Tone) resist regions. The resist relief image remaining on the wafer behaves as a stencil for subsequent processing (etching, metallisation, ...).

From Fig. 1. we can distinguish two main kinds of lithographies. The first kind, such as electron-beam lithography (EBL) and focused ion-beam lithography (FIBL), directly writes the patterns itself. The second kind of lithography, such as photo- and x-ray lithography, copies the pattern from a master („*reticle*" or „*mask*") to a wafer. The second

[1] currently with Leica Microsystems Lithography, Jena (Germany)

kind is called a *parallel system* because more groups of patterns from the mask are copied at once. Only this kind is used in mass production because of its high throughput.

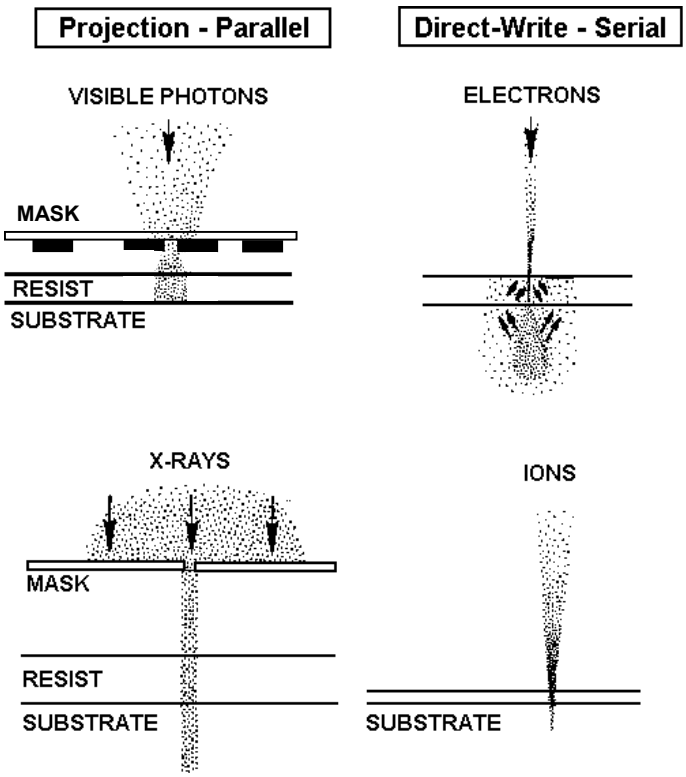

Fig. 1: Lithographic methods using photons (light and x-ray), electrons, and ions.

In our laboratory we use the most flexible direct-write electron-beam lithography technique in creating high resolution microstructures.

One of the most serious challenges to extending lithography by whatever radiation into the submicro- and nanometer regime is the mask manufacturing technology. Lithography is recognised as the key technology pacing the evolution of microelectronics and the introduction of nanoelectronics. As device design rules continue to shrink, on-mask patterns must experience a corresponding reduction in size. This need, coupled with the demand for improved Critical-Dimension (CD) uniformities, requires the use of an alternative lithographic method which allows to delineate the desired patterns on a substrate. Lithography is a technology with heavy global interdependence for equipment and materials.

The key elements of the micro-lithography infrastructure include:

- Exposure equipment (concepts, design, construction, and performance);
- Resist materials and processing equipment (masking layer needed to delineate the circuit level);
- Mask and mask equipment and materials, technology, and processes;
- Mask metrology and inspection equipment for CD and overlay, repair equipment.

Current Status: R&D and application possibilities in the laboratories of the Institute of Informatics of the Slovak Academy of Sciences

The laboratory of Electron-Beam Lithography (EBL) and microfabrication exists since 1980.

Maintaining and improving our clean room (ca. 200 m^2 down to class 1000 – 100, and better in local small areas) and equipment is also of a high priority during the course of our projects.

Our R&D team is involved in several research projects and was awarded international research grants by the East-West-Funds of the Austrian Academy of Sciences and by the European Community. The projects are closely linked with our technology efforts and with the good collaboration with foreign universities and research institutes from Austria, Germany, Greece, Italy, Poland, Czech Republic, Russia, and USA. Most of them are in the field of Microsystems Technology (MST).

The basic tool of the laboratory is a high-resolution *Variable-Shaped Electron-Beam Lithography System* (Electron-Beam Pattern Generator) with 30 kV accelerating voltage and 50 nm minimal shot size. This system has been systematically modified and improved by our own additional soft- and hardware components.

The R&D activities in the lithography and pattern transfer techniques into/onto the substrate material are oriented towards the development of reproducible and conformal patterning in micro-, submicro- and nanometer mask-structures for the creating of new microelectronic devices and multifunctional microsystems. According to the individual requirements the department develops and establishes know-how-oriented e-beam direct-write techniques and micro-processes to obtain high-resolution and high aspect ratio resist structures for deep anisotropic pattern transfer into the substrate material by using dry selective etching.

This facility supports R&D in the fabrication of new devices by:

- Fabrication of chromium master masks and reticles for conventional and deep-UV projection photolithography;
- Maskless Direct-EBL of multilayer submicro- and nanometer structures on semiconductor (bulk or membrane) wafers and/or Mix-and-Match lithography;
- Assistance and data generation for the design of new non-conventional microdevices;
- Fabrication of special (non-orthogonal and smooth curved) patterns and gratings for R&D by using newly developed chemically amplified resists in one single layer for deep dry pattern transfer into the substrate (SiO_2, Si, Nb, GaAs);
- Dry selective plasma (cryo-) etching techniques, and plasma processing of substrates;
- Thin film deposition techniques — special sputtering and evaporation processes.

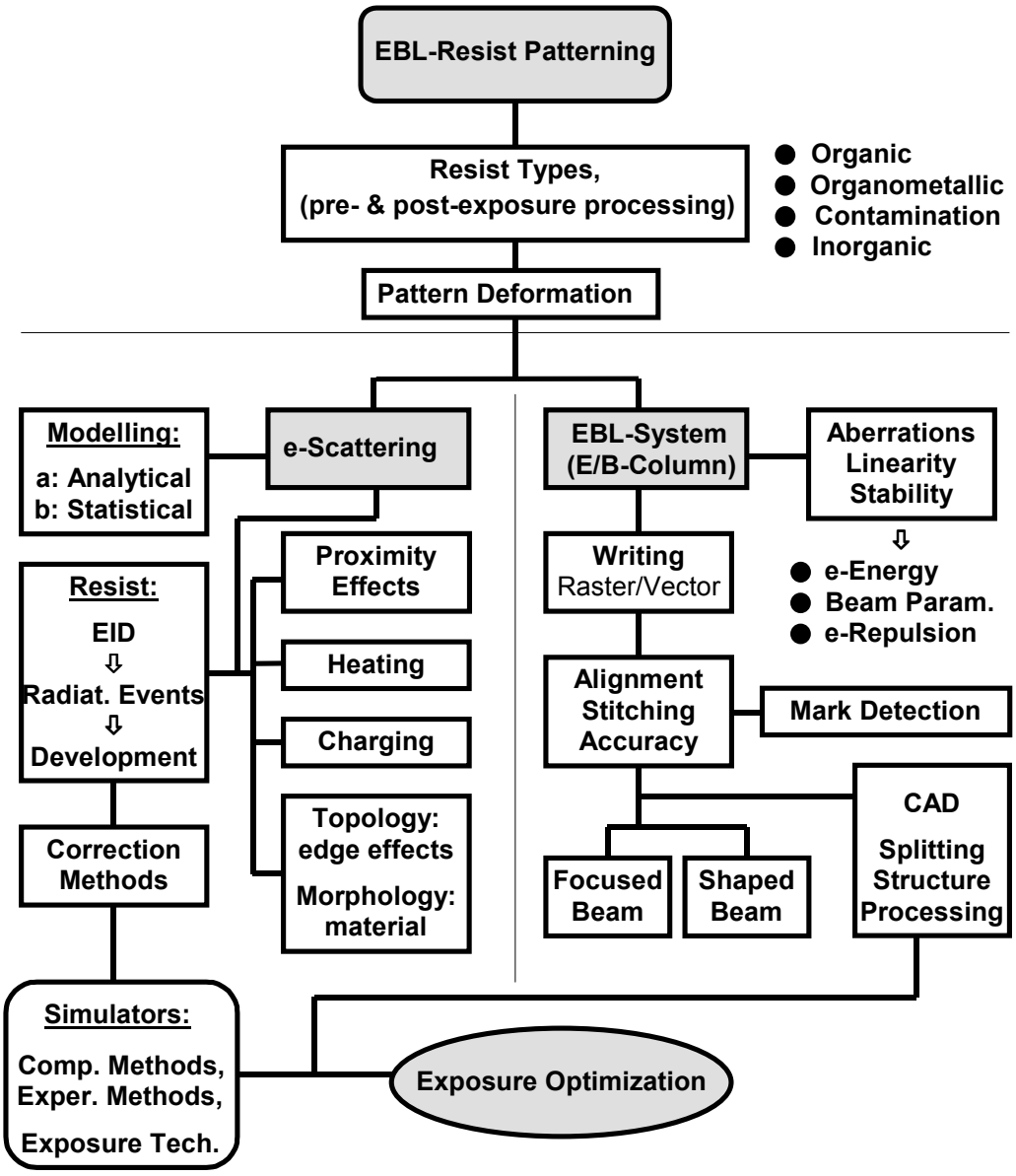

Fig. 2: Process flow of the physical and technical problems to solve for the optimisation of the e-beam exposure process to get conformal micro-patterning with minimal pattern deformation.

Within the field of the mentioned activities the research problems of our research team are as follows:

- Study and application of the theoretical and practical problems concerning the e-beam writing together with correction of the most of all pattern distortions as are proximity, local heating, and charging effects caused by the electron scattering in the substrate material (see Fig. 2);
- Methods of the technological treatments of thin-electron sensitive films (resists) before and after optimal exposure;

- Estimation of the main lithographic parameters of new and commercial (single and/or multilayer) resist systems for micro- and nanolithography;
- Inspection and measuring methods of resulting high-resolution submicro- and nanometer 3-dimensional relief structures;
- Special deposition techniques (patented and know-how-oriented) with determination of residual stress in layers also on the top of thin membranes (for example carbon layers) on large-area Open-Stencil Masks).

The process mask (creation of primary patterns into the resist)

Resists are materials used in the microtechnology to delineate patterns on the surface of a silicon wafer or other suitable substrates during the lithographic step. The resist layer is a film coating (organic, inorganic, organometallic, contamination) on top of the substrate whose chemical properties are radically altered by exposure to the suitable recording radiation. The resist must be capable of forming uniform pinhole-free films on a substrate by simple processes such as spinning, dip coating, or spraying. Requirements for resist strongly depend on the radiation sources of the lithography used and technological processes. Usually only *polymeric / organic materials* fulfil these requirements.

The exposure changes are created by a modification of the chemistry (chemical bonding) in some of the components of the resist. The goal of exposing a resist is to use a spatial variation in exposure energy (the aerial image) to create spatial variation in resist dissolution properties. The pattern in resist film is created in the development process after the exposure. For a *Positive Resist*, exposed areas become soluble (chain scissions of the irradiated polymer) in the developer while the unexposed areas remain insoluble. For a *Negative Resist* only the exposed areas remain on the wafer (cross-linking of the polymer chains), and the whole unexposed film will be removed in the development process.

In the early years of micro-lithography, the resist materials investigated were primarily Poly-Methyl-MethAcrylate (PMMA) and related polymers that undergo main chain scission upon irradiation (Positive Tone). Although the high resolution capability of this short-wavelength imaging technology was demonstrated, the low sensitivity and poor dry etch resistance precluded the manufacturing use these of PMMA-based resists.

Chemically Amplified Resists (CARs):

Key in the development of DUV lithography was the development of a new class of materials, the *Chemically Amplified Resists* (CARs). The new design, termed *chemical amplification*, involved the preparation of an acid reactive polymer, formulated with an "onium salt" Photoacid Generator (PAG). The critical feature is that the acid-labile group attached to the polymer would react with the photo-generated acid in such a way that a new molecule of acid would be generated, thus beginning a catalytic cycle. Thus, a molecule of photo-generated acid might produce 500 – 1000 chemical reactions (deprotection/deblocking steps).

CARs with new imaging mechanism have higher efficiency (fast photospeed) and dry etching resistance against the plasma-based pattern transfer processes. On the other hand, this new mode of lithography is paid for by increased processing complexity and also often by difficulties in CD control.

For *positive* CARs, formation of an environmental contaminated solubility surface layer causes the so called "*T-Top*" profiles, or "*Filling*" and "*Bridging*" effects (see Fig. 3).

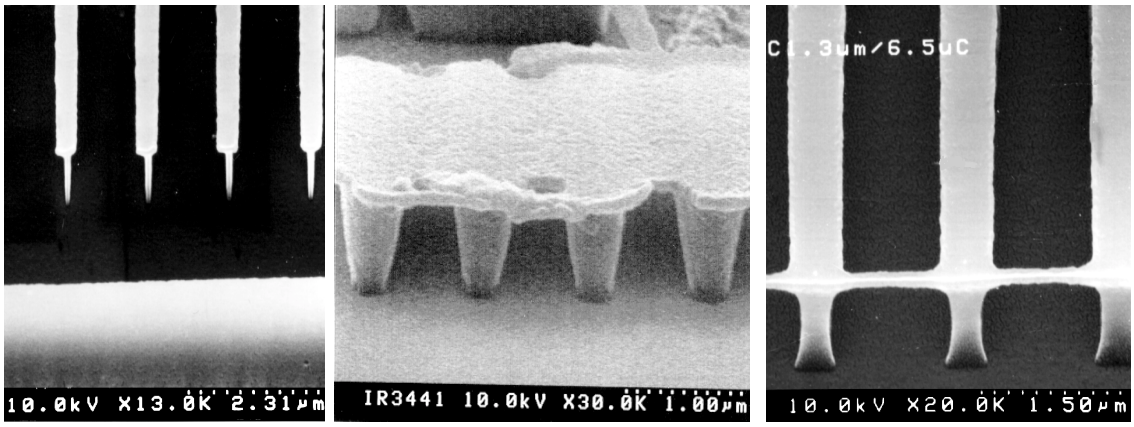

(a) (b) (c)

Fig. 3: SEM micrographs of more or less surface contaminated CARs after electron-beam exposure and post-processing: (a) "T-top" profiles of fine-line high aspect ratio (~ 20), (b)"Filling" and (c) Bridging" of resist patterns due to resist surface dissolution retardation effects in a DUV CAR

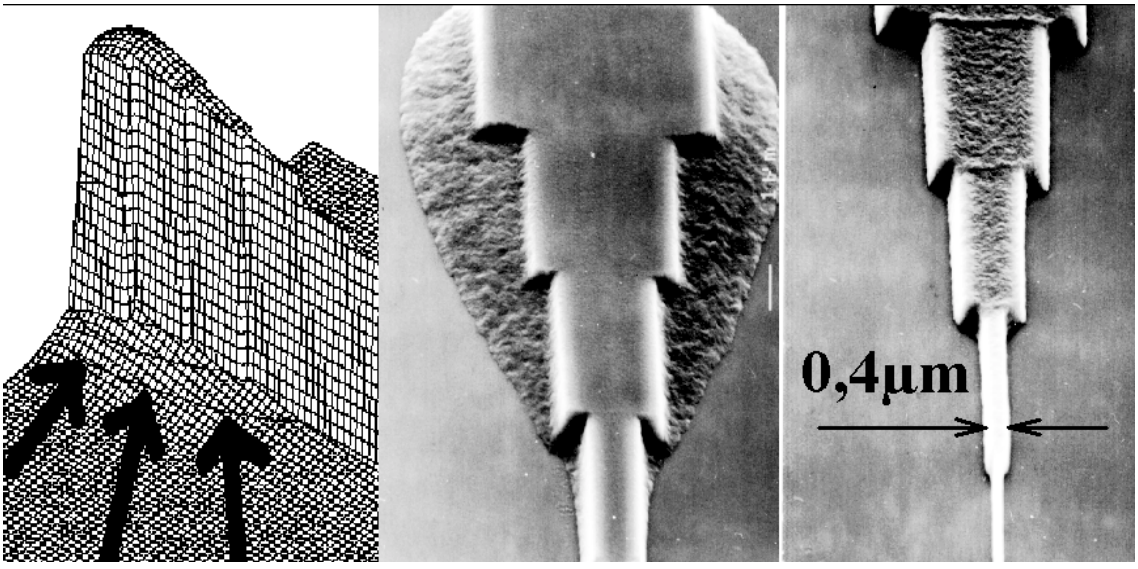

(a) (b) (c)

Fig. 4: Effect of gel formation in negative-tone CAR after EBDW lithography.
(a) The modelling shows a heightened outside exposure intensity (arrows).
(b) Resist pattern with residues around the overexposed region (gel).
(c) Corrected exposure of the same pattern.

Common to various recently emerged CARs is the *short lifetime* of the coated substrate prior to the exposure (shelf life). Most obvious problems connected with practical use of commercially available CARs are not only in discrepancies observed between the designed and obtained resist geometries (pattern dependent phenomena — proximity effects) but also in instabilities in the delay times between the resist exposure/processing periods.

In case of *negative* CARs the problems are connected with a gel formation effect at the resist-substrate interface (Fig. 4). It has been shown that these effects strongly deteriorate the resist pattern quality.

The new generation of DUV resist technology, ESCAP (Environmentally Stable Chemically Amplified Photoresist), currently being explored and introduced offers improved lithographic parameters along with significant enhancement and environmental stability.

Technologists are often interested in dry etching directly through a *single resist layer* (without additional top-surface imaging or multilayer techniques) deeply into the substrate; thicker resist film with vertical side walls of resist patterns are required then. It means that CD control requires here a high conformity not only in the lateral, but also in the 3rd (vertical) dimension along the relief contours. Therefore such deep submicrometer patterning in resist layers often resulted in features with high aspect-ratio (Fig. 5).

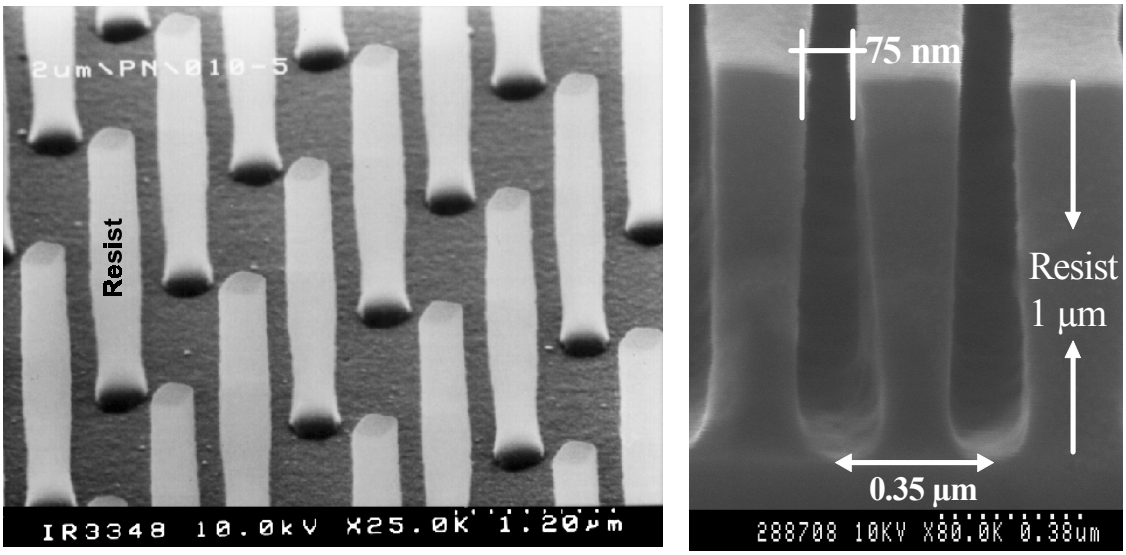

(a) (b)

Fig. 5: High aspect-ratio 3D patterns drawn by EBDW into relatively thick single-layer positive- and negative-tone CAR films. (a) AZ-PN 114 (Hoechst) Negative CAR patterns with an aspect-ratio of >15 and nearly vertical sidewalls (the diameter of pillars ~150 nm); and (b) sub-100 nm lines in 1 µm thick positive-tone UVIIHS (Shipley) CAR.

CARs that combine chemical amplification with more transparent resin material have recently demonstrated high resolution in the range of 0.17 µm to 0.25 µm with exposure doses below 25 mJ/cm^2 in the DUV.

Polymers with alicyclic groups are sufficiently transparent at 193 nm and have reasonable plasma-etch resistance. However, these resins in their "pure state" suffer from high hydrophobicity and adhesion problems. The improvements of these and other properties tend to decrease the plasma etch resistance significantly below that of Novolak-based resists. SL alicyclic polymer resists with acceptable adhesion and development parameters may not show etch resistance superior to that of the aromatic resins.

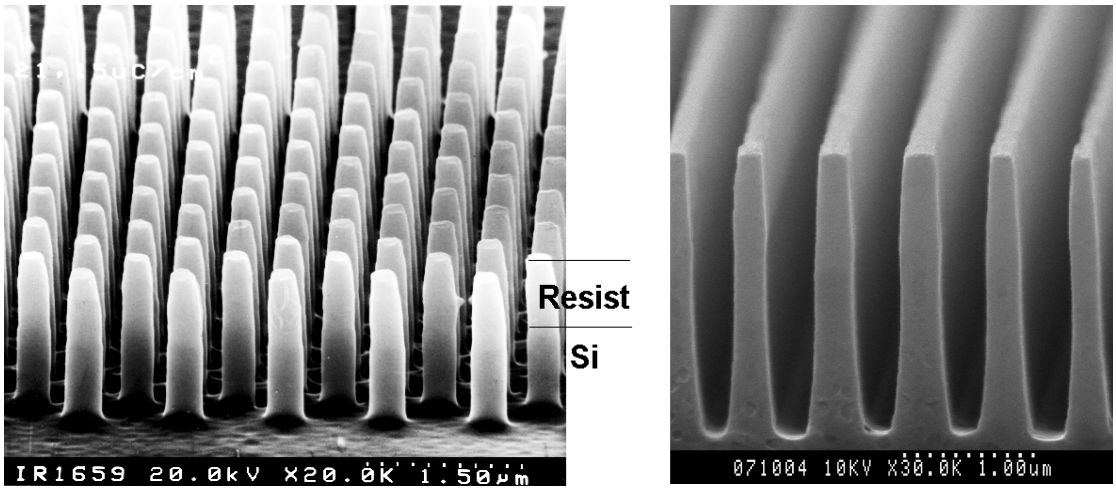

(a) (b)

Fig. 6: Transferred single-layer resist patterns using Reactive Ion Etching (RIE) into the substrate. (a) Fabrication of silicon "pillars" using the resist-mask from Fig. 5 (a). (b) Single-layer UVIIHS resist lines RIE-transferred deeply into SiO_2.

Pattern transfer using dry etching processes

Protecting well-defined regions of the substrate from all subsequent micro-technological processes is the primary purpose of resists, and thus the resist erosion/etch rate is a key parameter. The variety of substrate materials requires a number of different etch chemistries (too many to test on all developmental resists). Lithographic aspect ratios and other issues require that resist films be thinner (about 0,5 – 0.6 µm) for sub-200 nm devices. This, in turn, requires either greatly improved etch processes, or improved etch resistance of the resist, or both. Thus, excellent plasma etch resistance (preferably even better than earlier resist formulations) is a critical feature for realistic sub-200 nm resist formulations.

Summary: Patterning of thin ferromagnetic films

The high-resolution and reproducible patterning of thin ferromagnetic films requires precisely established dry-plasma-based etching through a multilayered masking system lithographically prepared by direct e-beam writing on the substrate, or by projection using photolithography. There are more possibilities how the primary resist-relief pattern could be transferred into the ferromagnetic layer. The etching mask should be a non-polymeric "hard mask" here (for example a pre-patterned aluminium thin film). The

hard mask will be patterned also by plasma etching through the primary single-layer polymer resist mask. The selective plasma etch process of the ferromagnetic layer is not established yet and will need an experimental phase. The required experiments can be carried out in our RIE/ECR plasma reactor made by Roth & Rau, Inc. (Germany), using Cl/F reactive process gases at higher temperatures, or using Ar/O_2 ion milling through a hard mask. A complementary process could be a "lift-off" of the deposited ferromagnetic thin film through a properly prepared and patterned resist relief mask having slightly undercut/retrograde profiles.

Magnetic Thin Film Sensors for Non-Destructive Evaluation

F. Schmidl, S. Wunderlich, S. Müller, A. Förster, L. Dörrer, S. Linzen, F. Schmidt, G. Kaiser[1], S. Lösche[2], O. Hesse[3], P. Seidel

Institut für Festkörperphysik, Friedrich-Schiller-Universität Jena, Helmholtzweg 5, D-07743 Jena, Germany

[1]ILK Dresden, FB Kryotechnik, Bertholt-Brecht-Allee 20, D-01309 Dresden, Germany

[2]Poly-Optik GmbH, Obere Marktstraße 3, D-07422 Bad Blankenburg, Germany

[3]IMG gGmbH Nordhausen, An der Salza 8a, D-99721 Nordhausen, Germany

The detection of magnetic signals in non-destructive evaluation (NDE) required in recent years a continuous improvement of the sensor sensitivity down to the pT range. The magnetic field sensors should exhibit this extreme sensitivity also at frequencies below 100 Hz. This sensitivity requirements were reached with high temperature superconducting sensors based on rf- or dc-SQUIDs (Superconducting Quantum Interference Devices) operating in unshielded environments [1] – [4].

We have developed different types of planar high-T_C dc-SQUID gradiometers on 10 x 10 mm^2 bicrystal substrates for our investigations [5]. Dependent on the field of application we can use gradiometers with adapted widths of the incoupling antennas (Fig. 1 (a)). We can tune the sensitivity of our sensors by two orders of magnitude by the explained variation of the antenna size as well as by a variation of the dc-SQUID inductance between 30 pH and 200 pH. Both methods make it possible to achieve a sufficiently high gradient field resolution of about 310 fT/(cm√Hz) in the white noise region and 700 fT/(cm√Hz) at 1 Hz in shielded environment at 77 K. Moving our sensor system into an unshielded and highly disturbed industrial environment we were able to achieve comparable results in the white noise region but an increased value of the field gradient resolution at 1 Hz with a value of 3 pT/(cm√Hz). For the operation of superconducting magnetometers we need a slew rate of the SQUID electronics of up to 10^7 Φ_0/s. This is one reason why SQUID magnetometers with effective sensing areas of the superconducting antennas above 0.1 mm^2 are mostly used for investigations in electrically and magnetically shielded rooms. Gradiometer concepts for the superconducting antennas allow the suppression of disturbances from far magnetic or electromagnetic sources. Their application usually applies larger effective areas of the gradiometer sensors. It is possible with this kind of sensor (gradiometer) to operate in an unshielded environment with reduced demands on the slew rate of the sensor electronics with values of 10^6 Φ_0/s and with a relatively small bandwidth of several kHz. Dc-SQUID mag-

netometers or gradiometers are often used in *Flux Locked Loop* (FLL) mode [6] for optimal operation. This operation mode reduces the dynamic range of this type of superconducting sensor especially in a highly disturbed environment and makes it difficult to integrate different sensors very close in an array configuration. Parasitic superconducting areas are the source of additional disturbances in such a sensor configuration, but it should also operate in an unshielded environment in the case of perpendicular fixed sensors.

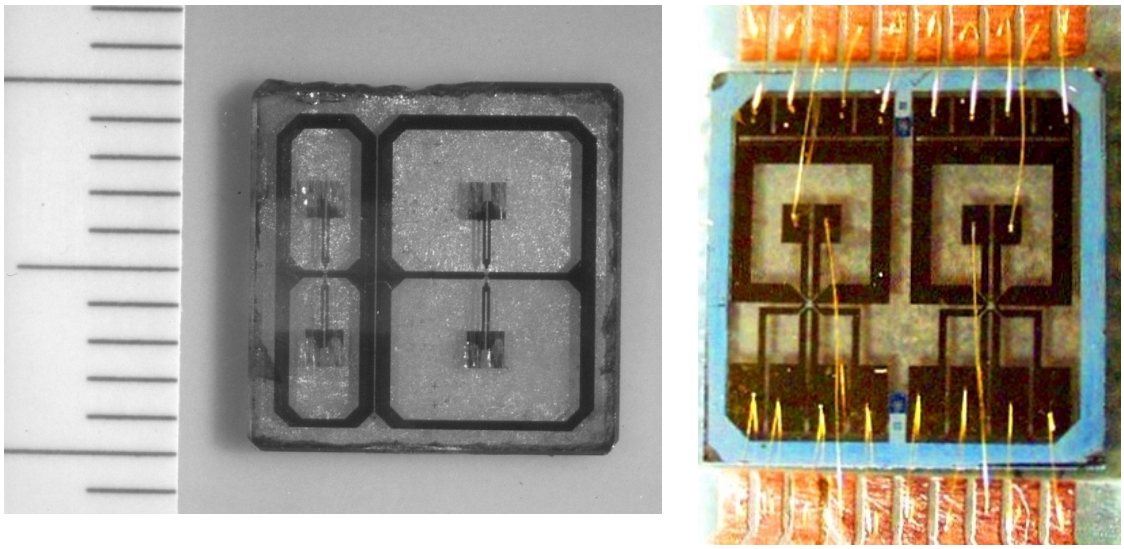

(a) (b)

Fig. 1: (a) Picture of a planar galvanically coupled High-T_C dc-SQUID-gradiometer for non-destructive testing on a 10 x 10 mm^2 bicrystal substrate. (b) Picture of a High-T_C-Hall magnetometer with superconducting antennas on a 10 x 10 mm^2 $SrTiO_3$ substrate.

The combination of superconducting antennas with other thin film sensors, based on Hall effect [7], magnetoresistive, or ferromagnetic materials [8], delivers several advantages for sensor applications (Fig. 1 (b)). The operation of combined sensors at 77 K can increase the sensor performance by a factor of about 100. This behaviour of combined (hybrid) sensors gives additional features for sensor applications. Arrays of robust and high sensitive magnetic field detectors allow the fast investigation of large area materials. The linear output characteristics of such sensor elements reduce the demands on the sensor electronics. It also makes possible the integration of the sensor electronics in the cooled part of the test equipment. Such a multi-channel NDE-system can operate with a specially developed small cryocooler [9].

We apply the magnetic field sensors in a scanning system for investigations in non-destructive evaluation. This system consists of a x-y-computer controlled positioning system, a fibre composite liquid nitrogen dewar for sensor cooling (necessary in the case of partially superconducting sensors), and sensor electronics, see Fig. 2 [10]. The positioning system allows a scanning area of 600 mm in x-direction and 400 mm in y-direction for a sample weight of about 10 kg with a positioning accuracy in the µm range. A special sample holder and the additional scanning program allow the sample motion in x- and y-direction as well as the sample rotation for investigation of symmet-

ric sample geometries. The maximum speed in the order of 30 mm per second enables the application of this system for NDE investigations in industrial quantities. Close to the sensor this experimental set-up is very sensitive for magnetic fields especially in unshielded environment. On that basis the whole scanning system is made of non-metallic and nonmagnetic materials. The motion of our DC-motors is translated by a system of ceramic rods to the sample which is moved under the cooled sensor in a fixed position to avoid electromagnetic disturbances from the DC motors (Fig. 3).

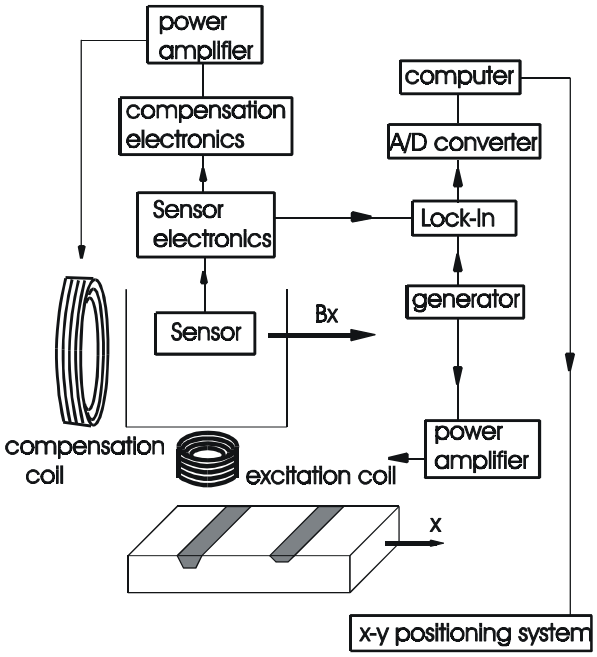

Fig. 2: Scheme of a system for non-destructive evaluation.

Fig. 3: Picture of our measurement system with dewar.

This system allows the detection of magnetic impurities or the application of eddy current techniques. The measured spatial resolution of the system limited by the warm-cold distance of the used dewar and the sensor position inside the dewar amounts to 2 mm.

The dewar allows the operation of superconducting sensors, and it also allows the cooling of other magnetic field sensors for comparison measurements of the sensor performance.

In our measurement system it is also possible to determine the effective area of our sensors experimentally [11]. We use for this sensor calibration a line-scan over a copper wire with the current flowing perpendicular to the scan direction measured at different distances and currents through the wire. From these calibration measurements we calculate the effective area of the sensor used especially in the case of complex geometries of the antenna structures. Based on these and additional noise measurements in shielded and unshielded environments we have an excellent method for the determination of the field sensitivity (magnetometers) or gradient field sensitivity (gradiometers).

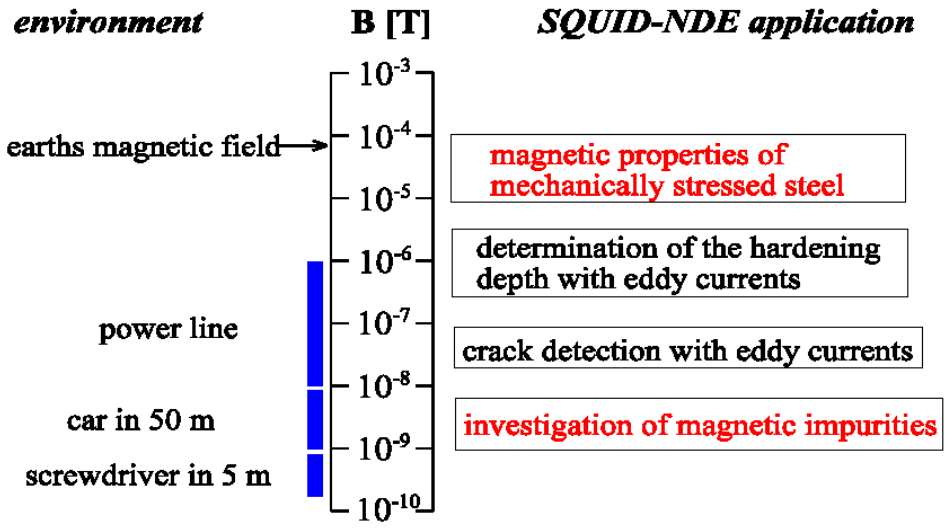

Fig. 4: Magnetic field strength of environmental disturbances compared to possible industrial applications in NDE with magnetic field sensors.

Figure 4 shows possible fields for industrial applications of magnetic field sensors and compares the required field resolution with typical environmental disturbances. The determination of weak magnetic signals in a background field, being several orders of magnitude higher, requires a special sensor layout as well as a sensor electronics which incorporates sensor control and methods for the compensation of permanent magnetic fields.

NDE applications often require less sensitivity compared to SQUID-based sensors but improved sensitivity compared to commercially available Hall detectors or magnetoresistive sensors, especially with respect to the behaviour in the low frequency noise region.

The investigation of weak magnetic signals in the field of NDE can be separated into two types of measurement, the measurement of weak permanent magnetic fields, or the measurement of ac-magnetic fields, for instance induced by an eddy current technique.

As an example for the detection of weak permanent magnetic fields we investigated hardened intake valves for motors of car engines (Fig. 5). The valves were inductively hardened at the first 20 mm of the cylindrical shaft. This hardening process produces a change in the permanent magnetisation of the material as well as a change in the permeability of the material. Line scans with additional rotation of the valves give a typical correlation of the gradiometer signal (magnetic field gradient) and the hardness of the investigated part of the valve. We can demonstrate clear differences between regular and less hardened valves on the basis of investigations of about 100 samples [12]. Another example is the location of magnetic impurities or magnetic markers in nonmagnetic materials with the intention of quality management, for instance in the treatment of nonmagnetic and multi-layered materials. The signal magnitude of several nT/cm, measured in an industrial (disturbed, magnetically unshielded) environment, extends the field of possible applications for superconducting and hybrid devices [13].

Fig. 5: Picture of a car intake valve

An eddy current technique allows to measure the response of the investigated sample leading to a signal in the sensor. The detected signal is not only a function of the frequency f of the eddy currents but also dependent on the relative permeability μ_r of the sample under investigation. The formula for the determination of the skin depth s (σ is the conductance and μ_0 the influence constant) indicates this fact:

$$s = \frac{1}{\sqrt{\pi \cdot f \cdot \sigma \cdot \mu_0 \cdot \mu_r}}$$

Figure 6 shows the measurement with a superconducting sensor for four different hardening depths of steel plates. The smallest hardening depth acts as a reference by which the other experimentally achieved data (three different depths) were modified. The two lines on the steel plates were hardened by electron beam with a depth between 0.4 and 1.5 mm. On the first line the hardening depth was varied, and the second line has the same depth and acts as a reference for these experiments. Under the dewar the excitation coil for the eddy currents is placed in a position where the superconducting sensor does not detect the excitation field of the coil (fixed frequency of about 1270 Hz) but the response of the steel sample. The correlation between hardening depth and measured magnetic field can be seen clearly. This result indicates that it is possible to use sensitive superconducting sensors for eddy current techniques on samples with high permanent magnetisation. In this special case a compensation technique was used. The main field of the application of superconducting sensors, i.e. measurements at low frequencies and with high sensor sensitivities, requires the additional use of compensation methods for the permanent magnetic field of the hardened material. First investigations with compensation techniques lead to a suppression of the permanent magnetic fields by a factor of 72.

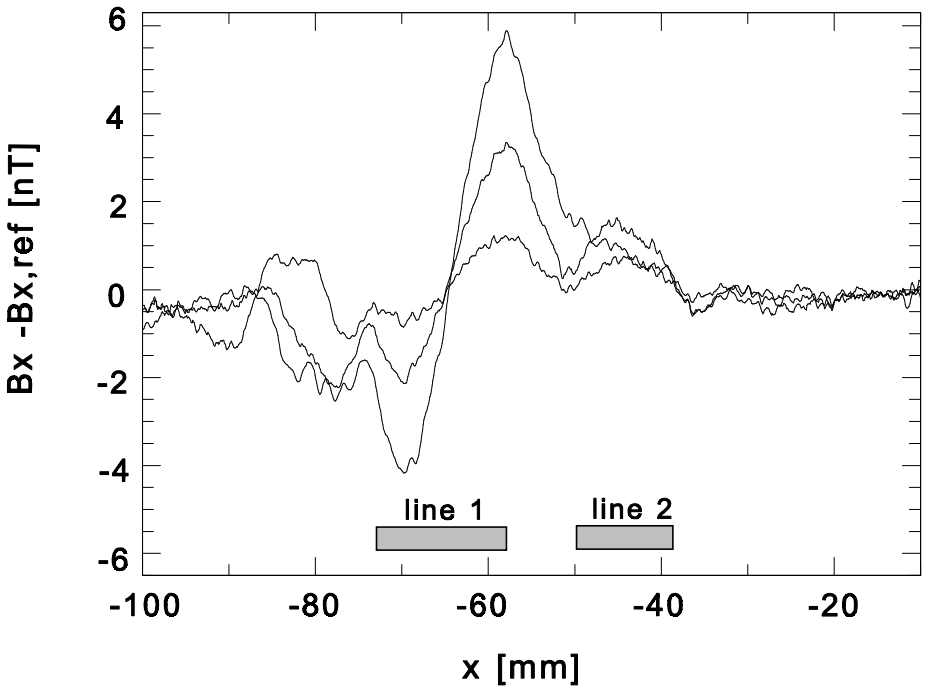

Fig. 6: Measured signal of steel plates with different hardening depths in line 1. (The amplitude increases with increasing hardening depth.)

Acknowledgements

We like to thank C. Steigmeier, U. Hübner and T. Vogt for their contributions to this work.

Partially supported by German BMBF (contract Nos 13 N 6808A, 13 N 7496 and 13 N 7497).

References

[1] D. Kölle, R. Kleiner, F. Ludwig, E. Dansker, John Clarke, High-transition-temperature superconducting quantum interference devices, Rev. Mod. Phys. 71, 631 (1999).

[2] H. Weinstock and R.H. Welsh, SQUIDs for nondestructive evaluation (NDE): A Review and a Callenge, Superconducting industry, Fall 1997, 23.

[3] A.I. Braginski, Superconducting Electronics Coming to Market, IEEE Trans. Appl. Supercond. 9, 2825 (1999)

[4] S. Wunderlich, F. Schmidl, H. Specht, L. Dörrer, H. Schneidewind, U. Hübner, P. Seidel, Planare gradiometers with high-TC DC-SQUIDs for non-destructive testing, Supercond. Sci. Technol. 11, 315 (1998)

[5] P. Seidel, L. Dörrer, F. Schmidl, S. Wunderlich, S. Linzen, R. Neubert, N. Ukhansky, S. Goudochnikov, Superconducting sensors for weak magnetic signals in combination with BiCMOS electronics at 77 K for different applications, Supercond. Sci. Technol. 13, 537 (2000).

[6] R.H. Koch, John Clarke, W.M. Goubau, J.M. Martinis, C.M. Pegrum, D.J. Van Harlingen, Flicker (1/f) noise in tunnel junction dc SQUIDs, J.Low Temp. Phys. 51, 207 (1981)

[7] G. Kaiser,S. Linzen, H. Schneidewind, U. Hübner, P. Seidel, First experimental investigations on thin film Hall magnetometer with a high temperature superconducting pick up antenna, Cryogenics 38, 625 (1998)

[8] G. Kaiser, M. Thürk, P. Seidel, F. Dettmann, U. Loreit, Properties of the commercially available magnetoresistive sensor KMZ10A in the temperature range between 50 and 290 K, Cryogenics 38, 187 (1998)

[9] S. Linzen, F. Schmidt, L. Dörrer, F. Schmidl, G. Kaiser, S. Wunderlich, P. Seidel, Combined HTSC-Hall-magnetometers with low temperature cryo-cooled electronics for NDE applications, Proc. Wolte-4, Noordwijk, June 2000

[10] F. Schmidl, S. Wunderlich, L. Dörrer, H. Specht, S. Linzen, H. Schneidewind, P. Seidel, High-TC DC-SQUID system for nondestructive evaluation, IEEE Trans. Appl. Supercond. Vol. 7 (2), 2756 (1997)

[11] S. Wunderlich, F. Schmidl, L. Dörrer, C. Steigmeier, F. Schmidt, U. Hübner, P. Seidel, The antenna efficiency of planar galvanically coupled dc-SQUID gradiometers and magnetometers on 10 x 10 mm2 bicrystal substrates, submitted to IEEE Trans. Appl. Supercond.

[12] P. Seidel, F. Schmidl, S. Wunderlich, L. Dörrer, T. Vogt, H. Schneidewind, R. Weidl, High-TC SQUID Systems for Practical Use, IEEE Trans. Appl. Supercond. Vol. 9 (2), 4077 (1999)

[13] P. Seidel, F. Schmidl, R. Weidl, S. Wunderlich, L. Dörrer, High-TC SQUID systems for biomagnetic clinical research and for non-destructive evaluation, Advances in Supercond. XI, Ed. N.Koshizuka, S.Tajima, Proc. of ISS‘98, Springer Tokyo, Vol. 2, 1193 (1999)

Activities of the PFM (Pôle Francilien Microsystèmes) on Permalloy Thin Films Deposition and Magnetic Devices

E. Martincic*, E. Dufour-Gergam*, A. Bosseboeuf*, J.-M. Quemper*, S. Cercelaru*, A.-M. Nguyen**, B. Ahamada***

* Institut d'Electronique Fondamentale, UMR 8622, Université Paris XI, Bât. 220, F-91405 Orsay Cedex, France
** Laboratoire de Génie Electrique de Paris, URA 128, Université Paris XI, Bât. 220, F-91405 Orsay, France
*** Laboratoire d'Electricité Signaux et Robotique, UPRESA 8029, ENS de Cachan, 61 av. du président Wilson, F-94235 Cachan Cedex, France

In this paper, past and present research activities of the Pôle Francilien Microsystèmes on permalloy thin films deposition and devices are presented. First, a short presentation of the different laboratories composing the PFM is made. Then the main results obtained on sputtered Ni-Fe and Ni-Fe-Mo thin films deposition and devices are briefly summarised. Finally, some results on the properties and patterning of electrodeposited permalloy thick films by micromolding are given.

Introduction

The Pôle Francilien Microsystèmes (PFM) is a network of four laboratories working on microtechnology and microsystems and located around Paris: IEF (Institute of Fundamental Electronics) and LURE (Laboratory of electromagnetic Radiation Use) which belong to the campus of Paris South University in Orsay, ESIEE (Engineering Superior School of Electronics and Electrotechnics) in Marne La Vallée, and ENS-Cachan (Ecole Normale Supérieure de Cachan). More generally the research activities of these laboratories range from material studies to system designs in the fields of microelectronics, optoelectronics, electrical engineering, nanotechnology, sensors, and actuators.

All technological work presented here on films deposition and device fabrication was performed in the clean room facilities of IEF by various teams of IEF, ENS Cachan, and LGEP (Laboratory of Electrical Engineering of Paris).

Deposition of Ni-Fe and Ni-Fe-Mo films by sputtering

Experimental conditions

Permalloy thin films deposition was started at IEF in 1993 and was continued during several theses from various teams of IEF and other laboratories. Ni-Fe and Ni-Fe-Mo films were deposited at room temperature by Ar rf sputtering in an MRC set up with a background pressure close to 10^{-7} mbar. Targets with a diameter of 6 inches and an anode-cathode distance of 6.5 cm were used for all depositions. Typical atomic compositions used for targets were $Fe_{19}Ni_{81}$ and $Fe_{15}Ni_{80}Mo_5$. Generally, 2 inches (100) silicon wafers were used as substrates. Unless otherwise indicated, film deposition was performed without a magnetic field during deposition.

Deposition rate and composition

Deposition rate and films composition were studied as a function of the working gas pressure and rf power. The deposition rate is approximately linear with the power density below 2 W/cm^2 and levels off beyond. The composition of the films was measured by x-ray microanalysis (EDS) and showed a percentage of iron lower than the target composition by approximately 2 %. Slight increases of Fe and Mo contents and a decrease of Ni content was observed by increasing rf power.

Magnetic properties

Magnetic measurements were carried out using an alternating gradient type magnetometer on 1 x 3 mm and 3 x 3 mm samples. An example of the hysteresis loops of FeNi and FeNiMo depositions is shown in Fig. 1. Depositions were realised at a pressure of 0.36 Pa and 0.55 W/cm^2 power. Saturation magnetisation is 0.68 T for NiFeMo and 0.87 T for NiFe and does not depend on the thickness.

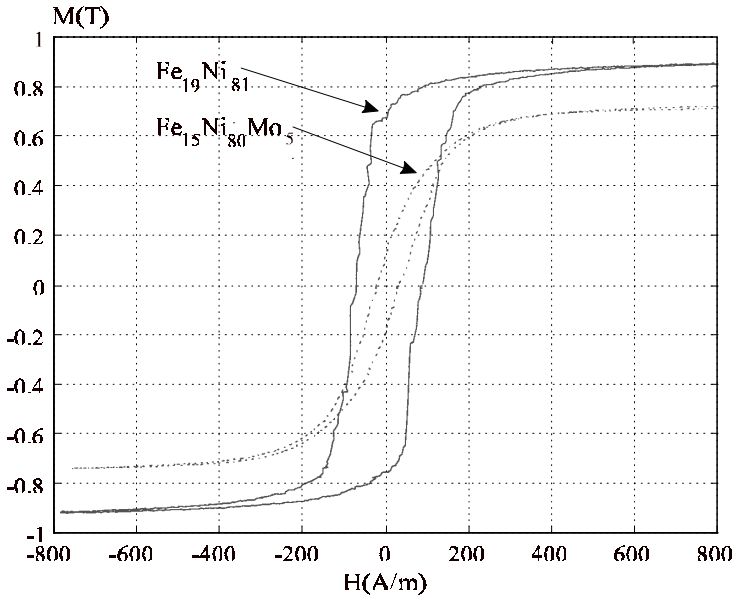

Fig. 1: Fe-Ni and Fe-Ni-Mo hysteresis loops comparison.

Coercive fields have been measured on various samples. The results obtained for 0.4 µm thick samples are summarised in Fig. 2. We observe a decrease in the value of the coercive field as a function of power. This effect might be related with smaller grain dimensions when the deposition rate is higher.

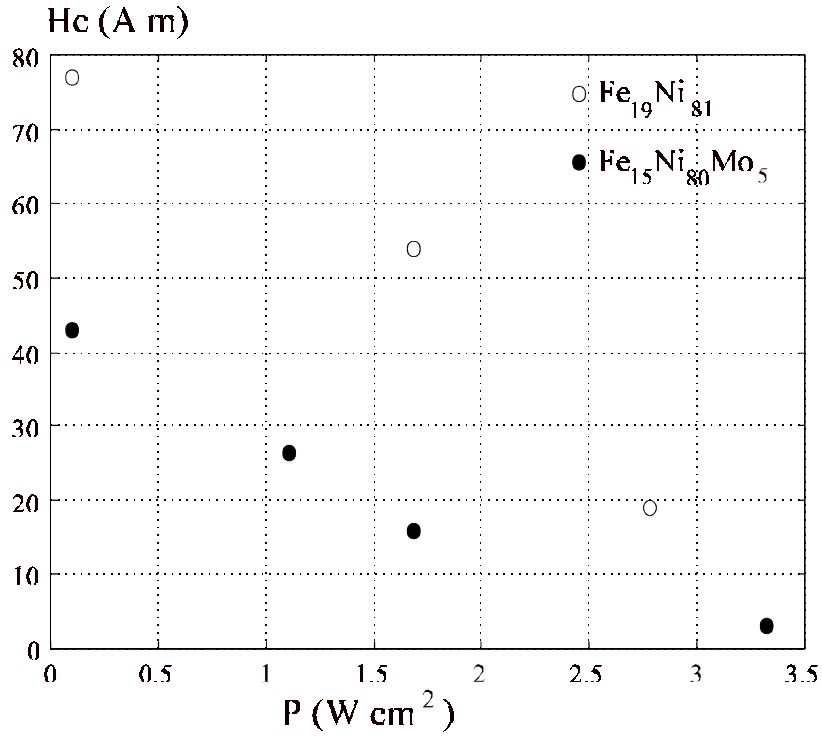

Fig. 2: Fe-Ni and Fe-Ni-Mo coercive field comparison as a function of the deposition power.

The effect of film thickness on the coercive field have also been evaluated on films deposited at 0.36 W/cm^2, 0.36 Pa. The coercive field decreases as the thickness increases: values obtained are from 67 A/m for 0.12 µm to 27 A/m for 0.4 µm.

The magnetisation anisotropy decreases with film thickness. For a film of 1 µm thickness, almost no difference can be seen between the hysteresis loops measured along the easy magnetisation axis and along the perpendicular magnetisation axis.

Electrical properties

The resistivity of the materials was measured with a 4-points probe. The results obtained are summarised in Fig. 3 as a function of the film thickness and rf power. The deposition pressure was 0.36 Pa when not indicated otherwise.

The average resistivity of NiFeMo films appears to be 3 times higher than for NiFe films. Films deposited at a higher pressure have also a higher resistivity compared with films of the same thickness and deposition power.

For both materials, thermal annealing produced a decrease of approximately 20% in the resistivity.

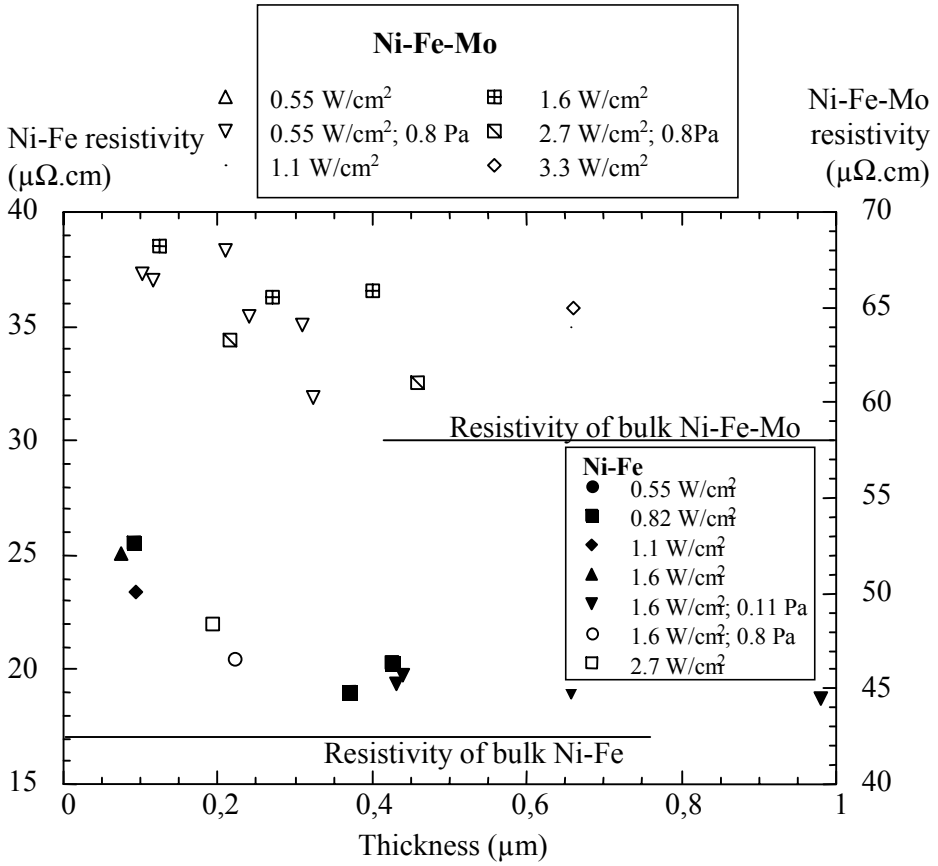

Fig. 3: Resisitivity of NiFe and NiFeMo films as functions of the thickness.

Devices with sputtered films

Some test devices were realised using sputtered permalloy films. Each application requires specific properties of materials.

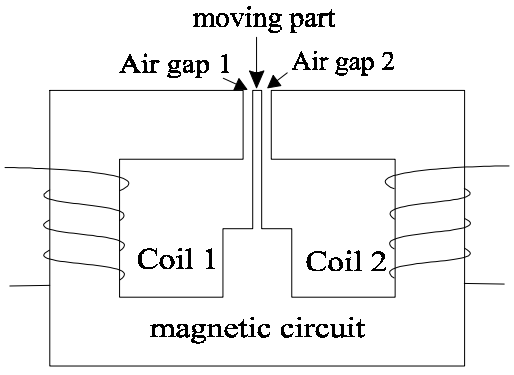

Fig. 4: Structure of the micro-relay [1].

Micro-relay

A study was realised at IEF on a bistable microrelay [1]. The conductors were realised by gold sputtering. A schematic representation of the device is shown in Fig. 4.

The operating cycle of the device can be described as follows: The current source 1 creates an electromagnetic field that moves the corresponding air gap until the magnetic path is closed. The remanent field keeps the contact closed. The current in coil 1 can then be removed.

The property of the permalloy that could be used for this application is a remanent electromagnetic field strong enough to keep the moving part in contact with the lateral parts when the current is removed from the coils. Anisotropy is not desirable in this application.

A two steps etching process (wet and dry etching) was used to release the moving part. It can be noticed that no deformation was observed when the moving part is released, as opposed to the deformations observed with silicon cantilevers released in one step.

Micro-electromagnetic sensors: permalloy magnetoresistors

A study on magnetoresistors was realised at LGEP (Laboratoire de Génie Electrique de Paris). All technological work was performed at the IEF. For this application, permalloy films were deposited with a magnetic field generated with a permanent magnet below the substrate. Figure 5 shows an example of a hysteresis loop measured for such films.

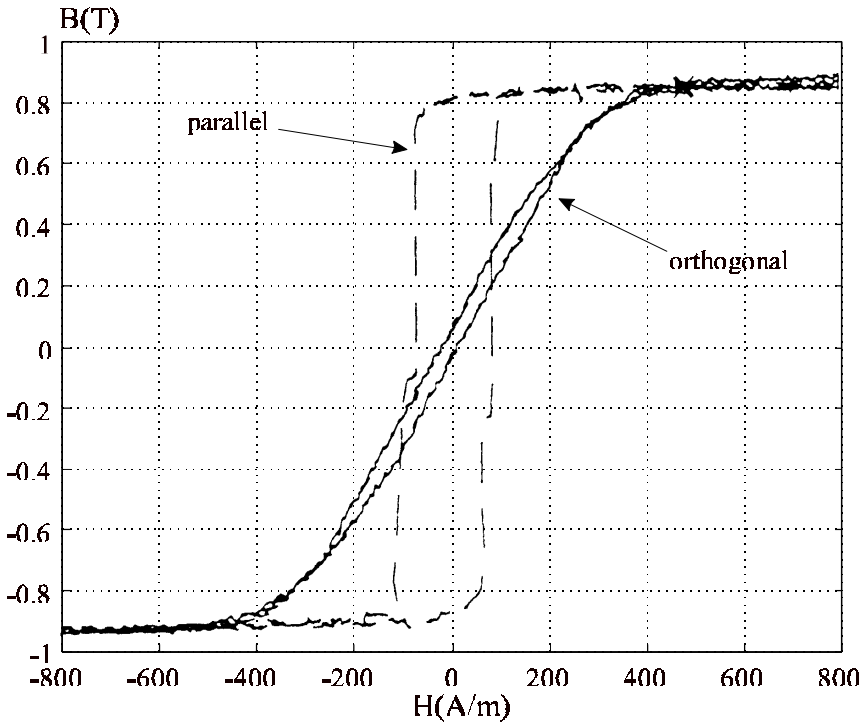

Fig. 5: Hysteresis loops of permalloy deposited under magnetic field in the parallel and orthogonal directions to the field [2].

Some test devices of magnetoresistors were realised with a single band structure, a barber pole structure and other structures in Wheatstone bridges configurations (Fig. 6). Experiments are in progress to obtain better balanced bridges which is the main technological difficulty.

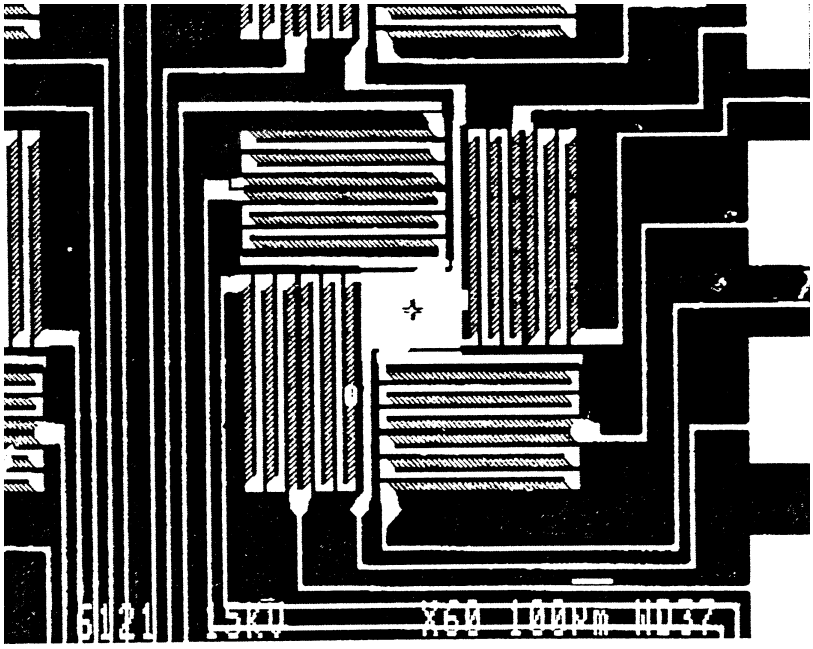

Fig. 6: SEM picture of a magnetic barber pole Wheatstone bridge structure sensor.

Electroplated NiFe alloys

Films of Ni-Fe alloys have also been realised by electrolytic growth. We present here some relevant results that were obtained at IEF.

The electrochemical cell used for Ni_xFe_y deposition is a two-electrodes system with a nickel anode in a 1 l glass beaker. The volume of the plating bath is approximately 450 ml with an interelectrode distance of 10 cm. DC current densities from 2 to 16 mA/cm^2 were applied at room temperature without stirring. A solution containing $NiSO_4$ (0.7 mol.l^{-1}), $FeSO_4$ (0.03 mol.l^{-1}), $NiCl_2$ (0.02 mol.l^{-1}) and saccharine (0.016 mol.l^{-1}) as a leveller was used as the electroplating bath. Boric acid (0.4 mol.l^{-1}) was added with the aim to obtain a good appearance of the deposit.

The film composition depends of the current density (Fig. 7).

The permalloy stoichiometry $Ni_{80}Fe_{20}$ is reached for a current density of 14.5 mA/cm^2. The variation of the mean film composition with current density shows the well known anomalous co-deposition effect of permalloy.

The magnetic properties of the $Ni_{80}Fe_{20}$ films were characterised using an alternative field gradient magnetometer. The coercive field is 28 A/m for a 680 nm thick film. These values were determined from the curves of flux density B as a function of the applied magnetic field H (Fig. 8).

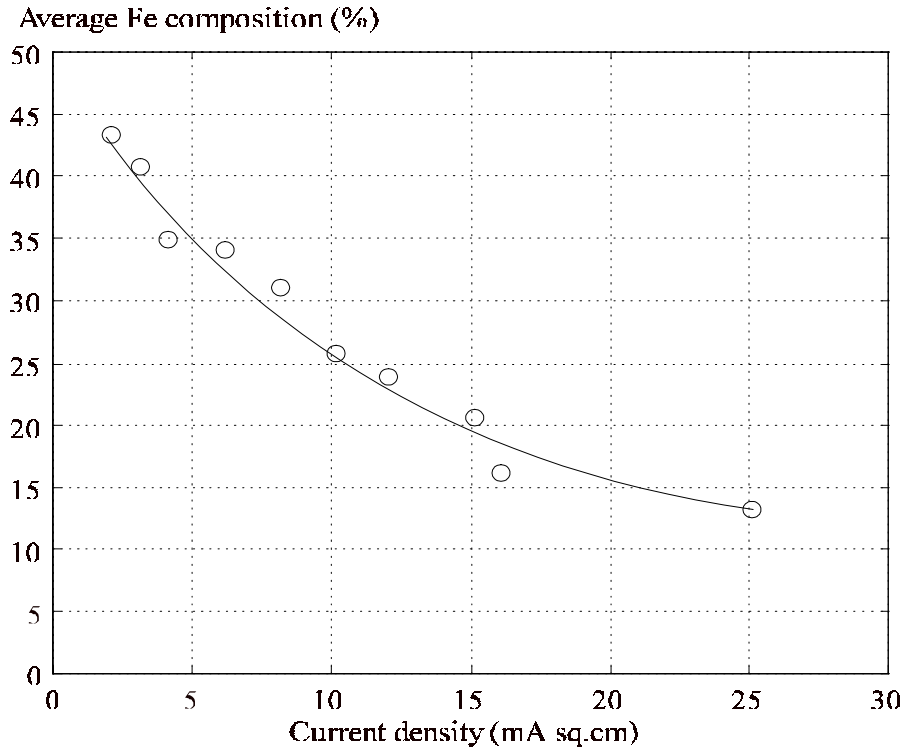

Fig. 7: Average Fe composition as a function of deposition current.

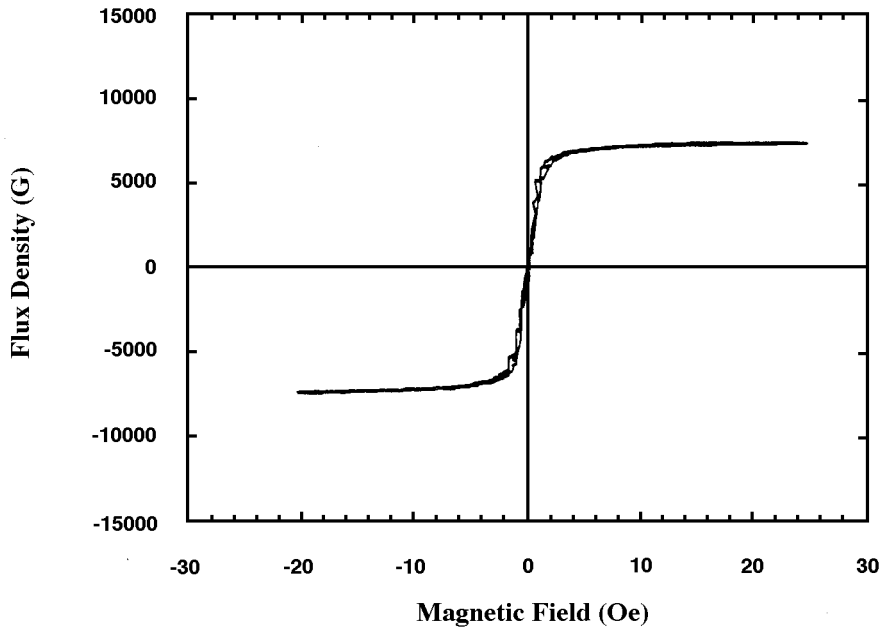

Fig. 8: Measured magnetic curve of electroplated permalloy.

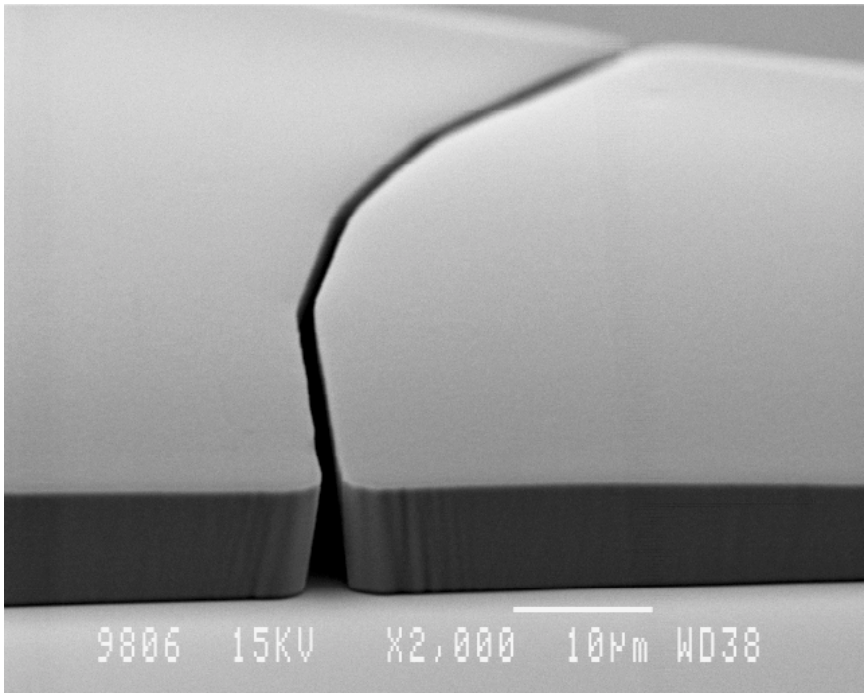

Fig. 9: 10 µm thick electrostatic motor realised by permalloy micromolding.

Conclusion

Current work is mainly focused on the optimisation of magnetic sensors for non-destructive evaluation using permalloy magnetoresistors in a barber pole structure, and on devices combining microcoils and permalloy films.

References

[1] S. Cercelaru, Étude de faisabilité d'un micro-interrupteur mécanique à commande électromagnétique, PhD thesis, June 1997, IEF, Université Paris-sud/Orsay.

[2] A.-M. Nguyen, Étude et réalisation d'un système micro-intégré de mesure du champ magnétique , PhD thesis, April 1997, LGEP, Université Paris-sud/Orsay.

[3] J.M. Quemper, S. Nicolas, J. P. Gilles, J. P. Grandchamp, A. Bosseboeuf, T. Bourouina, E.Dufour-Gergam, Permalloy electroplating through photoresist molds, Sensors and actuators A (physical) vol.A74, no.1-3; 20 April 1999; p.1-4.

[4] A.-M. Nguyen, S. Cercelaru, G. Tremblay, J.-C. Perron, P. Hesto, Magnetic and electrical characterizations of thin Ni-Fe and Ni-Fe-Mo films, Thin solid films, vol.275, no.1-2; 1 April 1996; p.231-234.

[5] S. Cercelaru, A.-M. Nguyen, P. Hesto, G. Tremblay, J.-C. Perron, A comparative study of the magnetic properties of thin permalloy films, Journal of Magnetism and Magnetic Materials. vol.160; July 1996; p.338-40.

Miniaturised Thin Film Magnetostrictive Delay Lines for Sensor Applications

E. Hristoforou

Laboratory of Physical Metallurgy, National Technical University of Athens,
9, Heroon Polytechniou Str., Zographou Campus, Athens 15780, Greece

A miniaturised arrangement based on the magnetostrictive delay line (MDL) mechanism, capable of being used as a sensor, is realised using thin films technology. In order to obtain high-performance miniaturised magnetostrictive delay line arrangements we used amorphous thin films of $Fe_{70}B_{20}Si_6C_4$ as magnetostrictive sensing elements because of their better magnetic and magnetoelastic characteristics than conventional magnetostrictive thin films. Improvements on signal to noise ratio are also discussed, focusing on the detection means.

Introduction

Among various types of magnetoelastic sensors, those based on the magnetostrictive delay line (MDL) technique attract an important attention because of their numerous applications for sensing displacement, force, position, pressure, and proximity [1], [2].

Due to the increased interest in magnetoelastic sensing applications, research has been focused on materials exhibiting two contradictory properties, namely, high saturation magnetostriction, and low magnetic anisotropy. The experimental investigations have shown that Fe-based amorphous alloys possess these two characteristics and also better magnetic and magnetoelastic properties compared to other magnetoelastic sensing elements [3].

Transition metal – metalloid amorphous alloys in the shape of ribbons and wires are suitable for a magnetostrictive delay line, but can not be adapted for miniaturisation. Magnetostrictive thin films are promising sensing materials for various magnetomechanical microsensors because they offer the following advantages: (1) magnetostrictive thin films require no power supply cable, being able to perform measurements in a non contact manner, (2) magnetostrictive thin films can be adapted for miniaturisation. In spite of this, only few works describing miniaturised MDL arrangements using magnetostrictive amorphous thin films as sensing elements have appeared.

We also report a special technological solution to improve the performance and to simplify the fabrication process of the miniaturised magnetostrictive delay lines (MDL) obtained by thin film technology. In order to increase the sensitivity level without adding new difficulties in the reliability of the sensing element, we conceived and realised a

new configuration of miniaturised MDL using a magnetoresistive sensing three-layered structure. According to this configuration, the MDL arrangement can be miniaturised, without the use of a receiving coil fabricated by thin film technology and photolithographic techniques, allowing thus a simple fabrication process and a high output signal level.

Fabrication and design of a miniaturised MDL arrangement

The miniaturised arrangement size is 33×1.2 mm^2. It uses 33 mm long Fe-based amorphous thin films as magnetostrictive delay line (MDL) media, with an exciting straight conductor (EC) deposited at one end of the delay line and a receiving coil (RC) at the other. The relative position of EC and RC is important in the design of the miniaturised magnetostrictive delay line arrangement, determining the delay time between the exciting and received signals and, consequently, the detection of a discrete MDL output signal. It has been found that the minimum distance necessary to obtain a discrete MDL output signal is of the order of 30 mm. The simplified operation principle of this miniaturised arrangement is based on the conventional MDL technique [4].

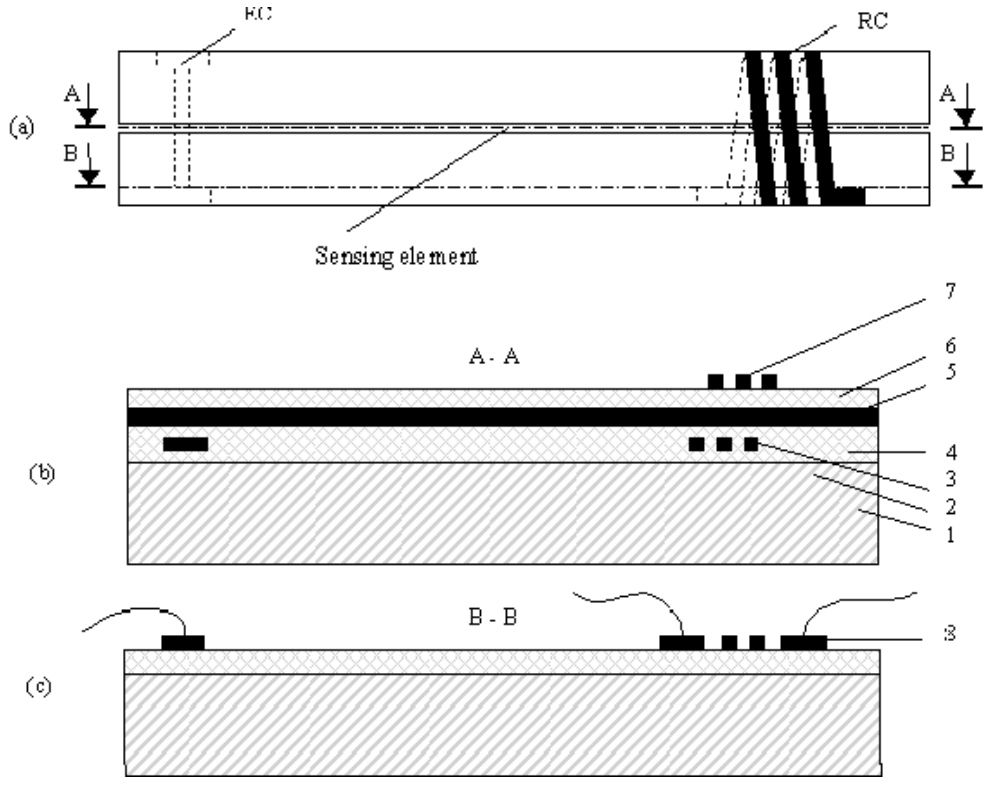

Fig. 1: The miniaturised arrangement of an MDL fabricated by thin film technology: (a) top view of the complete packaged thin film magnetostrictive delay line; (b) cross sectional view A — A: 1 – thin film wafer; 2 – insulating layer; 3 – first layer of Cu; 4 – insulating layer; 5 – $Fe_{70}B_{20}Si_6C_4$ amorphous thin films operating as MDL medium; 6 – insulating layer; 7 – last layer of Cu; (c) cross sectional view B — B: 8 – pads of exciting conductor and receiving coil.

The schematic arrangement of the miniaturised magnetostrictive delay line fabricated on a silicon wafer using a multilayer-like structure *X*/*Y*/*X*, where *X* is a multilayer structure of $SiO_2/Cu/SiO_2$ type and *Y* is the magnetostrictive material used as delay medium, is presented in Fig. 1.

The miniaturised MDL arrangement using an $Fe_{70}B_{20}Si_6C_4$ amorphous thin film 9500 Å in thickness as a sensing element is produced on silicon substrates using standard technological processes described in [5]. The deposited amorphous alloy, after mask formation in the shape of a narrow element, 0.5×33 mm, is the delay line medium. The excitation element is a copper or aluminium straight line orthogonal to the amorphous alloy, set at one end of it, separated by a silicon dioxide layer placed under the whole deposited amorphous alloy. Additionally, the receiving element can be realised arranging two arrays of conductors situated above and below the $Fe_{70}B_{20}Si_6C_4$ alloy, in order to form a receiving coil surrounding it. The insulating layers and amorphous thin films were deposited by r.f. sputtering. The lithography process used to form the exciting and receiving coils was based on the application of ordinary positive photo resist, exposure by ultraviolet contact photolithography, and development. The pattern is defined by wet chemical etching.

The above described technological solution, although offering a high level of sensitivity, is not an easy procedure concerning the flux change receiving means, adding possible difficulties in the reliability of the sensing element. Alternatively, the flux change sensing means is realised using the arrangement illustrated in Fig. 2. According to this, a $Ni_{81}Fe_{19}/SiO_2/Ni_{81}Fe_{19}$ three-layered MR structure is arranged below the $Fe_{70}Si_{15}B_{15}$ thin film, separated by a silicon dioxide layer. Another thin film layer made of $Fe_{70}Si_{15}B_{15}$ amorphous alloy is deposited below the three-layered MR structure, in order to increase the sensitivity of the flux change detection. The insulating layers and $Fe_{70}Si_{15}B_{15}$ amorphous thin films were deposited by the r.f. sputtering method. The $Ni_{81}Fe_{19}$ thin films (about 0.05 μm in thickness) were deposited by electron beam vacuum evaporation.

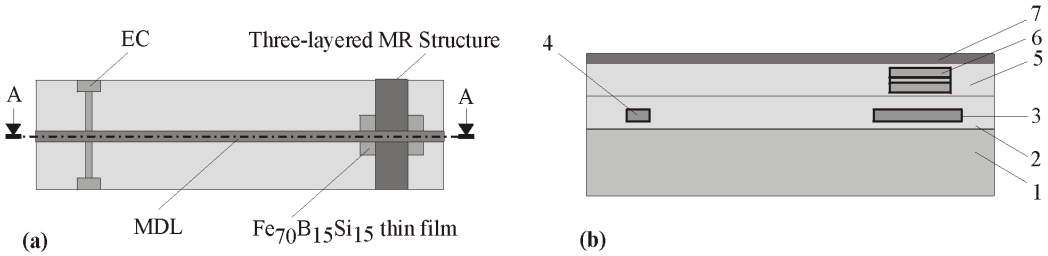

Fig. 2: The miniaturised arrangement of an MDL fabricated using a multilayer-like structure: (a) top view of the complete multilayer-like structure; (b) cross sectional view A — A: 1 – thin film wafer; 2 – insulating layer; 3 – $Fe_{70}B_{15}Si_{15}$ amorphous thin film; 4 – Cu thin film; 5 – insulating layer; 6 – three-layered MR sensing structure; 7 – $Fe_{70}B_{15}Si_{15}$ amorphous thin film operating as MDL medium.

Magnetic and magnetoelastic characteristics of sensing elements used for miniaturised MDL arrangements

In order to use $Fe_{70}B_{20}Si_6C_4$ amorphous thin films as sensing elements for the miniaturised MDL arrangements presented in this paper, the magnetic and magnetoelastic properties of technical significance for this application have been investigated.

The magnetic measurements of the Curie temperature, saturation magnetisation, and magnetic anisotropy field were made by a torque magnetometer. The saturation magnetostriction was measured using a capacitive cantilever technique. Based on values obtained for saturation magnetostriction λ_s and anisotropy constant k_u, we estimated the magnitude of the ΔE effect for investigated samples determining the values of the relative change of elasticity modulus $\Delta E/E$.

The Curie temperature T_C, saturation magnetisation M_s, and magnetic anisotropy field H_k are forming a triad of magnetic characteristics which in combination with magnetoelastic characteristics (saturation magnetostriction λ_s, magnetoelastic coupling coefficient $b^{\gamma 2}$, magnetoelastic coupling factor k and ΔE effect) determine the performance of the material used as a sensing element for the miniaturised MDL arrangement.

Among the crystalline materials, nickel thin films are good as sensing elements for miniaturised MDL arrangements. Various experiments show that the magnetomechanical coupling factor k and the ΔE effect for the amorphous alloy $Fe_{81}B_{13.5}Si_{3.5}C_2$ have larger values compared to nickel or any other magnetostrictive materials. It has been established that the magnitude of the ΔE effect depends on the ratio between the saturation magnetostriction constant λ_S and the magnetic anisotropy constant k_u. If E_s is the Young's modulus in magnetically saturated state and E is the Young's modulus in magnetically unsaturated state, the following equation gives information on the possibility of maximum changes of the sound velocities or the time of the signal delay for different materials used as sensing elements:

$$\frac{E}{E_{s\ \min}} = \left(1 + \left(\frac{9\lambda^2{}_s E_s}{2k_u}\right)\right)^{-1} \tag{1}$$

The study of the magnetic and magnetoelastic properties of Fe-based amorphous thin films shows that they exhibit ideal characteristics as a magnetostrictive delay line medium. The values of the relevant parameters of Fe-based amorphous thin films used as sensing elements for miniaturised MDL arrangements are presented in Table 1.

Thickness (Å)	T_C (°C)	σ_s (emu/g)	$\lambda_S \times 10^{-6}$	k_u (erg/g)	$b^{\gamma 2} \times 10^6$ dynes/cm^2	$D \times 10^{-10}$G^{-1}	$\Delta E/E$
9500	338	132	32	2×10^3	-30	425	0. 58

Table 1: The values of the relevant parameters for sensing element performance of $Fe_{70}B_{20}Si_6C_4$ amorphous thin films: Curie temperature T_C, saturation magnetisation σ_s, saturation magnetostriction λ_S, anisotropy constant k_u, magnetoelastic coefficient coupling $b^{\gamma 2}$, static stress sensitivity D and ΔE effect.

An other advantage of the use of amorphous thin films as magnetoelastic sensing elements, applicable for wide-range position sensors, is the large distance through which the magnetoelastic wave propagates. This advantage arises as the effect of the high electrical resistivity of amorphous thin films, resulting in low eddy current losses and a low value of the attenuation constant of the propagated magnetoelastic waves.

The three-layered MR sensing structure with a 5×0.05 mm^2 rectangular shape is presented in Fig. 3. The non-linear output in the applied magnetic field is avoided by applying a bias field in the direction perpendicular to the easy axis. Thus, the angle between magnetisation and current direction is maintained at 45° and the response of the $Ni_{81}Fe_{19}$ thin film to the magnetic field becomes linear. The bias field was achieved using the soft adjacent layer (SAL) biasing scheme.

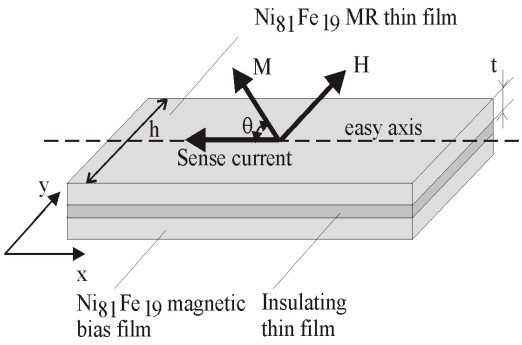

Fig. 3: The three-layered MR structure based on $Ni_{81}Fe_{19}/SiO_2/ Ni_{81}Fe_{19}$ thin films used for flux change sensing in the miniaturised MDL arrangement.

In SAL biasing, a $Ni_{81}Fe_{19}$ thin film is placed adjacent to the first $Ni_{81}Fe_{19}$ thin film and separated by an SiO_2 thin film with a thickness of 500 Å. The easy axis of the magnetic bias $Ni_{81}Fe_{19}$ thin film is in the *y*-direction, perpendicular to the easy axis of the first MR $Ni_{81}Fe_{19}$ thin film. The magnetic field generated by the current flowing in the $Ni_{81}Fe_{19}$ MR thin film magnetises the soft magnetic $Ni_{81}Fe_{19}$ thin film up to the saturation. The SAL, in turn, produces the field which biases the MR thin film. An uniaxial anisotropy was easily induced by depositing the $Ni_{81}Fe_{19}$ thin film in a weak magnetic field of about 100 Oe, applied in the film plane.

The response of the three-layered MR structure used in miniaturised MDL arrangements to the magnetoelastic waves which propagate in the MDL is under investigation.

Conclusions

The conventional arrangements of miniaturised MDL based on nickel thin films as material for the sensing elements have been improved by using amorphous thin films. In terms of sensitivity, dynamics, and versatility, it is possible to obtain high-performance microsensors if Fe-based amorphous thin films are used as a material for the magnetostrictive sensing element because of their better magnetic and magnetoelastic characteristics than conventional magnetostrictive thin films. Further improvements in performance of miniaturised MDL using Fe-based amorphous thin films as sensing ele-

ments can be achieved if two new miniaturised configurations of this device are used, targeting on its miniaturisation process, which will be considered a work in progress.

We have also presented a new miniaturised MDL arrangement fabrication technology and configuration using a three-layered MR structure based on $Ni_{81}Fe_{19}/SiO_2/Ni_{81}Fe_{19}$ thin films instead of a thin film receiving coil for flux change sensing. The use of the three-layered MR structure allows to simplify the fabrication process of the miniaturised device based on MDL technique and to maintain a high output signal level.

References

[1] Hristoforou E and Reilly R E 1994 IEEE Trans. Mag. 30 2728-2733

[2] Meydan T and Elshebani M S M 1992 J. Magn. Magn. Mat. 112 344-346

[3] Gibbs M 1994 Physics World January 40-45

[4] Hristoforou E and Niarchos D 1992 J. Magn. Magn. Mat. 116 177-188

[5] Chiriac H Hristoforou E Grigorica M and Moga A 1997 Sensors & Actuators 59 280-284

[6] Livingston J D 1982 Phys. Stat. Sol. (a) 70 591-596

[7] Gibbs M R J 1995 Sensors and their applications VII (Bristol IOP Publishing)

[8] Takemura Y Masuda S Yamada T and Kakuno K 1995 IEEE Trans. Mag. 31 3115-3118

[9] H. Chiriac, M. Pletea and E. Hristoforou, Proceedings of the 12th European Conference on Solid-State Transducers, 1998, 979-982

[10] U. Dibbern, Magnetoresistive Sensors, Magnetic Sensors, edited by R. Boll, K. J. Overshott, 1989, 341

Addresses of Workshop Participants

Dr. Giovanni A. **Battiston**

Istituto di Chimica e Tecnologie Inorganiche e dei Materiali Avanzati
Corso Stati Uniti 4
I-35127 Padova - Italy

e-mail: g.a.battiston@ictr.pd.cnr.it
Tel.: +39-049-829 5948
Fax: +39-049-870 2911
URL: http://www.pd.cnr.it/ist/ictr/ictr.html

Dr. Alain **Bosseboeuf**

Institut d'Electronique Fondamentale
Bat. 220 - Université Paris Sud
F-91405 Orsay Cedex France

e-mail: Alain.Bosseboeuf@ief.u-psud.fr
Tel.: +33-1-6915-7835
Fax: +33-1-6915-4000
URL: http://www.u-psud.fr/ief/

Prof. Dr. Joan **Cabestany**

UPC (Technical University of Catalunya)
Dept. of Electronic Engineering
Campus Nord - Gran Capità, s/n Building C4
E-08034 Barcelona - Spain

e-mail: cabestan@eel.upc.es
Tel.: +34-93-401 6742
Fax: +34-93-401 6756
URL: http://www-eel.upc.es/aha

Dr. Jaume **Esteve**

National Centre of Microelectronics
(Spanish Council for Research and Science, CSIC)
Campus Univ. Autonoma de Barcelona,
E-08193 - Bellaterra - Barcelona (Spain)

e-mail: jaume.esteve@cnm.es
Tel.: +34-93-594 7700
Fax: +34-93-580 1496
URL: http://www.cnm.es/

Prof. Dr. Wolfgang **Fallmann**

Institut für Industrielle Elektronik und Materialwissenschaften
TU Wien
Gusshausstrasse 27-29
A-1040 Wien

e-mail: wolfgang.fallmann@tuwien.ac.at
Tel.: +43-1-58801-36652
Fax: +43-1-58801-36699
URL: http://www.iemw.tuwien.ac.at

Dr. Heinrich **Grüger**

Fraunhofer-IMS - Institut für Mikroelektronische Schaltungen und Systeme
Grenzstrasse 28
D-01109 Dresden

e-mail: grueger@imsdd.fhg.de
Tel.: +49-351-8823-155
Fax: +49-351-8823-266
URL: http://www.ims.fhg.de

Ao.Prof. Dr. Hans **Hauser**

Institut für Industrielle Elektronik und Materialwissenschaften
TU Wien
Gusshausstrasse 27-29
A-1040 Wien

e-mail: hans.hauser@tuwien.ac.at
Tel.: +43-1-58801-36614
Fax: +43-1-58801-36695
URL: http://www.iemw.tuwien.ac.at

Prof. Dr.Ing. Ulrich **Hilleringmann**

Fachbereich Elektrotechnik
Fachgebiet Sensorik
Warburger Str. 100
D-33098 Paderborn

e-mail: Hilleringmann@sensorik.uni-paderborn.de
Tel.: +49-5251-602225
Fax: +49-5251-603743
URL: http://sensorik.uni-paderborn.de

Dr. Johannes **Hochreiter**

Institut für Industrielle Elektronik und Materialwissenschaften
TU Wien
Gusshausstrasse 27-29
A-1040 Wien

e-mail: wde@e355srv.tuwien.ac.at
Tel.: +43-1-58801-36634
Fax: +43-1-58801-36695
URL: http://www.iemw.tuwien.ac.at

Prof. Dr. Evangelos **Hristoforou**

Laboratory of Physical Metallurgy
National Technical University of Athens
9, Heroon Polytechnion
Zografon Campus
Athens 15780, Greece

e-mail: eh@metal.ntua.gr
Tel.: +30-1-772 2178
Fax: +30-1-772 2119
URL: http://www.ntua.gr

Dr. Peter **Hudek**

Leica Microsystems Lithography
Göschwitzer Strasse 25,
D-07743 Jena

e-mail: hudek.ui@savba.sk
Tel.: +49-3641-65-1969
Fax: +49-3641-65-1922
URL: http://ups.savba.sk/ebl

Prof. Dr. David **Jiles**

Ames Laboratory
Iowa State University
Ames, Iowa 50011, USA

e-mail: magnetics@ameslab.gov
Tel.: +1-515-294-9685
Fax: +1-515-294-8727
URL: http://www.iastate.edu

Dr. Ivan **Kostic**

Institute of Informatics
Slovak Academy of Sciences
Dúbravská 9,
SK-842 37 Bratislava, Slovakia

e-mail: kostic.ui@savba.sk
Tel.: +421-7-5941 2006
Fax: +421-7-5477 1004
URL: http://ups.savba.sk/ebl

Dr. Emile **Martincic**

Institut d'Electronique Fondamentale
Bat. 220 - Université Paris Sud
F-91405 Orsay Cedex France

e-mail: Emile.Martincic@ief.u-psud.fr
Tel.: +33-1-6915-4210
Fax: +33-1-6915-4080
URL: http://www.u-psud.fr/ief/

Dr. Terence **O'Donnell**

PEI Technologies
National Microelectronics Research Centre
University College
Lee Maltings
Prospect Row
Cork, Ireland

e-mail: terence.odonnell@nmrc.ie
Tel: +353-21-904165
Fax: +353-21-270271
URL: http://www.nmrc.ie

Dr. Eveline **Riedling**

Institut für Industrielle Elektronik und Materialwissenschaften
TU Wien
Gusshausstrasse 27-29
A-1040 Wien

e-mail: eveline.riedling@tuwien.ac.at
Tel.: +43-1-58801-36683
Fax: +43-1-58801-36692
URL: http://www.iemw.tuwien.ac.at

Ao.Prof. Dr. Karl **Riedling**

Institut für Industrielle Elektronik und Materialwissenschaften
TU Wien
Gusshausstrasse 27-29
A-1040 Wien

e-mail: karl.riedling@tuwien.ac.at
Tel.: +43-1-58801-36658
Fax: +43-1-58801-36699
URL: http://www.iemw.tuwien.ac.at

Dr. Frank **Schmidl**

Institut für Festkörperphysik,
Friedrich-Schiller-Universität Jena
Helmholtzweg 5
D-07743 Jena, Germany

e-mail: schmidl@dpserv1.ifk.uni-jena.de
Tel. +49-(0)3641-947410
Fax: +49-(0)3641-947412
URL: http://www.physik.uni-jena.de/~tief/

Dr. Dieter **Schrottmayer**

Schiebel Elektronische Geräte GmbH
Margaretenstrasse 112
A-1050 Wien

e-mail: disc@schiebel.com
Tel.: +43-1-54626-0
Fax: +43-1-5452339
URL: http://www.schiebel.com/

Günther **Stangl**

Institut für Industrielle Elektronik und Materialwissenschaften
TU Wien
Gusshausstrasse 27-29
A-1040 Wien

e-mail: guenther.stangl@tuwien.ac.at
Tel.: +43-1-58801-36672
Fax: +43-1-58801-36699
URL: http://www.iemw.tuwien.ac.at

Prof. Dr. Gábor **Vértesy**

Hungarian Academy of Sciences
Research Institute for Technical Physics and Materials Science

H-1525 Budapest, P.O.B. 49, Hungary

e-mail: vertesyg@mfa.kfki.hu
Tel.: +36-1-392 2677
Fax: +36-1-3959284
URL: http://www.mfa.kfki.hu

Dr. Pierino **Zanella**

Istituto di Chimica e Tecnologie Inorganiche e dei Materiali Avanzati
Corso Stati Uniti 4
I-35127 Padova - Italy

e-mail: p.zanella@ictr.pd.cnr.it
Tel.: +39 049 8295948
Fax: +39 049 8702911
URL: http://www.pd.cnr.it/ist/ictr/ictr.html

ISBN: 3-85465-007-8